UNIVERSITY OF OKLAHOMA

GRADUATE COLLEGE

MANUFACTURING AND MICROSTRUCTURAL MODELING OF GEOMETRICALLY COMPLEX COMPOSITE COMPONENTS PRODUCED BY BLADDER ASSISTED COMPOSITE MANUFACTURING (BACM)

A DISSERTATION

SUBMITTED TO THE GRADUATE FACULTY

in partial fulfillment of the requirements for the

Degree of

DOCTOR OF PHILOSOPHY

By

JACOB PRESTON ANDERSON
Norman, Oklahoma
2013

MANUFACTURING AND MICROSTRUCTURAL MODELING OF GEOMETRICALLY COMPLEX COMPOSITE COMPONENTS PRODUCED BY BLADDER ASSISTED COMPOSITE MANUFACTURING (BACM)

A DISSERTATION APPROVED FOR THE
SCHOOL OF AEROSPACE AND MECHANICAL ENGINEERING

BY

_____
Dr. M. C. Altan, Chair

_____
Dr. Shivakumar Raman

_____
Dr. J. David Baldwin

_____
Dr. Mrinal C. Saha

_____
Dr. Zahed Siddique

© Copyright by JACOB PRESTON ANDERSON 2013
All Rights Reserved.

ACKNOWLEDGEMENTS

I would like to thank Dr. M.C. Altan, my advisor, for his continuous guidance and unwavering support throughout the course of this dissertation. I would also like to thank him for allowing me the honor and privilege to work with him as a Graduate Research Assistant, which gave me the opportunity to work on various interesting research activities.

I would like to express my thanks to Newport Adhesives and Composites Inc., and TenCate® Composites for their donations of the prepreg materials. As well as the Oklahoma EDGE program, the SEAM center at the University of Oklahoma whose research grant partially supported the research conducted in this dissertation, the Robert Hughes Centennial Fellowship, and my committee members.

Special thanks to Dr. Levent Aktas, Orhan Ozcelik, Charbel Chaghouri, and Scott Bowen for their numerous helpful conversations. Last but not least, I would like to thank my parents Daniel and Joyce Anderson, wife Kali Brownell, and family for their continued support without which none of this would be possible.

TABLE OF CONTENTS

Acknowledgements iv

Table of Contents v

List of Tables x

Table of Figures xi

Abstract xvi

Nomenclature xviii

1. Introduction 1

1.1 Composite Manufacturing Techniques 1

1.2 Void Formation in Composites 3

1.3 Voids Effects on the Mechanical Properties of Composite Laminates 5

2. Properties of Composite Cylinders Fabricated by Bladder Assisted Composite Manufacturing (BACM) 8

2.1 Introduction 8

2.2 Materials and Experimental Procedure 11

2.2.1 Geometry and Materials Used 11

2.2.2 Sample Fabrication Process 12

2.2.3 Void Analysis Procedure 16

2.2.4 Mechanical Testing 18

2.2.4.1 Cylinders 20

2.2.4.2 Flat Laminates 23

2.3 Results and discussion 23

2.3.1 Energy Consumption 24

2.3.2 Processing Pressure Effect 25

2.3.3 Laminate Quality 28

2.3.4 Flexural Properties 33

2.4 Conclusions 36

3. Reduction of Microvoids in Composite Laminates Fabricated by Bladder Assisted Composite Manufacturing (BACM) 38

3.1 Introduction 38

3.2 Materials and Experimental Procedures 41

3.2.1 Prepreg Material Used 41

3.2.2 BACM Curing Processes 41

3.2.2.1 Original Configuration 41

3.2.2.2 Sealed Configuration 43

3.2.2.3 Bleeder Configuration 43

3.2.2.4 Combined Seal/Bleeder Configuration 44

3.2.7 Characterization of Flexural Properties 47

3.2.8 Measurement of Fiber Volume and Void Content 50

3.3 Results and Discussion 52

3.3.1 Energy Consumption during Manufacturing 52

3.3.2 Mold Configuration Effect on Fiber Volume Fraction 54

3.3.3 Wet-Conditioned Laminates Results 55

3.3.3.1 Bulk Void Content in Wet-Conditioned Laminates 55
3.3.3.2 Wet-Conditioned Laminates Flexural Properties 57
3.3.3.3 Wet-Conditioned Laminates Void Morphology 59
3.3.4 Dry-Conditioned Laminates Results 64
3.3.4.1 Bulk Void Content in Dry-Conditioned Laminates 64
3.3.4.2 Dry-Conditioned Laminates Flexural Properties 65
3.3.4.3 Dry-Conditioned Laminates Void Morphology 67
3.6 Conclusions 70

4. Formation of voids in composite laminates: coupled effect of humidity exposure and cure pressure 72

4.1 Introduction 72

4.2 Materials and Methods 75

4.2.1 Fabrication Procedure 75

4.2.2 Moisture Content 76

4.2.3 Void Content Measurement 78

4.3 Results and Discussion 78

4.3.1 Moisture Diffusion in Uncured Prepregs 78

4.3.2 Humidity and Pressure Effect on Void Formation 80

4.4 Proposed Model 82

4.4.1 Model Development 82

4.4.2 Model Fit to Experimental Data 84

4.4.3 Model Validation 86

4.5 Conclusions 88

5. Mechanical properties of composite laminates: coupled effect of microvoids and fiber content 90

5.1 Introduction 90

5.2 Materials and Methods 93

5.2.1 Fabrication Procedure 93

5.2.2 Void and Fiber Volume Content Measurement 94

5.2.3 Characterization of Laminate Tensile Properties 95

5.3 Results and Discussion 97

5.3.1 Processing Conditions Effect 97

5.3.2 Tensile Properties of Laminates 100

5.4 Conclusions 105

6. Conclusions and Recommendations 106

6.1 Conclusions 106

6.2 Recommendations for Future Work 108

References 110

Appendix A: BACM Process Controller 118

A.1: BACM Control Scheme 118

A.2: BACM Controller VB6 Code 119

Appendix B: Void Content 130

B.1: Derivation of ASTM D2734 130

B.2: Void Content Uncertainty 131

B.2.1: Sample Uncertainty Calculation 133

Appendix C: Ring Flexural Properties 134

C.1: Ring Flexural Modulus 134

C.1.1: Flexural Strain Energy 135

C.1.2: Shear Strain Energy 136

C.1.3: Circumferential Deformation Strain Energy 137

C.2: Ring Flexural Strength 139

Appendix D: Dissertation Publications 144

Journal Article 144

Conference Proceedings 144

LIST OF TABLES

Table 1: Fitting parameters of Eq. (13) for the experimental data. 86

Table 2: Predicted void contents compared to the actual void content of the laminates exposed to separate humidity cycles. 88

Table 3: Values used for Uncertainty Calculations 133

Table 4: Calculated Uncertainty Values 133

Table 5: Comparison of Equations used for Calculating the Elastic Moduli 138

TABLE OF FIGURES

Figure 1- Mold assembly, heating element and bladder used to fabricate composite cylinders. 15

Figure 2- BACM mold half with the heating/cooling manifold attached. 15

Figure 3- Typical BACM cure cycle showing process temperature and pressure. 16

Figure 4- Procedure used for the determination of the bulk composite and epoxy resin densities. 18

Figure 5- Diagram of (a) how the manufactured cylinders rings were cut and (b) how these rings were further processed (if necessary) to create the required test specimen. Note: All the listed dimensions are in millimeters. 19

Figure 6- A 50.8mm composite cylinder fabricated by the BACM method. A 12.7mm wide ring, ring segment, and a flat test specimen obtained from a hot pressed laminate are shown in the figure. 20

Figure 7- Typical load-deflection behavior of the composite rings during testing. 22

Figure 8- Typical stress-strain behavior of the curved flexure samples during testing.. 23

Figure 9- Comparison of BACM and Oven Heating energy consumption during the processing of composite cylinders. Note: Error bars represent the 95% confidence interval for n=5. 25

Figure 10- Effect of processing pressure on fiber volume fraction 27

Figure 11- Spatial variation of fiber volume fraction in cylinders produced using BACM. 28

Figure 12- Density of specimen as the fiber volume % is increased. The average void content is shown to be below 5% for all specimens. Note: The increase in marker size is used to illustrate increase in pressure applied during processing. 31

Figure 13- Void % as processing pressure is increased normalized by number of plies present..... 31

Figure 14- Representative void morphologies in composite cylinders fabricated by BACM method observed at 100x and 200x magnification. Bladder pressure: (a) 345 kPa and (b) 621 kPa. 32

Figure 15- Difference between the maximum and minimum void fractions (%) obtained for fabricated composite cylinders (i.e., Void $\%_{max}$ – Void $\%_{min}$) as processing pressure is increased. 32

Figure 16- Effect of processing technique and fiber content on measured elastic modulus. The dashed line shown is a trend line fit to all data points present. 35

Figure 17- Failure strength of fabricated specimens. 36

Figure 18- Void effects on the flexural strength of composite specimens. The dashed markers indicate specimen with void fractions above the 1.9% threshold. None of the hot pressed specimen exceeded the threshold value of 1.9%. 36

Figure 19- Schematics of the (a) I-, (b) S-, (c) B-, and (d) C-BACM mold configurations. 45

Figure 20- BACM cure cycle showing the effect the mold configurations had on cure profile temperature stability. The average temperature profiles shown for the sealed and bleeder configurations were recorded by thermocouples placed between the second and third plies, 6.4mm from each end of the lay-up. 47

Figure 21- Schematic representation of the (a) rings cut from BACM processed cylinders and (b) how these ring specimens were cut to allow for the characterization of the laminates elastic modulus and flexural strength. Note: all dimensions are in mm. . 49

Figure 22- Effect of varying span to depth ratio on the flexural strength of TenCate® EX-1522/Plain Weave carbon fiber/epoxy prepreg. Note: Error bars represent the 95% confidence interval for n=5. 50

Figure 23- Variations in energy consumption by the BACM curing processes. The effect of changing the BACM mold configurations on the energy consumed was found to be insignificant. Note: Error bars represent the 95% confidence interval for n=4..... 53

Figure 24- The effect of mold configuration on fiber volume fraction. Note: Error bars represent the 95% confidence interval for n=6..... 55

Figure 25- Void contents of the cylinders produced using each of the mold configurations. Note: Error bars represent the 95% confidence interval for n=6. 57

Figure 26- Mold configuration and fiber content effect on measured elastic modulus of the cylinders. Note: Error bars represent the 95% confidence interval for n=6. 58

Figure 27- The failure strengths of the cylinders produced using each of the mold configurations. Note: Error bars represent the 95% confidence interval for n=6. 59

Figure 28- SEM images of the 207 kPa processed specimens manufactured by the (a) I-, (b) S-, (c) B- and (d) C-BACM mold configurations at 50x, and 200x. 61

Figure 29- SEM images of the 483 kPa processed specimens manufactured by the (a) I-, (b) S-, (c) B- and (d) C-BACM mold configurations at 50x, and 200x. 62

Figure 30- Schematic representations of the (a) I-BACM and (b) B-BACM configurations. The effect of the bleeder is shown in the (b) B-BACM configuration. In the I-BACM configuration, the absence of a bleeder leads to resin outflow along the circumference of the laminate. In the B-BACM configuration, the presence of bleeder leads to higher resin outflow and higher fiber volume fractions. 63

Figure 31- Void content of laminates using the hot-press and B-BACM manufacturing techniques. Note: Error bars represent the 95% confidence interval for n=6. 65

Figure 32- Manufacturing technique, preconditioning, and fiber volume content effect on measured elastic modulus. Note: Error bars represent the 95% confidence interval for n=6. 66

Figure 33- Manufacturing technique, preconditioning, and fiber volume content effect on flexural strength. Note: Error bars represent the 95% confidence interval for n=6. . 67

Figure 34- SEM images of the dry-conditioned B-BACM specimen processed at (a) 207 kPa and (b) 483 kPa at 50x, and 200x. 69

Figure 35- SEM images of the dry-conditioned hot-pressed specimen processed at (a) 207 kPa and (b) 483 kPa at 50x, and 200x. 69

Figure 36- Hypothesized effect of increasing from (a) low to (b) high fiber volume content on the morphology of voids. 70

Figure 37- Temperature cure profile used to manufacture the laminates in this chapter. 75

Figure 38- Total moisture transmission of a representative prepreg specimen. 77

Figure 39- Time dependent moisture transmission rate of a representative prepreg specimen. 77

Figure 40- Moisture content of TenCate® BT250/7781 exposed to humidity environments of 99%, 45%, and 25% relative humidity at 25°C until saturation was reached. The fit of the Fickian 1-D diffusion model, i.e. Eq. (9), is also shown. Note: Error bars represent the 95% confidence interval for n=3. 80

Figure 41- Effect of humidity environment and processing pressure on the formation of voids. Note: Error bars represent the 95% confidence interval for n=8. 81

Figure 42- Fiber bundle hierarchy of laminates manufactured at (a) 69 kPa and (b) 483 kPa whose prepreg plies were conditioned at 25% RH for 24 hrs. 82

Figure 43- Fit of the model Grunenfelder and Nutt [21] used, Eq. (12), when fit to the data points at each cure pressure separately along. Note: The model was unable to be fit to the entire data set. Note: Error bars represent the 95% confidence interval for n=8. 85

Figure 44- Fit of the model proposed in this chapter, Eq. (13), to the complete data set. Note: The model is capable of predicting void contents at all pressure/humidity levels and the error bars represent the 95% confidence interval for n=8. 85

Figure 45- The two humidity exposure cycles of the prepreg plies which composed the laminates used to verify the proposed model. Note: The temperature at the time of the exposure cycles was 25°C. 87

Figure 46- Moisture content of the prepreg plies composing the verification laminates during their humidity cycles shown with the predicted moisture content using Eq. (9). Note: Error bars represent the 95% confidence interval for n=3..... 88

Figure 47- Cure profile used to manufacture the laminates in this chapter. Note: Three laminates were manufactured at 69 kPa, 207 kPa, 345 kPa, and 483 kPa producing a total of 12 laminates. 94

Figure 48- Tensile test specimen geometry used to determine the effect of voids. 97

Figure 49- Effect of humidity environment and processing pressure on the formation of voids. Note: Error bars represent the 95% confidence interval for n=8. 99

Figure 50- Effect of cure pressure on the fiber volume content of the manufactured laminates. Note: Error bars represent the 95% confidence interval for n=8. 99

Figure 51- Tensile modulus of the specimen as void and laminate fiber volume content is increased. Note: Error bars represent the 95% confidence interval for n=16. 102

Figure 52- Tensile strength of the specimen as void and laminate fiber volume content is increased. Note: Error bars represent the 95% confidence interval for n=16. 103

Figure 53- Variation of the strength reduction coefficient as fiber volume content is changed. 103

Figure 54- SEM images taken at 75x that show the morphologies and locations of voids in specimen as fiber volume contents are increased. 104

Figure 55- Effect of increasing laminate fiber volume content on the aspect ratio of voids. Note: Error bars represent the 95% confidence interval for n=5. 104

Figure 56- The BACM process controllers' decision flow chart. 119

Figure 57- Free-body diagram of a cylindrical ring that is laterally compressed. 134

Figure 58- Free-body diagram of a curved beam subject to bending. 139

Figure 59- Error of using classical beam theory to calculate flexural strengths of curved beams of varying radius to depth ratios. 143

ABSTRACT

In the first part of the dissertation a new manufacturing method, Bladder Assisted Composite Manufacturing (BACM), to fabricate geometrically complex, hollow polymeric composite parts is presented. The BACM process utilizes a bladder to provide the necessary consolidation pressure and cures the part by circulating heated air inside the bladder. The feasibility of this manufacturing process is demonstrated by fabricating laminated composite cylinders using multiple numbers of plies, cure pressures, and mold configurations. Using the described process, a number of 2-, 4-, and 6-ply composite cylinders made of either Newport 321/7781 glass/epoxy or TenCate® EX-1522/plain weave carbon/epoxy prepregs were prepared as test samples. Cylinders were cured at the manufactures recommended cure temperatures and hold times using bladder pressures ranging from 207 kPa (30 psi) to 621 kPa (90 psi). The fiber volume fraction, void content, mechanical properties, and energy consumed during the curing of the composite cylinders, are investigated and compared to traditional manufacturing techniques. The fiber volume fraction and the void content of the cylinders were determined from resin burn-off experiments and density measurements. The mechanical responses of these cylinders were characterized by diametrically compressing sample rings and loading ring segments in three-point bending configuration. The fiber volume fractions of the cylinders were observed to be dependent on both the bladder pressure and mold configuration used, reaching a maximum of 66% for the cylinders made from the TenCate® material. The elastic moduli and failure strengths of the cylinders were found to increase with fiber volume fraction regardless of mold configuration used, reaching maximums of 61.5 GPa and 1272 MPa respectively for the TenCate® material. The void content was found to be dependent on mold configuration and was minimized

to 0.2%. Compared to conventional bladder manufacturing methods, the BACM process reduced the energy required to cure the cylinders by more than 50%.

The second part of the dissertation involves the development of new void formation and mechanical effect models. These models were developed by manufacturing eight-ply laminates from TenCate® BT-250/7781 prepreg at cure pressures ranging from 69 kPa (10 psi) to 483 kPa (70 psi) by hot-press. For each cure pressure, a laminate was fabricated from prepreg, which were direct from the bag and conditioned at 25%, and 99% relative humidity for 24hrs at 25°C. The manufactured laminates' void contents were found to vary from 1.6-5.0% depending on humidity environment and the applied cure pressure and were observed to approach an asymptotic value of approximately 1.6% as cure pressure was increased. The available predictive model for process-induced voids was not found to be capable of accounting for this. Therefore, the model was modified by the addition of a pressure reduction and asymptotic void content terms. The integration of these two terms resulted in a void formation model, which shows excellent agreement with experimental data. The experimental evidence indicates that the presence of voids only affects tensile strength significantly and the effect of voids on strength increases with fiber volume content. For example, the tensile strength of the laminates were found to decrease by 2.7%-23% for every 1% void content as the fiber volume content was increased from 45%-57%. This effect is explained by the voids becoming increasingly in contact with and elongated along the fibers as fiber volume content is increased. These findings resulted in a void effect model capable of accurately predicting the influence of voids as fiber volume content is varied.

NOMENCLATURE

A- Cross-sectional area of tensile specimen (mm^2)

A_v- Model fitting parameter (atm)

B- Empirical fitting parameter

B_v- Model fitting parameter (atm)

C_{sat}- Moisture concentration on void surface (g/mm^3)

D- Moisture diffusion coefficient (mm^2/h)

E- Elastic modulus (GPa)

F_{mass}- Fiber mass (g)

I- Moment of inertia (mm^4)

L- Support span (mm)

M_c- Moisture content of a prepreg at any time "t" (%)

M_{fiber}- Mass of fiber after burn-off (g)

M_{fluid}- Mass of solution in pycnometer (g)

M_{H2O}- Molecular weight of water (g/mol)

M_i- Initial moisture content of a prepreg (%)

M_m- Saturation moisture content of a prepreg (%)

$M_{specimen}$- Mass of composite specimen before burn-off (g)

OD- Outer diameter

P- Applied load (N)

P_{max}- Maximum applied load carried (N)

P_g- Pressure (atm)

P_R- Pressure reduction coefficient

R- Radius of cylinders (mm)

R_g- Ideal gas constant (mm^3/molK)

RH- Relative humidity (%)

S- Resin solubility coefficient (%)

S_{mass}- Specimen mass (g)

T- Temperature (K)

V_v- Volume % void content

V_{cup}- Volume of pycnometer (cm^3)

V_{fiber}- Volume % of fibers

V_{matrix}- Volume % of matrix

V_m- Characteristic volume element of a composite (mm^3)

V_{min}- Theoretical minimum obtainable void content (%)

Vol_{fiber}- Fiber volume (cm^3)

$Vol_{specimen}$- Specimen volume (cm^3)

W_{fiber}- Weight fraction of fiber reinforcement

W_{matrix}- Weight fraction of matrix

$\%W_{fiber}$- Weight % fiber reinforcement

$\%W_{matrix}$- Weight % matrix

b- Specimen width (mm)

d- Depth of beam (mm)

d_v- Final void diameter (mm)

h- Thickness of prepreg used for moisture uptake (mm)

m- Slope of the initial load-deflection curve (N/mm)

t- Time of moisture exposure (hr)

δ- Deflection (mm)

$\Delta\sigma_T$- Difference between two tensile stress values (MPa)

$\Delta\varepsilon$- Difference between two tensile strain values (%)

ρ_{fiber}- Density fiber reinforcement (g/cm^3)

ρ_{matrix}- Density matrix (g/cm^3)

$\rho_{specimen}$- Measured density of composite specimen (g/cm^3)

σ_f- Flexural failure stress (MPa)

$\sigma_{f0\%}$- Strength of composite material with 0% void content (MPa)

σ_T- Tensile failure stress (MPa)

1. INTRODUCTION

1.1 COMPOSITE MANUFACTURING TECHNIQUES

The manufacturing of high quality, geometrically complex, hollow parts made of composite materials has presented significant challenges. Injection and compression molding of short fiber reinforced parts is currently the most economical and obvious choice for the fabrication of geometrically complex parts [1]. However, parts manufactured using these techniques suffer from a decrease in mechanical performance when compared to parts with continuous fiber reinforcement. As a result, in industries, such as defense and aerospace where the strength/weight ratio is important, continuous fiber reinforced composite materials are often used. Currently, pultrusion and filament winding are the two most commonly used processes to create hollow, structural composite components that contain continuous fiber reinforcement. However, despite achieving good surface quality, low microstructural defects and excellent structural performance, composite parts fabricated using these processes are generally axis-symmetric with limited geometric complexity and have uniform wall thicknesses [2, 3].

To address the shortcomings of filament winding and pultrusion, the composites industry has used variations of bladder molding to fabricate hollow composite parts with increased geometric complexity, non axis-symmetric shapes, and varying wall thicknesses. In conventional bladder molding, an inflatable mandrel (bladder) presses a composite material against a female metallic mold, which is subsequently heated in an oven or autoclave to process the part. This technique has been used with manufacturing techniques such as resin transfer molding (RTM) successfully [4, 5]. Lehmann and

Michaeli [4] produced hollow composite components using a braided tube preform and RTM/bladder molding, and found several processing difficulties. Specifically, the obtainable fiber volume fractions were limited by the permeability of the preform, which was governed by bladder pressure. As a result, the use of prepregs may be desirable in bladder molding, as resin infusion would not be affected by bladder pressure, and thus would allow higher fiber volume fractions to be obtained. Bladder molding has been used as well for both thermoplastic and thermoset prepregs [6, 7]. Salomi et al. [6] fabricated hollow composite components from a thermoplastic prepreg using bladder molding in an oven. It was reported that for all parts produced, the void contents remained below 5% and the fiber mass fraction remained within ±0.5% of the average value of 60.9% [6]. Parts such as "bubble" golf shafts, composite bicycle frames, bicycle stems and composite propeller blades are examples of parts that have been produced using conventional bladder molding [5, 8-10].

Generally, in an oven/autoclave, heat is transferred by convection to a conductive mold as well as the tooling or bagging placed around the part, which in turn, transfers the heat to the part to facilitate curing. As a result, a large amount of energy is expended in heating both the air inside the oven/autoclave, tooling, and the part, which increases operating costs. In addition, the thermal inertia of the curing system used can limit the achievable heating/cooling rates, resulting in prolonged process cycles. Additionally, the heating rate must often be maintained between 1-4°C min^{-1} to avoid a runaway increase in laminate temperature caused by the exothermic reaction of the matrix system [11]. Because of the large capital investment required and the disadvantages discussed

above, the use of an autoclave based process generally results in higher part production costs when compared to out-of-autoclave processes [1].

Finding a replacement for the autoclave curing process capable of producing comparable part quality has been actively pursued due to the disadvantages outlined above. The Quickstep™ process is to date one of the most successful out-of-autoclave processes developed that produces parts with comparable quality to autoclave cured laminates. The Quickstep™ process functions by curing a composite component between two fluid filled pressure membranes which heat the mold/part [12]. Due to the way in which the part is heated, the heating rate can be increased beyond the typical rate for autoclave processed parts. In fact, Davies et al. [11] showed the Quickstep™ process can use heating rates as high as 10°C min^{-1} to cure composite components with void contents below 2%. They also found that the process could produce parts with fiber fractions as high as 60.2% with flexural and interlaminar shear strengths comparable to autoclave processed parts [11]. Additionally, due to the decrease in manufacturing time this process serves to increase production rates, resulting in a reduction of per part cost [13]. The Quickstep™ process solves the thermal inertia and exothermic heating problems associated with the autoclave. However, the required capital investment remains high and a large amount of energy is expended in heating the fluid chambers.

1.2 VOID FORMATION IN COMPOSITES

Voids are one of the most common defects in composite laminates and are known to degrade there performance considerably [14-16]. As a result, the void content of a laminate is often used to assess its quality, and thus, to determine if it is acceptable for a

particular application. Experimental studies available in literature have attempted to address the cause of void formation in composite laminates and have primarily focused on either the effect of curing pressure or moisture content [17-23]. Boey and Lye [17] for example examined the effect of processing pressure on the formation of voids in laminates laid-up from a glass/epoxy prepreg and manufactured by the autoclave process. They found that as the autoclave pressure was increased from 100 kPa to 400 kPa void content dropped marginally from 38% to 35% [17]. They believed the marginal decrease in void content indicated that in this pressure range the internal pressure of the voids, caused by vaporized moisture, reached equilibrium with the resin pressure. Thus, as pressure was continued to be increased from 400 kPa to 1100 kPa the void content dropped to below 3% [17]. Following the previous work, Grunenfelder and Nutt [21] explored how moisture dissolved in the resin, caused by humidity exposure, would affect the formation of voids in prepreg laminates manufactured by both the vacuum-bag-only (VBO) and autoclave processes. They found, that the void contents in the VBO laminates, which were manufactured at atmospheric pressure (101 kPa), would increase parabolically with the relative humidity level at manufacturing while the autoclave laminates' void contents remained approximately zero regardless of the relative humidity exposure [21]. The dissimilar behavior of the two processes with relative humidity was explained by the higher pressure in which the autoclave operates (609 kPa) which caused the moisture to remain in solution during manufacturing preventing the formation and expansion of voids [21].

Upon reviewing the models available in literature which attempt to explain void formation, one finds that they are predominantly centered around a diffusion-based void

growth model proposed by Kardos et al. which predicts final average void diameter [18, 22]. According to this model, voids are spherical and formed due to the moisture in the resin diffusing to air voids, vaporizing and pressurizing the voids in the resin. As a result, voids are predicted to grow until the internal void pressure becomes equal to that of the surrounding resin. Therefore, according to Kardos et al. [18, 22], the final average diameter of a void present in the resin is a function of the resins' moisture content, temperature profile, process time, and pressure profile. As an extension to the Kardos model, Boey and Lye [17] suggested that by calculating the volume of the predicted void and using a characteristic volume element, the void content of any particular laminate could be determined provided the processing conditions are known. This approach was used successfully by Grunenfelder and Nutt [21] for laminates manufactured by vacuum bag only (VBO) prepregs which were processed at different initial moisture contents and constant processing pressure. However, this approach is unproven when the laminates are manufactured using different processing pressures.

1.3 VOIDS EFFECTS ON THE MECHANICAL PROPERTIES OF COMPOSITE LAMINATES

Voids are one of the most common manufacturing defects in composite materials and are known to adversely affect the mechanical properties of composite laminates [19, 24, 25]. This affect is believed to be caused by the presence of voids on the fiber-matrix interface which limits the ability of the matrix to transfer applied loads to the fiber reinforcement, and acts as crack initiation planes [17, 26, 27]. In general, the in-plane elastic modulus is reported to be minimally affected because it is primarily dependent on the fiber property [28-30]. However, the failure strength of a composite can be

significantly affected. For example, Judd and Wright [14] surveyed twenty-four articles and concluded that for each volume percent of voids the flexural, tensile, compressive, and interlaminar shear strengths will be reduced by at least 3% or as much as 20%. As a result, the void content of a laminate is often used to assess its quality, and thus, to determine if it is acceptable for a particular application. Because of the wide ranging effects of voids the aerospace industry's current rule of thumb is to accept structural composite components that contain less than 1% voids and nonstructural components with less than 5% [17, 19, 31, 32].

Studies available in literature to distinguish the effect of voids on the various failure strengths of composite materials have typically focused on void content and have assumed the effect of fiber volume content to be insignificant [15, 19, 24, 25, 31-35]. For example, Almeida and Neto [31] examined the effect of voids on the flexural strength of woven carbon/epoxy laminates. Four laminates were manufactured with void contents ranging from 1% to 6% while maintaining a fiber volume fraction of approximately 61%. After testing, the laminates flexural strengths were found to be reduced by as much as 16% at a void content of 6%. They suggested this reduction was caused by matrix fractures occurring at voids lying on the fiber-matrix interface [31]. In addition, they proposed a critical void content of 3% exists which must be surpassed before voids will begin to have an effect on the strength of a composite component. Following this work, Chambers et al. [15] examined the effect of voids on the flexural strength of unidirectional carbon fiber laminates by manufacturing laminates at five vacuum levels producing laminates with void contents ranging from 2% to 3%. The flexural strengths of these laminates were reduced by as much as 20% at the highest

void content which conflicted directly with the results of Almeida and Neto [31]. They therefore concluded the critical void content concept put forth by Almeida and Neto [31] was too simplistic and that void morphology most likely drives the reduction in flexural strength [15, 36].

A study by Wisnom et al. [36] examined the effect of void aspect ratio on the interlaminar shear strength (ILSS) of carbon/epoxy laminates. They varied the void aspect ratio of the laminates from 1-4 by embedding PTFE monofilaments of various lengths while maintaining a constant fiber volume fraction. Subsequent, flexural testing of these laminates showed their ILSS was reduced by 25% as void aspect ratio was increased. This result raises the question as to what governs the void aspect ratio of manufactured composite laminates. The author believes the answer to this question is the final fiber volume fraction of the laminate. However, upon review of literature, little work has been done relating the effect of fiber volume fraction on the observed void aspect ratios and their effect on composite laminates.

2. PROPERTIES OF COMPOSITE CYLINDERS FABRICATED BY BLADDER ASSISTED COMPOSITE MANUFACTURING (BACM)

2.1 INTRODUCTION

The ability to manufacture high quality hollow composite parts, which are geometrically complex and have superior mechanical properties, has presented significant challenges. Currently, the injection and compression molding of short fiber reinforced parts is the most economical choice to fabricate geometrically complex components [1]. However, the parts manufactured using these techniques often suffer from a decrease in mechanical performance when compared to parts with continuous fiber reinforcement. As a result, when the strength/weight ratio is important, continuous fiber reinforced composite materials are often used. The most common techniques currently in use to create continuously reinforced hollow, structural composite components is pultrusion and filament winding. However, these techniques are generally only able to produce components with limited geometric complexity [2, 3].

In order to produce parts with increased geometric complexity, the composite industry has investigated bladder molding. In conventional bladder molding, a bladder presses a composite material against a female metallic mold, which is subsequently heated in an oven or autoclave to process the part. This technique has been used with manufacturing techniques such as resin transfer molding (RTM) successfully [4, 5]. Lehmann and Michaeli [4] produced hollow composite components using fiber preforms and RTM/bladder molding, and encountered several processing difficulties. First, the resin injection pressure cannot be more than 0.2 MPa greater than the bladder pressure or the

bladder will collapse. Second, the obtainable fiber volume contents are limited by the permeability of the fiber preform, which is governed by the applied bladder pressure. As a result, the use of prepregs may be desirable in bladder molding, as resin infusion would not be affected by bladder pressure, and thus would allow higher fiber volume fractions to be obtained. Salomi et al. [6] fabricated hollow composite components from a thermoplastic prepreg using bladder molding in an oven. It was reported that as processing temperature and pressure was increased from 185°C-215°C and 0.03 MPa-0.05 MPa, respectively, the void content of the components decreased from 4.16% to 1.97%. Ref. [6] attributed the effect of temperature and pressure to the lower viscosity of the thermoplastic matrix at elevated temperatures and improved impregnation of the fiber reinforcement.

High-performance composite components are generally manufactured using prepregs with a thermoset matrix due to their greater stiffness and dimensional stability. These components are typically manufactured in an oven/autoclave, where heat is transferred by convection to a conductive mold as well as the tooling or bagging placed around the part, which in turn, transfers the heat to the part to facilitate curing. As a result, manufacturing hollow shapes is difficult and a large amount of energy is expended in heating both the air inside the oven/autoclave, tooling, and the part, which increases operating costs. In addition, the thermal inertia of the curing system used can limit the achievable heating/cooling rates, resulting in prolonged process cycles. Additionally, the heating rate must often be maintained between 1-4°C min^{-1} to avoid a runaway increase in laminate temperature caused by the exothermic reaction of the matrix system [11]. Because of the large capital investment required and the disadvantages discussed

above, the use of an autoclave based process generally results in higher part production costs when compared to out-of-autoclave processes [1].

Finding a replacement for the autoclave curing process capable of producing comparable part quality has been actively pursued due to the disadvantages outlined in the preceding paragraph. The Quickstep^{TM} process is currently one of the most successful out-of-autoclave processes developed. The Quickstep^{TM} process functions by curing a composite component between two fluid filled pressure membranes which heat the mold/part [12]. Due to the heating dynamics, the heating rate can be increased beyond the typical rate for autoclave processed parts. In fact, Davies et al. [11] showed the Quickstep^{TM} process can use heating rates as high as 10°C min^{-1} to cure composite laminates with void contents less than 2% which is statistically identical to the same laminates manufactured by autoclave. In addition, the Quickstep^{TM} processed laminates obtained fiber volume contents within 4% of the autoclave (60.2% vs. 64.1%) and with a flexure strength of 1755 MPa, which is only 168 MPa less than that of the autoclave processed, laminate (1923 MPa). Additionally, due to the decrease in manufacturing time this process serves to increase production rates, resulting in a reduction of per part cost [13]. The Quickstep^{TM} process solves the thermal inertia and exothermic heating problems associated with the autoclave. However, the required capital investment remains high, a large amount of energy is expended in heating the fluid chambers, and manufacturing hollow composite structures remains difficult.

The bladder molding technique introduced in this chapter, Bladder Assisted Composite Manufacturing (BACM) eliminates the conventional external heating of the tooling/mold in an oven or autoclave by moving the heating to the inside of the

mold/part. Due to the change in heating dynamics, the temperature of the composite part is controlled accurately by circulating and venting air inside the bladder, thus improving the process quality. The heating and cooling rates can also be increased, resulting in a reduction in the required cycle time. Because of the change in heating source and location, the mold material is no longer required to be conductive which results in several advantages. Particularly, direct internal heating yields efficient energy utilization and allows for the use of nontraditional, cost effective mold materials with low thermal conductivity.

The aim of this chapter is first to introduce and assess the feasibility of the BACM process in manufacturing high-quality composites in a cost effective manner. This was achieved by producing a number of composite cylinders using processing pressures of 207 kPa (30 psi), 345 kPa (50 psi), 483 kPa (70 psi), and 621 kPa (90 psi). The elastic moduli, failure strength, and void content of the cylinders produced were compared to laminates fabricated using hot press molding at similar consolidation pressures. Additionally, the energy consumption of BACM is compared to that of a conventional bladder molding technique.

2.2 MATERIALS AND EXPERIMENTAL PROCEDURE

2.2.1 GEOMETRY AND MATERIALS USED

Cylindrical samples (D=50.8mm and L=101.6mm) were made using Newport® 321/7781 prepreg. This prepreg is composed of an eight-harness woven E-glass fabric with a 121°C cure epoxy system. The epoxy system used is toughened and has a glass transition temperature of 149°C [37]. Tomblin et al. [37] processed the material in a

vacuum bag with an absolute pressure of 76 kPa producing laminates with a nominal fiber volume fraction of 46% and elastic modulus of 27.5 GPa. As a result of its desirable properties, the material is currently in use in general aviation aircraft [38].

2.2.2 SAMPLE FABRICATION PROCESS

Two separate methods were used to fabricate the cylinders in this chapter. The first was the conventional bladder molding technique, which used an oven to heat an uninsulated aluminum mold externally. The air inside the bladder was not heated but was pressurized to provide the consolidation pressure during curing. Five cylinders were fabricated using this method while recording the energy consumption for each cycle. The goal was to obtain the average energy consumption per cure cycle when curing is performed via an external heating source. Later the energy requirements of conventional bladder manufacturing molding and the newly developed BACM process are compared.

The second curing method, the BACM process, utilized a bladder, heating/cooling module, and a thermally insulated mold made of aluminum. Eager Plastics P50 RTV silicon, which has a maximum operating temperature of 343°C, was used to produce the bladders used during curing of the composite cylinders. The cylindrical bladders had an outer diameter of 47.6mm and length of 203.2mm. The heating/cooling module was composed of a heating element inside the bladder and an air-pressure regulation system. The heating element used was a 450W cartridge heater with a maximum operating temperature of 870°C. Heaters such as these are commonly used in the hot runners of injection molds. An air regulator and an electronic air valve, which intermittently vented air to reduce laminate temperature gradient, controlled the air pressure and flow inside the bladder (a more thorough explanation of the BACM cycle controller may be

found in Appendix A). It should be noted that the mold was insulated to increase the energy efficiency of the BACM process by minimizing the heat loss to the environment. The optimal thickness of the mold walls and the insulation may likely depend on the part geometry and the cure cycle. The aluminum mold was insulated by incasing it in 20mm of gypsum (plaster of paris) which has a thermal conductivity of 0.6 W/m-°C [39]. The resulting mold assembly was composed of two layers: an outer minimally conductive gypsum casing and an inner aluminum shell (6.4mm thick) which formed the mold cavity. In Figure 1, a schematic representation of the bladder, heating/cooling module, and mold assembly is shown and in Figure 2, one mold half along with the heating/cooling module is shown.

A number of 101.6mm long composite cylinders with 2-, 4-, and 6-plies were manufactured with bladder pressures of 207 kPa (30 psi), 345 kPa (50 psi), 483 kPa (70 psi), and 621 kPa (90 psi). The cylinders were laid-up by wrapping a single piece of prepreg material around an aluminum mandrel 2, 4, or 6 times depending on the required number of plies, while allowing for an overlap of 6.4mm at the seam of the cylinders. One thermocouple was placed in the center of the laminates at each end of the cylinders during layup for process control purposes. The process of curing the parts consisted of placing and centering the layup on the bladder, placing the bladder-layup assembly into the mold, pressurizing the bladder, and performing the cure cycle. The cylinders were cured using a cure cycle consisting of a 1°C/min ramp from 25°C to 121°C where they were held for two hours before being cooled to 60°C and removed from the mold. Two cylinders were fabricated for each of the pressure/ply combinations resulting in the production of 24 cylinders. A power meter measured the

total energy consumed during the manufacturing of each of the cylinders. A typical BACM cure cycle is shown in Figure 3. It is evident from Figure 3 that the temperature lag between the set point and the composite part is minimal and that the temperature difference at both ends of the laminate remains less than 3.1°C. The bladder pressure was maintained constant at one of the four processing pressures, 621 kPa in this case, throughout the cure cycles. The average deviation from the set-point temperature for the complete cure cycle was 3°C with a maximum deviation of 5°C, which indicates a thermally stable cure process. A number of small variations in pressure seen in Figure 3 were due to venting heated air to minimize the temperature gradient across the laminate.

In addition to the BACM process, 4-ply flat composite plates were fabricated using the same cure cycle in a hot press. In this case, compressive forces of 4800 N, 8000 N, 11200 N, and 14000 N were used to produce four 152mm x 152mm laminates. The compressive forces used resulted in the laminates experiencing consolidation pressures equivalent to the bladder pressures used in fabricating the cylinders. The properties of these flat laminates establish baseline values, which could be used to compare the properties of the cylinders produced by BACM. These comparisons are expected to help assess the quality of the composite cylinders and thus validate the viability of the BACM process. The bladder pressure maintained during the cure cycle and the cure pressure applied during hot pressing will be referred to as processing pressure while comparing the properties of the composite samples.

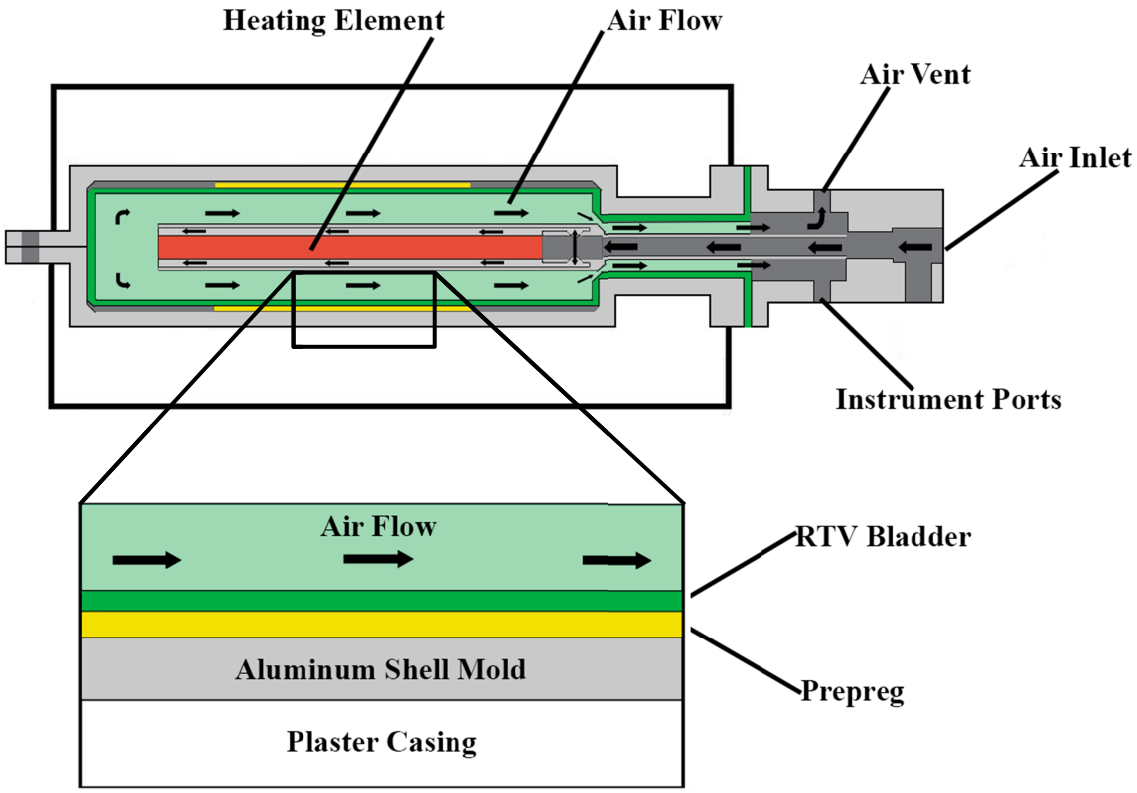

Figure 1- Mold assembly, heating element and bladder used to fabricate composite cylinders.

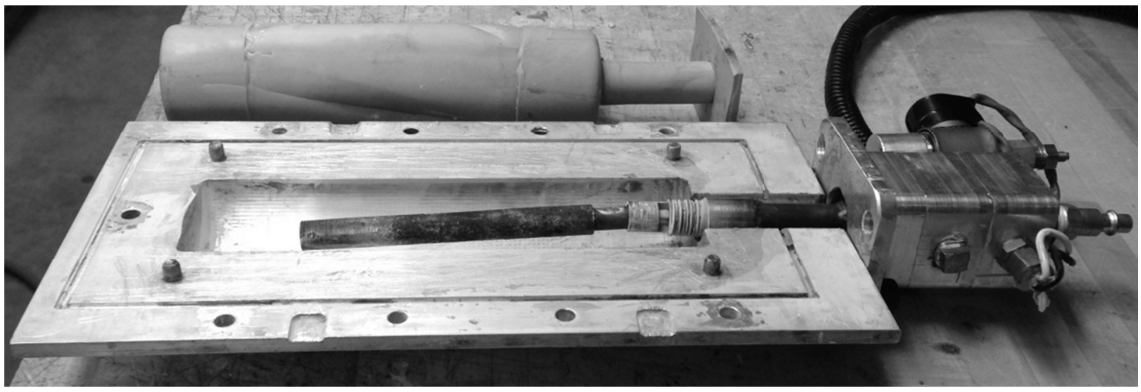

Figure 2- BACM mold half with the heating/cooling manifold attached.

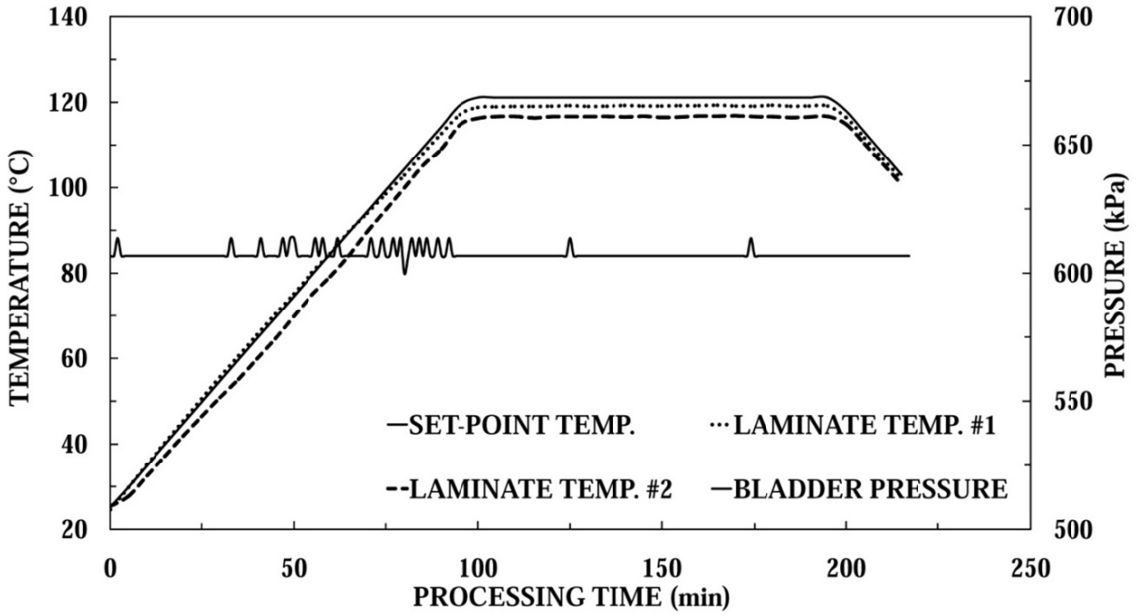

Figure 3- Typical BACM cure cycle showing process temperature and pressure.

2.2.3 VOID ANALYSIS PROCEDURE

Comparing void contents would be useful in assessing the quality of the cylinders and flat laminates produced. Several methods such as water absorption, microscopy, ultrasonic C scan, radiography, and density are available to determine the void fraction of composite products [14]. By measuring the density of the composite, its void content can be determined without requiring sophisticated equipment. Void contents of the composite samples can be accurately determined using this technique if the density values of the bulk composite and its constituents can be accurately measured. By suspending the composite and the resin samples in a liquid medium, their densities can be determined within ±0.001 g/cm^3.

The density of the bulk composite specimens were determined by reducing the density of Cargill Labs 2.49 g/cm^3 Heavy Liquid by slowly adding water to the liquid until the specimens were suspended in the solution. Once a specimen was suspended, the solution density was determined using a pycnometer. Similarly, the resin density (1.224

g/cc) was determined by suspending multiple bubble free specimens in a water/glycol solution. These resin samples were obtained from the cured epoxy, which was squeezed out of the composite parts during the cure. A schematic representation of the procedure is shown in Figure 4. The density of the fiber reinforcement (2.635 g/cc) was determined using a helium pycnometer. The weight fraction of both the fiber reinforcement and matrix was determined by removing the matrix using the burn-off technique recommended by ASTM D2584-08. Using the weight fractions and density measurements, the void content of the specimens were calculated from Eq. (1) as recommended by ASTM D2734-09,

$$V_v = 100 - \rho_{specimen}\left(\frac{W_{fiber}}{\rho_{fiber}} + \frac{W_{matrix}}{\rho_{matrix}}\right) \quad (1)$$

By using the outlined procedure, the void content was resolved within ±0.22% (refer to Appendix B for detailed analysis). This level of accuracy indicates the suspension/burn-off method is useful even for composite laminates with void contents below 1%.

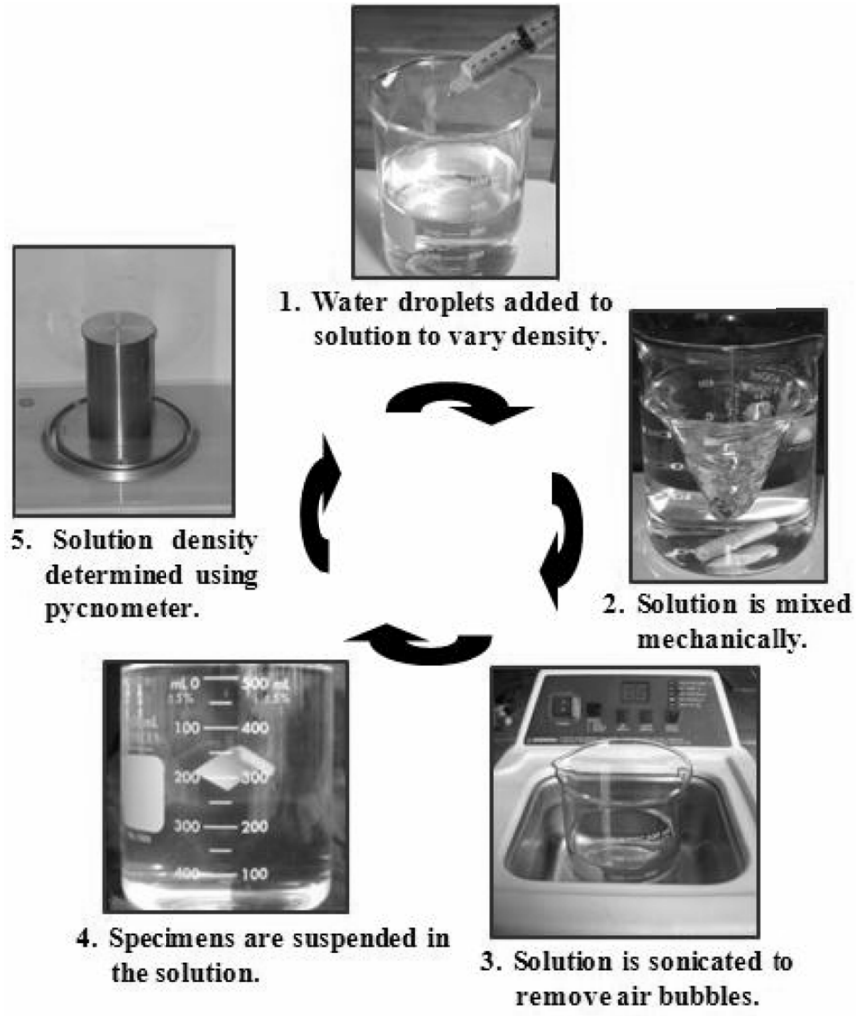

Figure 4- Procedure used for the determination of the bulk composite and epoxy resin densities.

2.2.4 MECHANICAL TESTING

To demonstrate the quality of the hollow parts made by the BACM process, flexural modulus and strength of the composite cylinders and hot pressed laminates were determined. Six 12.7mm (0.5") wide ring specimens from the center of each cylinder were obtained with the fibers oriented longitudinally and around the circumference of the cylinder resulting in twelve ring specimens for each of the pressure/ply combinations. Three rings from each cylinder were quartered producing 24 ring segments for each of the pressure/ply combinations. In addition to the cylinder

specimens, 10 flat 50.8mm x 12.7mm (2" x 0.5") specimens were cut from each of the four hot pressed laminates. Thickness and width measurements were taken of all specimens tested and used in the determination of flexural properties. In Figure 5, a diagram of the test specimens are shown. Figure 6 displays an example of the cylinders produced and the specimens used for testing.

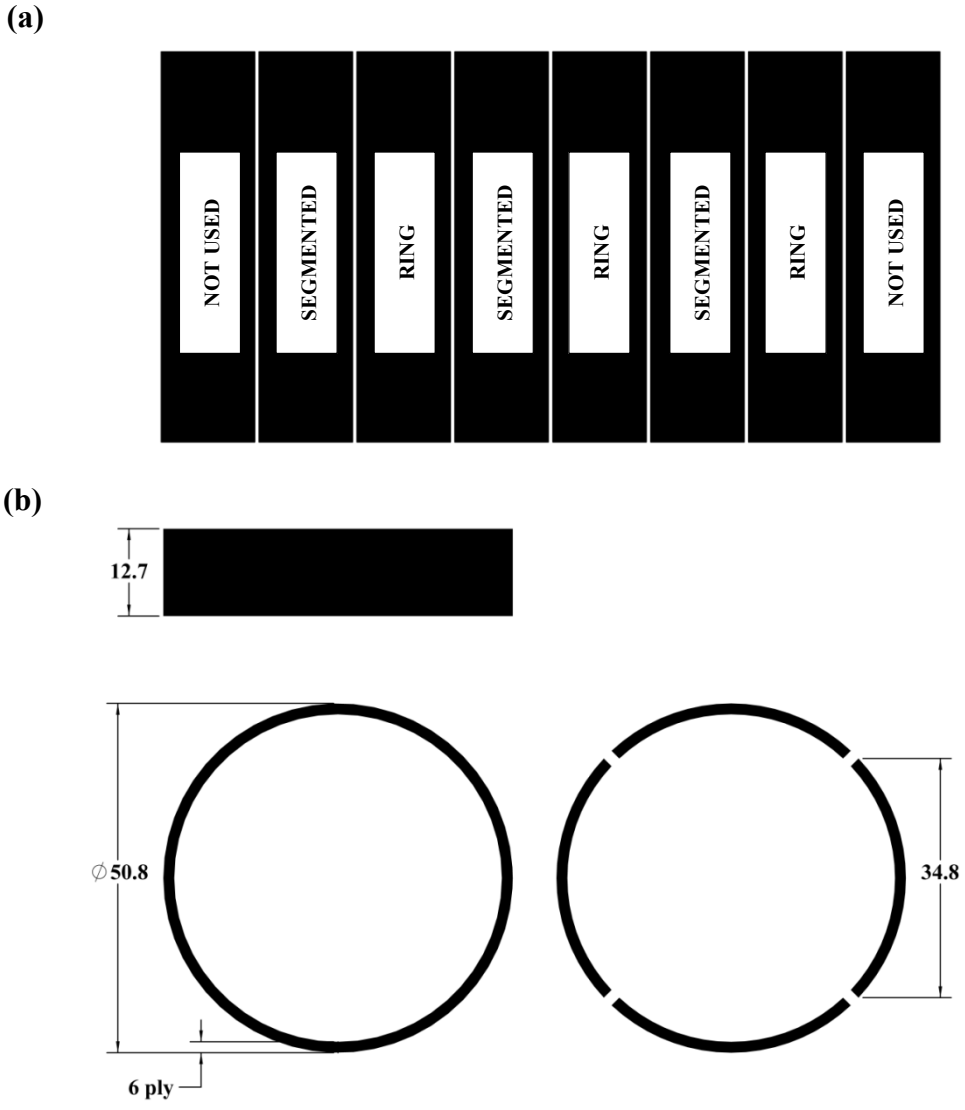

Figure 5- Diagram of (a) how the manufactured cylinders rings were cut and (b) how these rings were further processed (if necessary) to create the required test specimen. Note: All the listed dimensions are in millimeters.

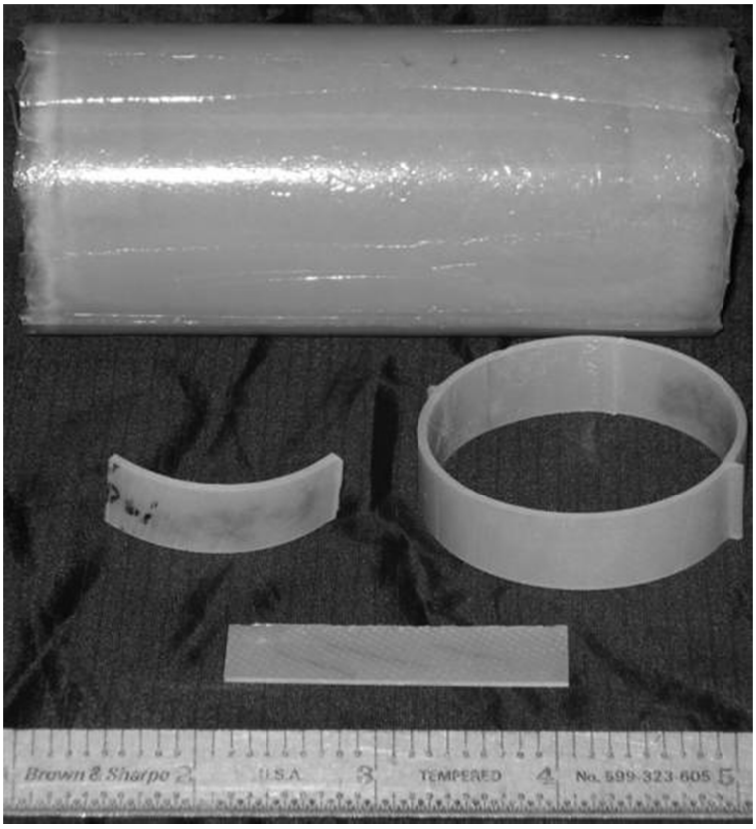

Figure 6- A 50.8mm composite cylinder fabricated by the BACM method. A 12.7mm wide ring, ring segment, and a flat test specimen obtained from a hot pressed laminate are shown in the figure.

2.2.4.1 Cylinders

The elastic moduli of the rings were found by laterally compressing them between two flat platens using a Com-Ten® 705TN testing system. For quasi-static loading as in Ref. [40], the rings were compressed between two parallel platens at a rate of 2mm/min. The rings were compressed to 10% (5.08mm) of their original diameter at which point the test was terminated. Six specimens were tested for each of the pressure/ply combinations using this procedure. The elastic moduli of the rings were determined as recommended by ASTM D2412-10a at a deflection of 2.50mm using Eq. (2). A typical load-deflection diagram of the ring samples in this dissertation is shown in Figure 7.

$$E = \frac{0.149PR^3}{I\delta}\left[1 + \frac{\delta}{4R}\right]^3 \quad (2)$$

Because of the nonlinear behavior of the composite rings used to determine the cylinders elastic moduli as shown in Figure 7, the flexural strength of the BACM processed laminates were determined by testing quarter ring segments in three-point bending using a Com-Ten® 705TN testing system as described in Ref. [41]. The support span for all tests was set at 25.4mm resulting in span to depth ratios that varied from 18 to 60 and were contingent on ply number and processing pressure. The specimens were placed concave side down on support pins to reduce the effect of geometric nonlinearities [42]. The ring segments were loaded at a rate of 2mm/min until an outer surface rupture occurred. This procedure was used to test twenty-four ring segment specimens from each pressure/ply combination. The high thickness to radius ratios for the ring segments ensured that the flexural strength of the samples can be obtained without accounting for sample curvature (for further discussion refer to Appendix C) [43]. Therefore, the flexural strengths of the BACM processed ring segments were found using simple beam theory as outlined in Section 2.2.4.2.

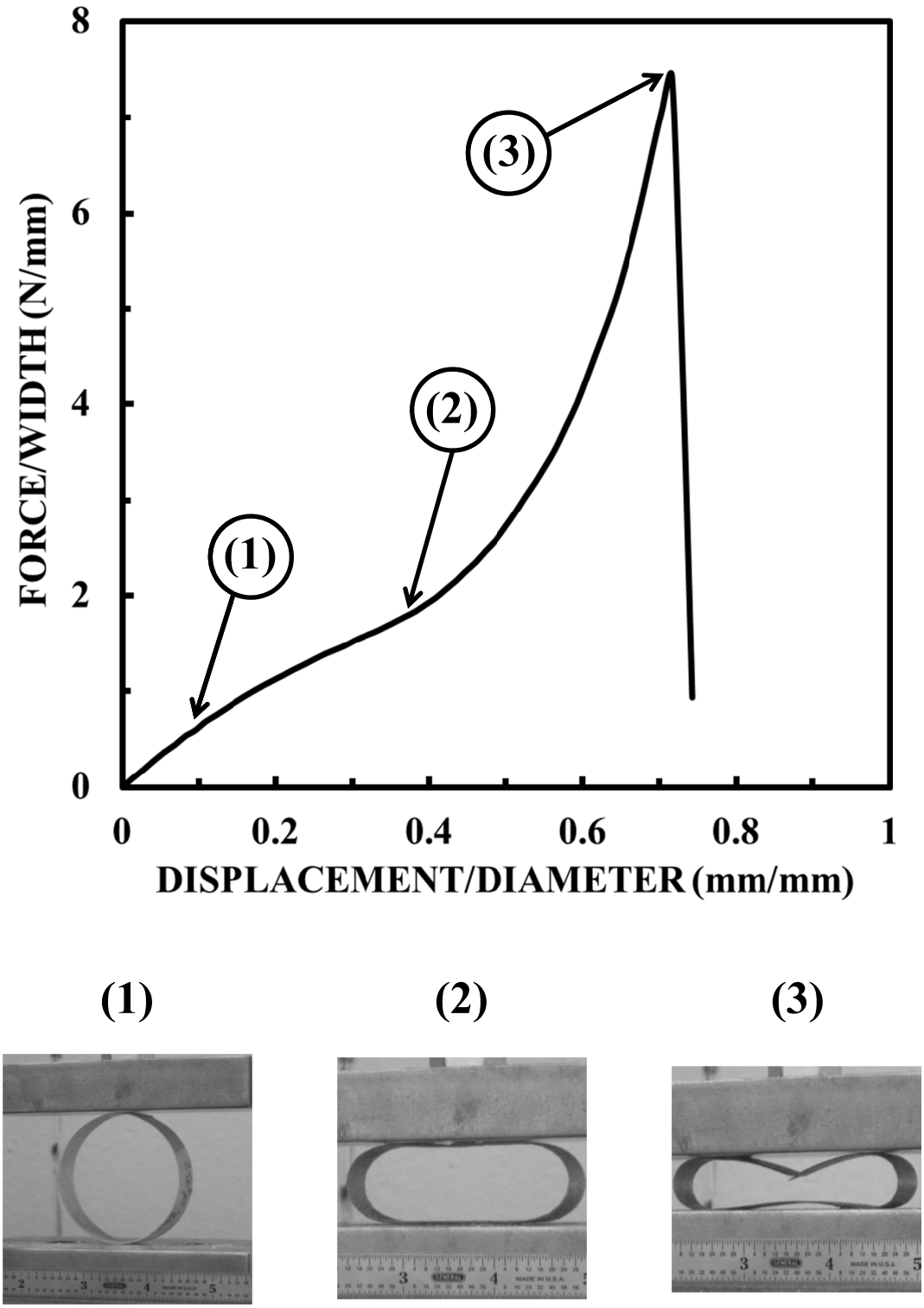

Figure 7- Typical load-deflection behavior of the composite rings during testing.

2.2.4.2 Flat Laminates

The flexural properties of the flat laminates and quarter ring segments were determined by testing specimens in three-point bending. The support spans for all the tests were chosen such that a 16:1 or greater span to depth ratio was obtained. The specimens were then loaded at a rate of 2mm/min until failure occurred. Five specimens from each of the four hot pressed laminates were tested. The elastic modulus and stress at failure were found using Eq.'s (3) and (4) respectively as recommended by ASTM D790-10. A typical stress-strain diagram of the curved flexure samples in this chapter is shown in Figure 8.

$$E = \frac{L^3 m}{4bd^3} \tag{3}$$

$$\sigma_f = \frac{3PL}{2bd^2} \tag{4}$$

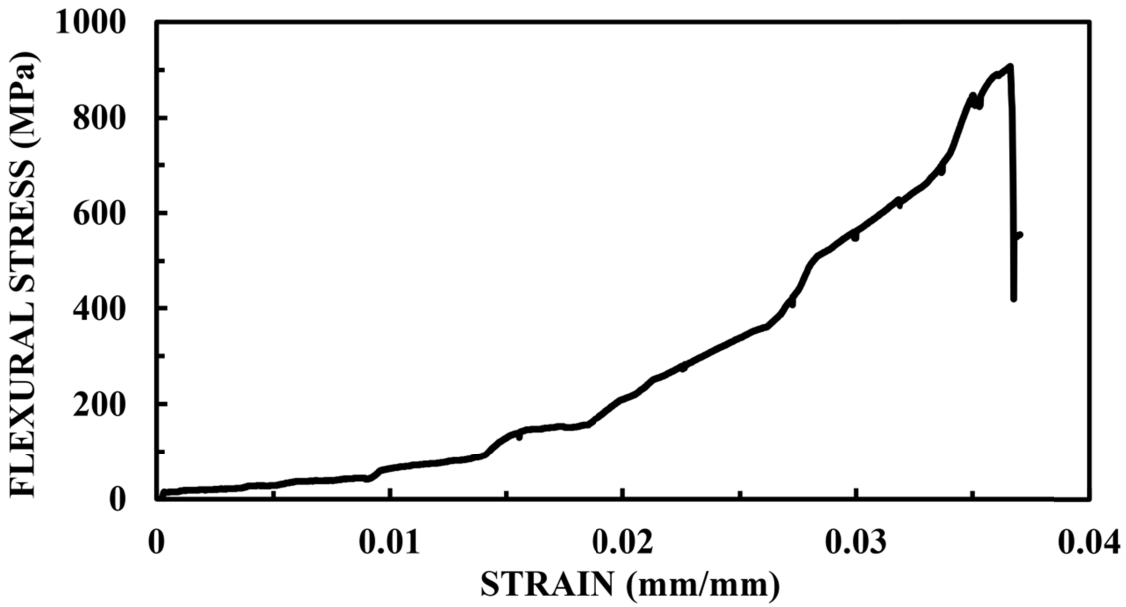

Figure 8- Typical stress-strain behavior of the curved flexure samples during testing.

2.3 RESULTS AND DISCUSSION

2.3.1 ENERGY CONSUMPTION

In the current manufacturing atmosphere, where the environmental effect of manufacturing are under increasing scrutiny, companies are progressively looking to introduce green manufacturing processes [44]. These manufacturing processes tend to focus on reducing both energy consumption and operational wastes. In addition to lessening environmental impact, a reduction in energy use can have the effect of reducing operational costs. Figure 9 compares the energy consumption of a bladder assisted manufacturing process that utilizes an external heat source (i.e., placing the uninsulated mold assembly in an oven of appropriate size for cure) with that of BACM using an internal heating module for cure. It is shown that the energy consumed during the processing of cylinders using the same cure cycle was reduced by approximately 50% (from 1.09 kW-h to 0.56 kW-h). As a result, the BACM process would be a cost effective manufacturing process if the laminate quality and mechanical properties could be shown as equivalent to a commonly used manufacturing process such as hot press molding.

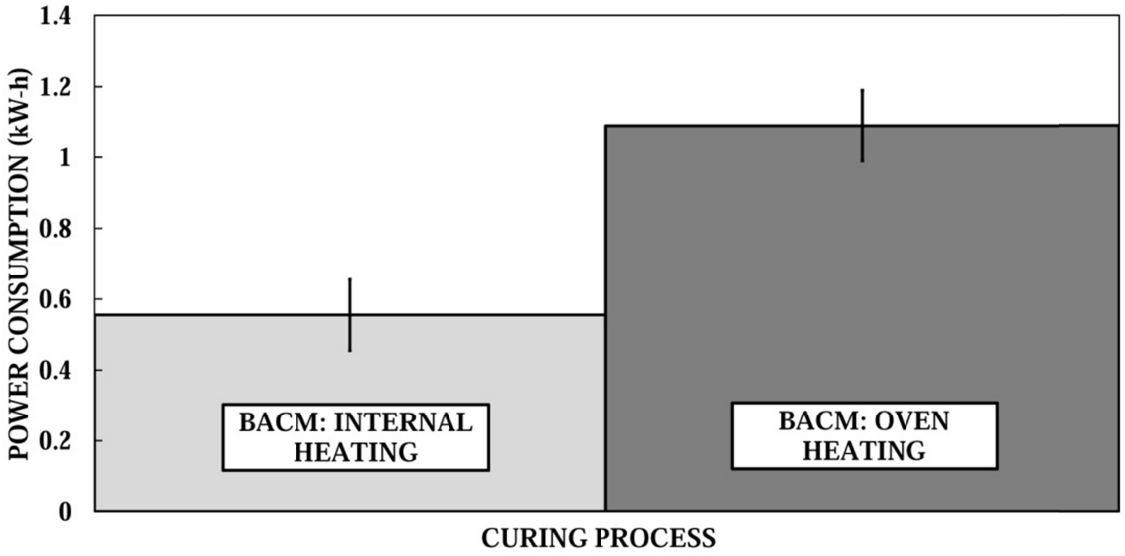

Figure 9- Comparison of BACM and Oven Heating energy consumption during the processing of composite cylinders. Note: Error bars represent the 95% confidence interval for n=5.

2.3.2 PROCESSING PRESSURE EFFECT

If a composite part is cured at higher pressure, the fiber volume fraction is expected to increase, as more resin is likely to be squeezed out during cure. Thus, the composite parts cured under increased processing pressure will likely approach a theoretical maximum fiber volume fraction as determined by packing factor or the weave pattern of the prepreg. Obviously, if the resin flow is restricted during cure, the increase in fiber volume fraction may not materialize as expected. Figure 10 illustrates the effect of pressure on the fiber volume fractions obtained from both BACM and hot press cured parts. From the figure, the dependence of fiber volume fraction on the applied pressure is clearly observed. In addition, the numbers of plies present in the laminate were not found to affect the final fiber volume fraction significantly. Also note that as the processing pressure is increased the fiber volume fractions of both the BACM and hot pressed parts increase at approximately the same rate until 621 kPa. At 621 kPa, the fiber volume fraction of the BACM parts began to reduce while the hot pressed parts

continued to increase. The BACM process displays one of its unique attributes in this result. As processing pressure is increased, a critical point is reached in which the RTV silicon bladder begins to restrict resin flow and eventually seal both ends of the cylindrical part causing the fiber volume fraction to become reduced at elevated pressures. The seal point will vary with composite thickness and appears to be located between 483 kPa and 621 kPa for the cylinders produced. The sealing of the part by the bladder would most likely result in an increase in the hydrostatic pressure of the resin. Several studies have examined the effect of resin pressure on void fractions and have concluded that increases in resin pressure will serve to decrease the void fractions of parts produced [18, 22, 45, 46].

In addition to the macroscale effect of processing pressure on fiber volume fraction, the spatial variations of fiber volume fraction throughout the parts produced are of interest as well. Such variations are, in most cases, undesirable and may lead to unexpected variations of properties within a composite product. Hence, the variation of fiber volume fraction inside produced parts must be minimized. The fiber volume fraction in the laminates produced using the hot press was found to vary by no more than ±0.63% of the average value of 58%. A nominal variation comparable to that of hot pressed specimens was needed in order for the BACM process to be considered viable. Spatial variation of the BACM processed cylinders are shown in Figure 11. As expected, the fiber volume fraction for each of the cylinders increases with pressure, reaching the maximum average value of 55.5% at 483 kPa and then regresses slightly to 54.9% at 621 kPa. The average fiber content of all cylinders was determined to be 53.4%, a small reduction compared to the 58% reported for the hot pressed laminates. Despite

this slight reduction, the spatial variation of the fiber volume fraction for the cylinders was minimal for all pressure levels as depicted in Figure 11. The maximum variation was limited to ±0.61% for the BACM processed cylinders, which was slightly less than the variation observed in the hot pressed parts. Using the rule of mixtures, the fiber fraction variations found in both processes equate to a change in the elastic modulus by approximately 1%. Clearly, this low level of spatial inhomogeneity is inherent in most material systems and does not adversely affect the actual design and use of composite products. From this viewpoint, one can conclude that the BACM process introduced in this chapter is capable of producing macroscopically homogeneous, hollow composite products.

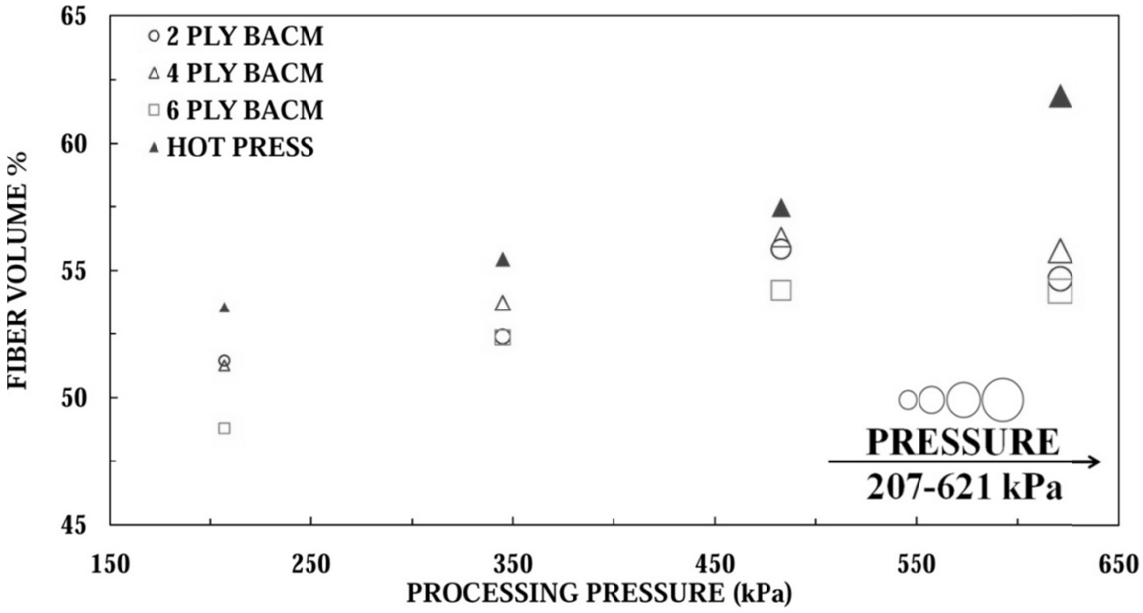

Figure 10- Effect of processing pressure on fiber volume fraction

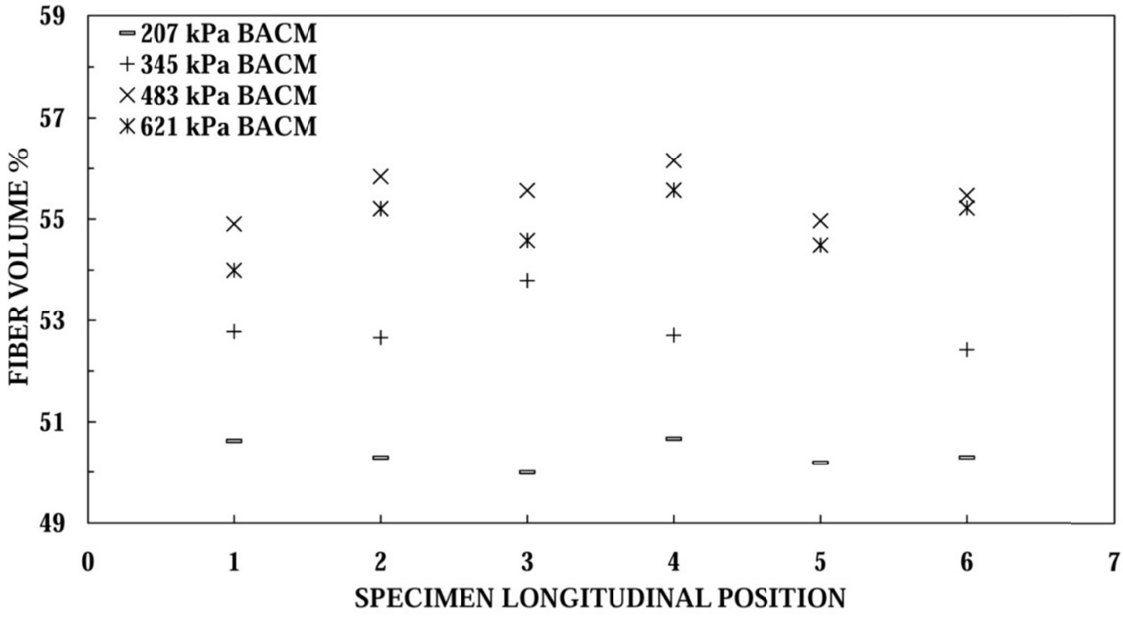

Figure 11- Spatial variation of fiber volume fraction in cylinders produced using BACM.

2.3.3 LAMINATE QUALITY

It is important to consider void volume fraction (i.e., often referred to as void content) when assessing the quality of composite laminates. In industrial applications, the overall void content of a laminate is often times utilized to determine if that component is acceptable for a particular application. The component acceptance threshold usually varies depending on intended use. For example, aerospace structures generally contain less than 1% voids but for other less demanding applications, void contents of up to 5% are acceptable [17, 19, 31, 32, 47]. Boey and Lye [17, 47] examined the effects of voids on the flexural strength and modulus of composite laminates fabricated in an autoclave. They found flexural strength to degrade by approximately 5% and the modulus by 2% for every 1% of voids present. The applicability of the BACM process for producing high performance components is therefore reliant on its ability to produce components with low void content at high fiber fractions.

The presence of voids will decrease the density of a composite when compared to one with negligible voids and comparable fiber volume fraction. As a result, the relative void fractions of composite specimens can be assessed from the specimen density versus fiber fraction plots. Hence, in Figure 12 the average densities of 10 specimens for each of the pressure/ply combinations are shown plotted against their average fiber volume fraction. In addition, the lines of theoretical density of the material with 0% and 5% voids are shown. All the pressure/ply combinations fabricated using both BACM and hot press manufacturing processes were found to contain void fractions below 5%. Interestingly, the void fractions seem to vary little for each of the ply/process groupings regardless of fiber volume fraction and processing pressure. A close examination of the figure also seems to indicate that void fraction is slightly increasing with ply number for the BACM specimens. This may indicate that as plies are added, air or moisture is increasingly trapped in the prepared laminates. Kardos et al. [18, 22] developed a void growth model which showed that the application of an absolute pressure greater than 35.5 kPa would prevent the formation of voids by moisture. Specimens in this chapter were processed with pressures well above this limiting pressure. Therefore, the voids present in the processed specimens are less likely to be environmentally driven and are most likely caused by the entrapment of air mechanically. The void content in the processed specimens normalized with ply number is shown in Figure 13. The normalized void content of the BACM specimens are shown to exhibit similar trends as processing pressure is increased. The results for the 4- and 6-ply specimens appear to be identical but the 2-ply specimens depict a slightly higher void content per ply. The lay-up process itself may be the cause of this increase.

Considering that the act of wrapping the prepreg around the mandrel may be serving as a debulking process, the addition of plies could cause greater normalized compaction (i.e., lower per ply thickness), which would in turn reduce the volume of trapped air per ply [46]. It is also interesting to note that above 207 kPa the void content/ply for the BACM specimens remain nearly constant. This seems to indicate that the resin and not the voids are removed as processing pressure is increased. Cross-sectional micrographs of a select number of specimens were taken to observe the morphology of the voids present and to determine if evidence of void mobility by resin flow could be found. A select number of these micrographs are shown in Figure 14. From the figure, the voids are found to have become immobilized by coming into contact with the fiber tows in the laminate and elongated along the tows as processing pressure is increased.

Because of Figure 13 and Figure 14, the variation of void content along the length of the cylinders was of interest. At lower pressures, the void content in the center of the cylinders were found to be less than the void content at the edges of the cylinders. This variation is indicative of void mobility along the length of the cylinders. However, as pressure was increased, the difference in maximum and minimum void content observed in a particular cylinder was found to decrease as shown in Figure 15, indicating that the voids are becoming less mobile at higher processing pressures. The reduction in mobility of the voids may be due to: (i) the sealing of the cylinders' ends by the bladder, and (ii) their increased perimeter at higher pressures, which leads to greater adhesion to the fibrous preform [31]. Figure 12-Figure 15 support the belief that the primary mechanism for the removal of voids in the BACM process is consolidation and resin flow. It can be inferred from Figure 10 that the increased fiber volume fraction and

the lower void content in the hot pressed specimens are a result of greater resin flow during cure.

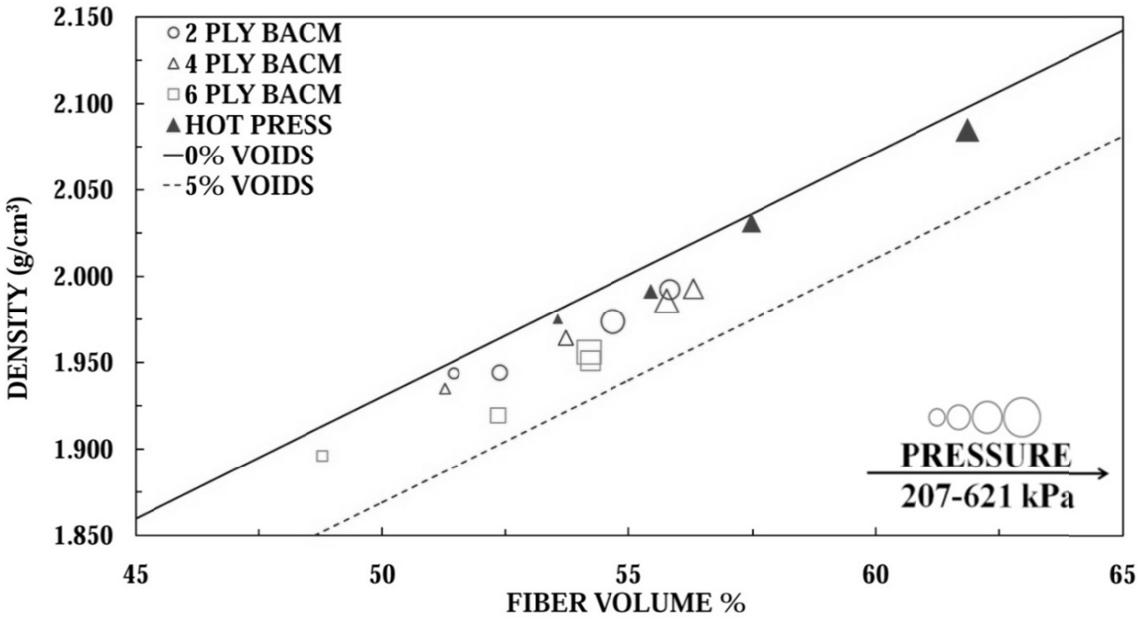

Figure 12- Density of specimen as the fiber volume % is increased. The average void content is shown to be below 5% for all specimens. Note: The increase in marker size is used to illustrate increase in pressure applied during processing.

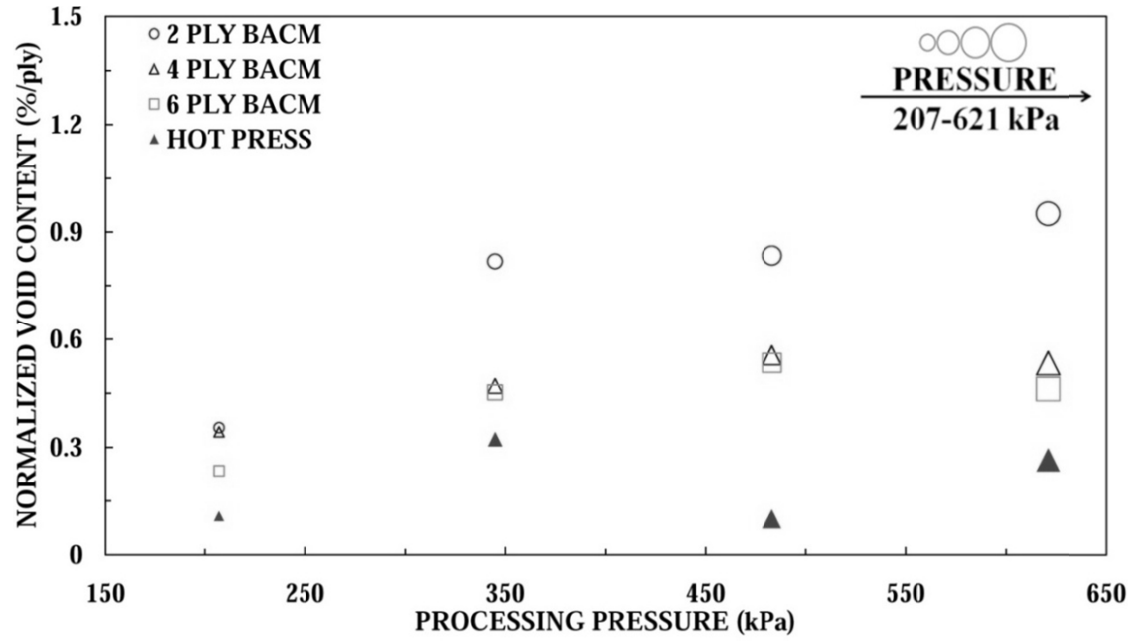

Figure 13- Void % as processing pressure is increased normalized by number of plies present.

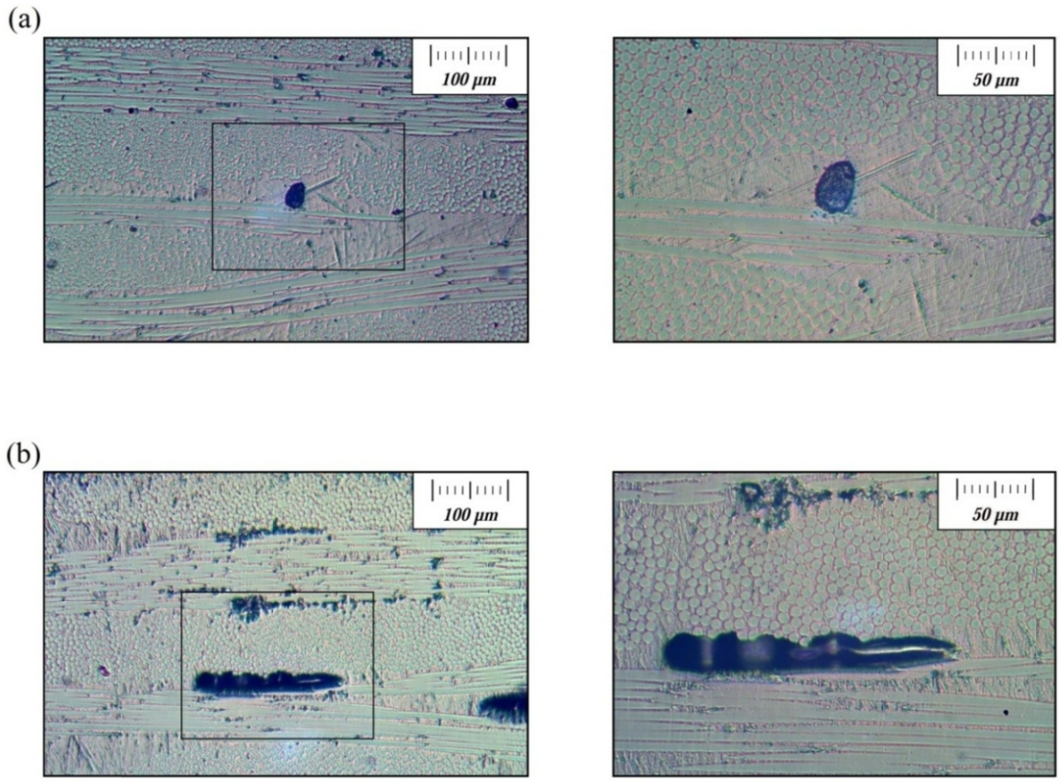

Figure 14- Representative void morphologies in composite cylinders fabricated by BACM method observed at 100x and 200x magnification. Bladder pressure: (a) 345 kPa and (b) 621 kPa.

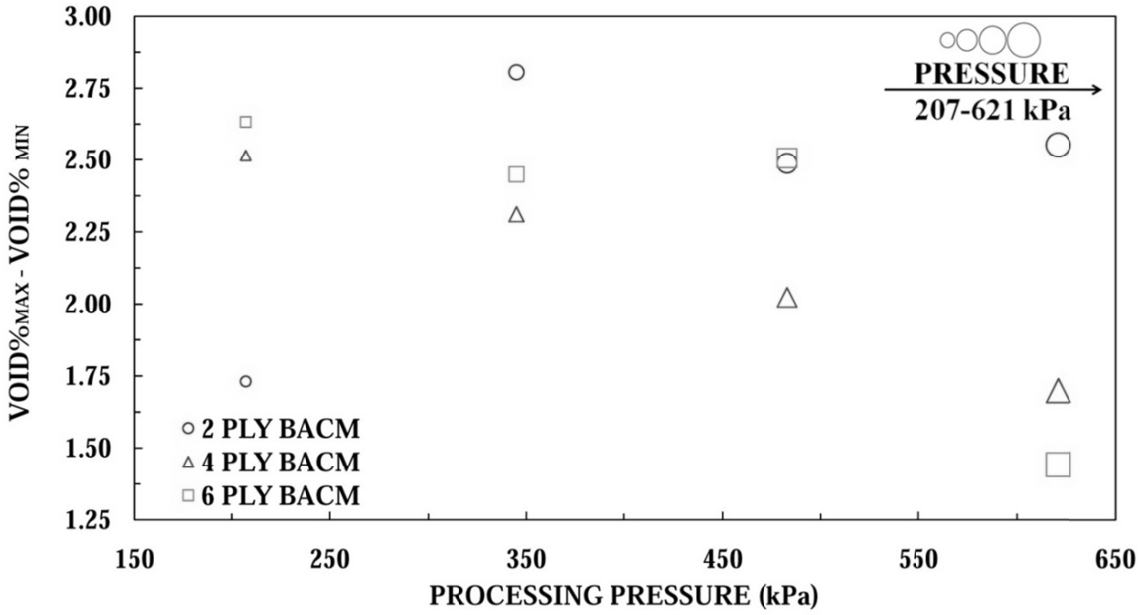

Figure 15- Difference between the maximum and minimum void fractions (%) obtained for fabricated composite cylinders (i.e., Void $\%_{max}$ – Void $\%_{min}$) as processing pressure is increased.

2.3.4 FLEXURAL PROPERTIES

The flexural properties of composite components produced by different manufacturing process can be used to assess the effectiveness of these processes in manufacturing high-quality, structural components. By comparing flexural properties, most process-induced effects such as compaction, volume fraction variations, voids, degree of cure, etc. are considered. As a result, the subtleties of process-induced properties become evident. The effects of processing technique on the elastic moduli of the various specimens are shown in Figure 16. As expected, the elastic moduli of the samples show a clear uptrend as the fiber volume fraction is increased. Moreover, it is shown that the elastic moduli of the BACM processed specimens are comparable to the hot pressed laminates and greater than that reported by Tomblin et al. [37]. The improvement in moduli is not surprising, as the mechanical properties reported were obtained from laminates with a fiber volume fraction of 46% [37]. However, if a trend line is fit to the BACM results, a good correlation with Tomblin et al. [37] is found. The moduli of the BACM specimens showed no discernible dependence on ply number and were found to increase following the same trend as the hot pressed specimens. The presence of voids did not appear to have a significant effect on the elastic moduli of the specimens. This is believed to be a result of the high fiber volume fractions and low amount of voids present in the tested specimens. It is also well known that the elastic modulus is primarily dependent on the fiber property [19, 24, 25, 48].

The failure strength of a composite is dependent on both the ability of the matrix to transfer an applied load to the fiber reinforcement and the fiber volume fraction present in the composite. As a result, for a composite with minimal voids, the failure strength

of the material is expected to increase with fiber fraction. Figure 17 shows how the change in fiber volume fraction affected the failure strength of the fabricated specimens. It is observed that the data tends to cluster within a band regardless of the processing technique and exhibit a general upward trend as fiber volume fraction is increased. However, Figure 17 does not directly illustrate the effect of voids present, which can significantly affect the measured failure strength. This effect is due to the voids reducing the efficiency of the matrix in transferring loads to the fiber reinforcement and also acting as the crack initiation planes. As a result, the failure strength is expected to not only increase with fiber volume fraction but decrease as void content is increased. It is worth noting that the effect of voids may not be significant if the void content can be maintained below a certain level. For example, Almeida and Neto [31] developed a fracture model which showed that the presence of voids in a composite laminate would not significantly affect its strength until a critical void fraction is surpassed. This critical fraction has been observed experimentally by Refs. [49, 50] to be between 2-3% and is dependent on laminate toughness, the ratio of constituent shear moduli and Poisson's ratio, and finally the strength of a laminate with no voids present. The specimens in this chapter were found to contain void fractions from a minimum of 0.2% to a maximum of 3.4% with an average of 1.9%. Because of this, the failure strengths of the tested specimens were placed in to two groups. The first consisted of specimens with void fractions below 1.9% and the second for those with void fractions above 1.9%. The average void content of the first and second group was 1.19% and 2.27%, respectively. The failure strength of the specimens tested and the trends of the associated void groupings are shown in Figure 18. As expected, the failure strength of both groups show

an upward trend as fiber volume fraction is increased. The slopes of the low and high void groupings were found to be 12.3 and 11.7 MPa/V_{fiber} respectively. Hence, the rate of strength increase is not believed to be affected by the presence of voids due to the very similar values of these slopes. However, the presence of voids has caused the trend lines of the two groups to be offset by 5% as void contents increase above 1.9%. For example, the flexural strength of a sample that contains 50% fibers is estimated to be 694 MPa for the group that has less than 1.9% voids. This value decreases to 657 MPa when the void fraction surpasses 1.9%. Flexural strength reductions such as these are common and have been reported by multiple researchers for composites processed by autoclave and hot plate pressing [19, 24, 25, 31].

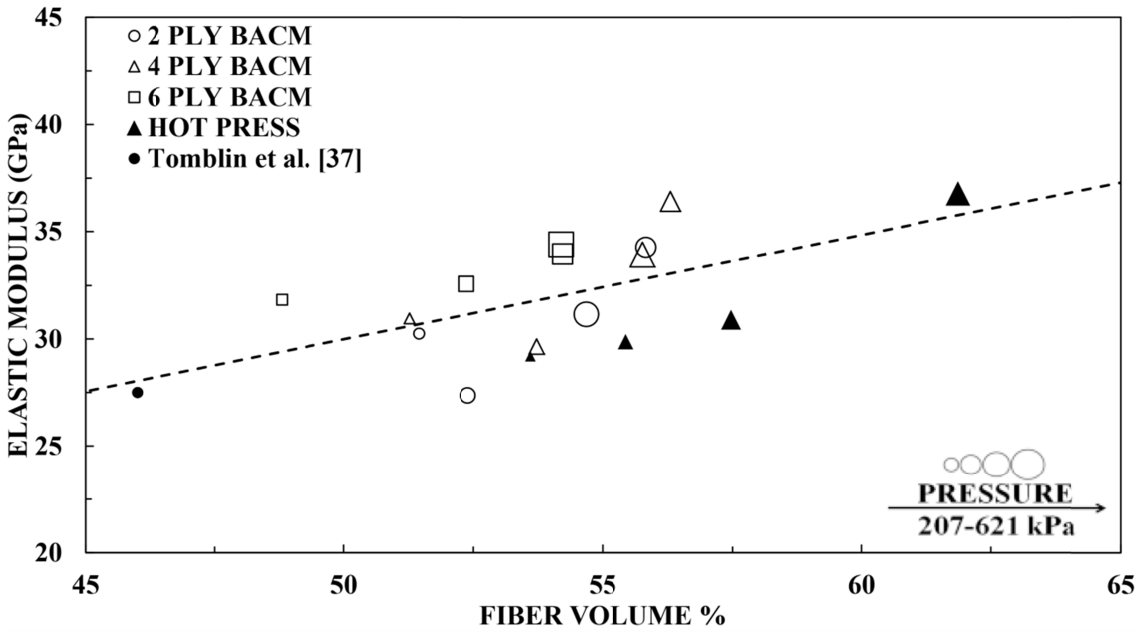

Figure 16- Effect of processing technique and fiber content on measured elastic modulus. The dashed line shown is a trend line fit to all data points present.

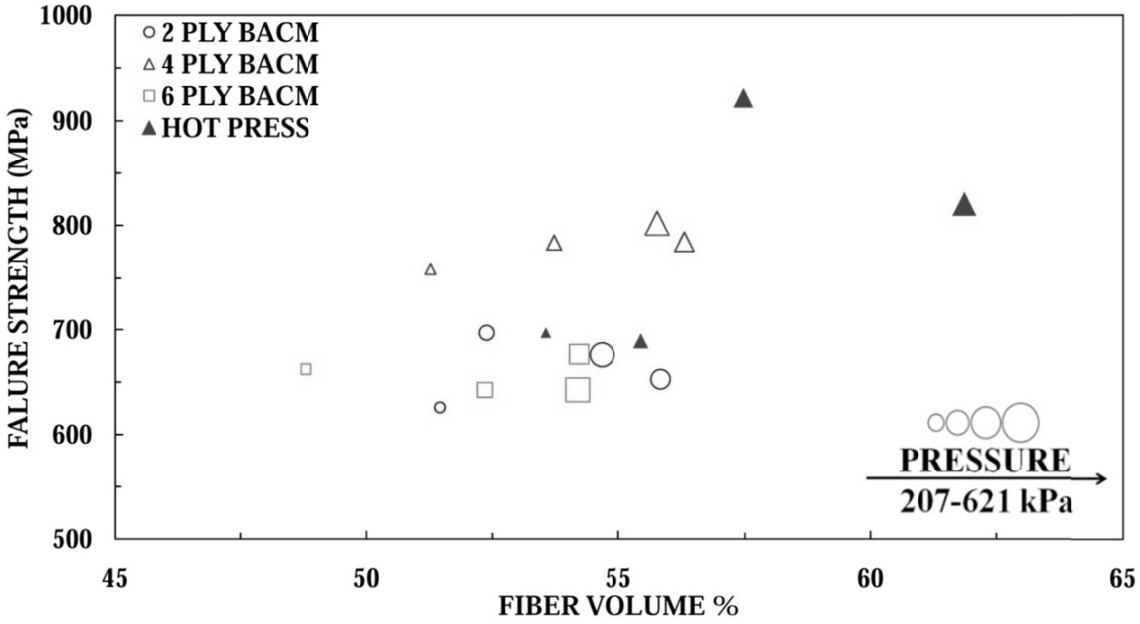

Figure 17- Failure strength of fabricated specimens.

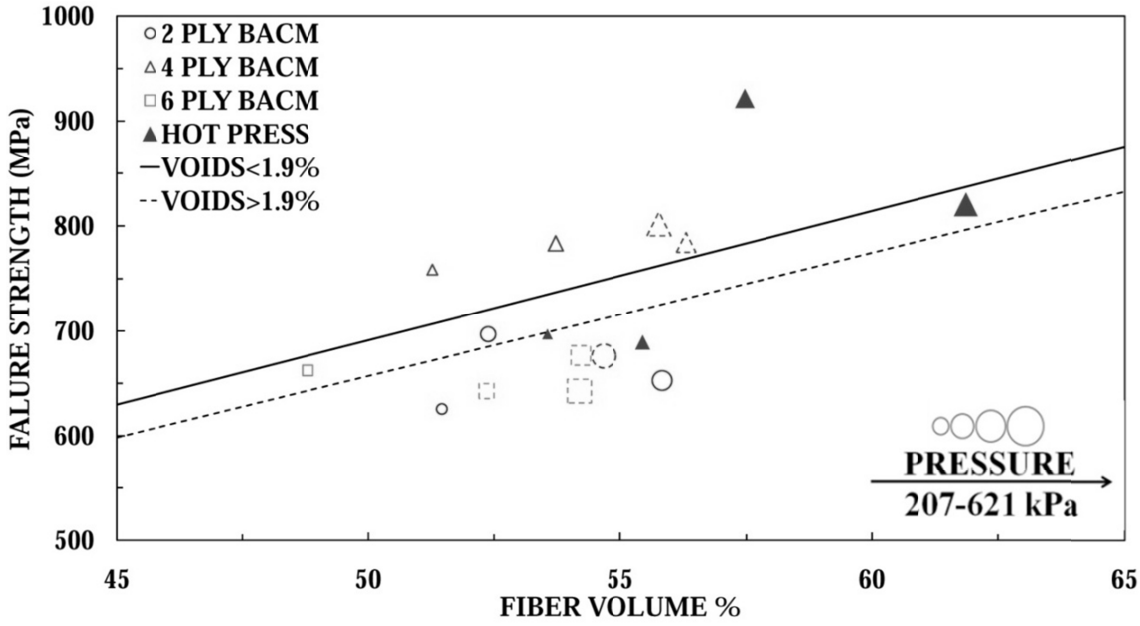

Figure 18- Void effects on the flexural strength of composite specimens. The dashed markers indicate specimen with void fractions above the 1.9% threshold. None of the hot pressed specimen exceeded the threshold value of 1.9%.

2.4 CONCLUSIONS

A new, cost-effective manufacturing process, Bladder Assisted Composite Manufacturing (BACM) has been presented. The BACM process can fabricate hollow,

geometrically complex structural composite components using a variety of prepreg material. Unlike conventional oven or autoclave curing, the heating of the composite to be cured is provided by hot air circulated inside of a pressurized bladder. The proposed process was shown to produce composite cylinders; (i) in a more energy efficient manner when compared to traditional cure processes with an external heat source; (ii) with a spatial fiber volume deviation <0.75%; (iii) with fiber volume fractions as high as 55% at a bladder pressure of 483 kPa; (iv) with void fractions<5%; (v) with flexural properties comparable to hot pressed components. It was also shown that the properties of the cylinders fabricated were not dependent on number of plies. The BACM process has demonstrated its capability to produce high quality components that contain less than 5% voids. As a result, the BACM process can be considered as a viable alternative to filament winding, pultrusion or autoclave curing for the production of medium to large, structural composite components used in aerospace and defense applications.

3. REDUCTION OF MICROVOIDS IN COMPOSITE LAMINATES FABRICATED BY BLADDER ASSISTED COMPOSITE MANUFACTURING (BACM)

3.1 INTRODUCTION

Variations of bladder molding have been used in the past by the composites industry to fabricate non axis-symmetric, geometrically complex, composite components. "Bubble" golf shafts, composite bicycle frames/stems and composite propeller blades are all examples of components produced using the conventional bladder molding process [5, 8-10]. In conventional bladder molding, a bladder presses a composite material against a female mold, which is subsequently heated in an autoclave or oven to cure the component. Bladder Assisted Composite Manufacturing (BACM), which was introduced in Chapter 2, is a recently developed out-of-autoclave/oven process designed to fabricate high-quality, hollow polymeric composite components [51]. In Chapter 2, the BACM process was used to produce composite cylinders from Newport® 321/7781 glass/epoxy prepregs using bladder pressures of 207 kPa (30 psi), 345 kPa (50 psi), 483 kPa (70 psi), and 621 kPa (90 psi) [51]. The fiber volume contents of these cylinders were found to reach a maximum of 55.4% at a processing pressure of 483 kPa. When the pressure was increased to 621 kPa the fiber volume content was found to stagnate. This was believed to be a result of the bladder sealing the ends of the cylinder during manufacturing. The void contents of the cylinders were maintained below 3.5% which is acceptable for secondary composite components but not for primary components. As a result, there is a need to find techniques to reduce void content of components produced using the BACM manufacturing process.

For composite laminates made of prepregs, achieving the required fiber volume fraction while maintaining a low void content and dimensional accuracy can be challenging. Although the initial fiber volume fraction of a prepreg is specified by the supplier, proper consolidation pressure should be applied during cure to facilitate resin flow, which in turn increases the fiber volume fraction. Clearly, fiber volume fraction can be judiciously controlled by the application of consolidation pressure as excess resin can be squeezed out from the laminate edges. In addition to applying consolidation pressure, restricting resin outflow can be used as an effective tool to attain the desired fiber content. By sealing the mold or laminate periphery, the resin outflow can be limited, thus causing the final fiber volume fraction to remain within the proximity of the initial fiber content of the uncured prepreg. As an important benefit, the seal will cause the resin to develop an internal static pressure, which can in turn cause the entrapped air or microvoids in the resin to collapse or reduce in size. The effectiveness of this void mitigation technique in RTM manufacturing was shown by Barraza et. al [52] who found void content could be reduced by as much as 6.5% when resin pressure was increased to 300 kPa. Conversely, the inclusion of a porous bleeder cloth on one side of the prepreg can facilitate resin flow through the laminate thickness, which may result in higher fiber volume fractions. Moreover, the presence of the bleeder may serve to reduce the distance voids must travel to escape the laminate and reduce the likelihood of a void becoming in contact with fiber tows which can result in it become entrapped in the laminate [53].

The removal of voids or reduction of their average size while trying to achieve a sufficiently high fiber volume content is desirable as the presence of excessive voids are

known to considerably reduce the performance of composite laminates [31-33]. In particular, the presence of voids at the fiber-matrix interface has been reported to weaken the interfacial region and serve as crack initiation sites [17, 47]. For example, Boey and Lye [17, 47] examined the effects of voids on the flexural modulus and strength of composite laminates fabricated in an autoclave. They reported modulus and strength reductions of 2% and 5% respectively for every 1% of voids present. Hence, components used for high performance applications are generally expected to contain less than 1% voids while for nonstructural or less critical components void contents as high as 5% may be acceptable [17, 31-33, 47, 49].

In this chapter, three variations of the BACM process are introduced to reduce the void content of composite components by facilitating or limiting resin flow out of the laminate during curing. The first variation was made by placing a porous fabric (bleeder) between the laminate and pressurized bladder and was expected to result in higher fiber volume contents. The second variant was composed of a seal that extends along the periphery of the laminate, is intended to reduce resin outflow, and was expected to result in laminates with lower fiber volume contents. The final version was composed of both a seal and bleeder. These three versions of the BACM process are expected to reveal possible strategies to control and manipulate fiber volume contents as well how to reduce or eliminate the process-induced voids, which were observed in the original BACM configuration outlined in Chapter 2.

3.2 MATERIALS AND EXPERIMENTAL PROCEDURES

3.2.1 PREPREG MATERIAL USED

TenCate® EX-1522/plain weave, a carbon/epoxy prepreg, was used to manufacture the cylindrical samples (OD=50.8mm and L=101.6mm). This material is composed of a balanced plain-woven IM-7 fabric and a toughened epoxy matrix, which cures at 127°C with a glass transition temperature of 180ºC. TenCate® EX-1522/plain weave and similar woven carbon/epoxy prepregs have been commonly used in aerospace applications because of its high specific stiffness/strength [1, 38, 54-57].

3.2.2 BACM CURING PROCESSES

3.2.2.1 Original Configuration

The original insulated BACM configuration (I-BACM), schematically shown in Figure 1, utilizes a flexible RTV bladder, a heating/cooling module, and a thermally insulated aluminum mold. In the BACM process, the desired number of prepreg plies are stacked and placed between the flexible bladder and the inner surface of a two-piece, metallic mold. The composite laminate is then pressed against the inner surface of the mold cavity during cure. Hence, geometrically complex and hollow composite parts can be manufactured with relative ease by using the BACM process. The required temperature profile and consolidation pressure during cure is achieved by controlling the heating element placed inside the pressurized bladder as shown in Figure 1. The composite laminate is cured by the heated air inside the bladder and is not placed in a vacuum bag as in the case of conventional autoclave curing. Although not shown in Figure 1, release

films can be used on both sides of the laminate, thus facilitating easy part removal after the completion of the cure cycle.

As in Chapter 2, the bladders (Length=203.2mm and OD=47.6mm) used to fabricate the composite cylinders were manufactured from Eager Plastics P50 RTV silicon. Heating and cooling of the system was achieved using a custom-made temperature and air regulation system. Thermal uniformity during curing was achieved by opening an air valve to induce air flow in the bladder when the longitudinal temperature gradient along the composite laminate exceeded a predetermined value (i.e., 5.6ºC). This air flow removes temperature gradients formed by any localized heating within the bladder. After the completion of the cure cycle, the air valve is kept open to facilitate cooling of the mold/part. To minimize heat loss to the environment, increase energy efficiency, and eliminate the potential for the injury of laboratory personnel the mold was insulated with a 20mm thick gypsum casing.

As mentioned in the introduction, three different BACM mold configurations were used to investigate the effect of restricting or facilitating resin flow on the void content of the cured cylinders. These three alternative BACM configurations were expected to vary the fiber volume fraction by controlling resin outflow and reduce void content by inducing increased levels of resin pressure during consolidation. Of particular interest was to achieve a desirable increase in fiber volume fraction as well as a reduction in voids. Therefore, the I-BACM configuration described above was used to establish a baseline in which the effectiveness of the three subsequent mold configurations could be compared. A cross-sectional view of the I-BACM configuration is shown in Figure 19a for reference.

3.2.2.2 Sealed Configuration

The sealed configuration (S-BACM), shown in Figure 19b, was composed of a thermally insulated aluminum mold with seals, bladder, and cylindrical laminate. The seals were prepared from Viton 4.76mm cord stock, which was extended longitudinally along the length of the laminate. These seals, located on each side of the cylinder, contain the resin, which would normally be squeezed out of the laminate. Because the resin flow would be impeded by the seal, the fiber volume fraction is likely to be lower compared to the I-BACM configuration. However, the obstruction of resin flow is expected to induce an increase in internal resin pressure, which would facilitate a reduction of void content and average microvoid size. Considering that the concept of increasing pressure by obstructing or restraining resin flow has been successfully used to reduce microvoids in various molded parts [16, 45, 52], this configuration was expected to produce laminates with void contents significantly lower than the I-BACM configuration. It should be emphasized that having two longitudinal seals on both sides of the cylinder does not completely eliminate resin outflow. Both ends of cylinder are not sealed and thus, some longitudinal resin flow into the small gap between the bladder and the mold is expected.

3.2.2.3 Bleeder Configuration

The bleeder configuration (B-BACM), shown in Figure 19c, was composed of a thermally insulated aluminum mold, the cylindrical bladder, a thin layer of porous bleeder fabric wrapped around the bladder, and the cylindrical laminate. Clearly, the presence of a porous fabric on the surface of the laminate considerably reduces the resin flow-path distance, and thus leads to a one-dimensional, through-the-thickness flow. As

a result of the increased resin outflow from the laminate, a fiber volume fraction greater than that of the I-BACM configuration is anticipated. In addition, the reduction in resin flow-path length increases the probability that more mobile voids will be removed before the resin gels [58]. Although a lower resin pressure is expected due to the presence of the highly compressible and porous bleeder, removal of mobile voids across the laminate thickness may result in an overall reduction in void content when compared to the I-BACM configuration.

3.2.2.4 Combined Seal/Bleeder Configuration

The combined seal/bleeder configuration (C-BACM), shown in Figure 19d, utilizes both seals and a bleeder within the BACM mold assembly. Put differently, it was composed of a thermally insulated aluminum mold with two longitudinal seals, a porous bleeder around the bladder, and the cylindrical laminate. The fiber volume fraction of the components produced using this configuration is likely to be similar to the B-BACM configuration. Moreover, the presence of seals is expected to increase resin pressure causing a reduction in void size. This reduction is not predicted to be as significant as in the S-BACM configuration since the resin pressure will not be as high due to the presence of the bleeder. Instead, the through-the-thickness resin flow is expected to increase, making the removal of the smaller and more mobile voids likely.

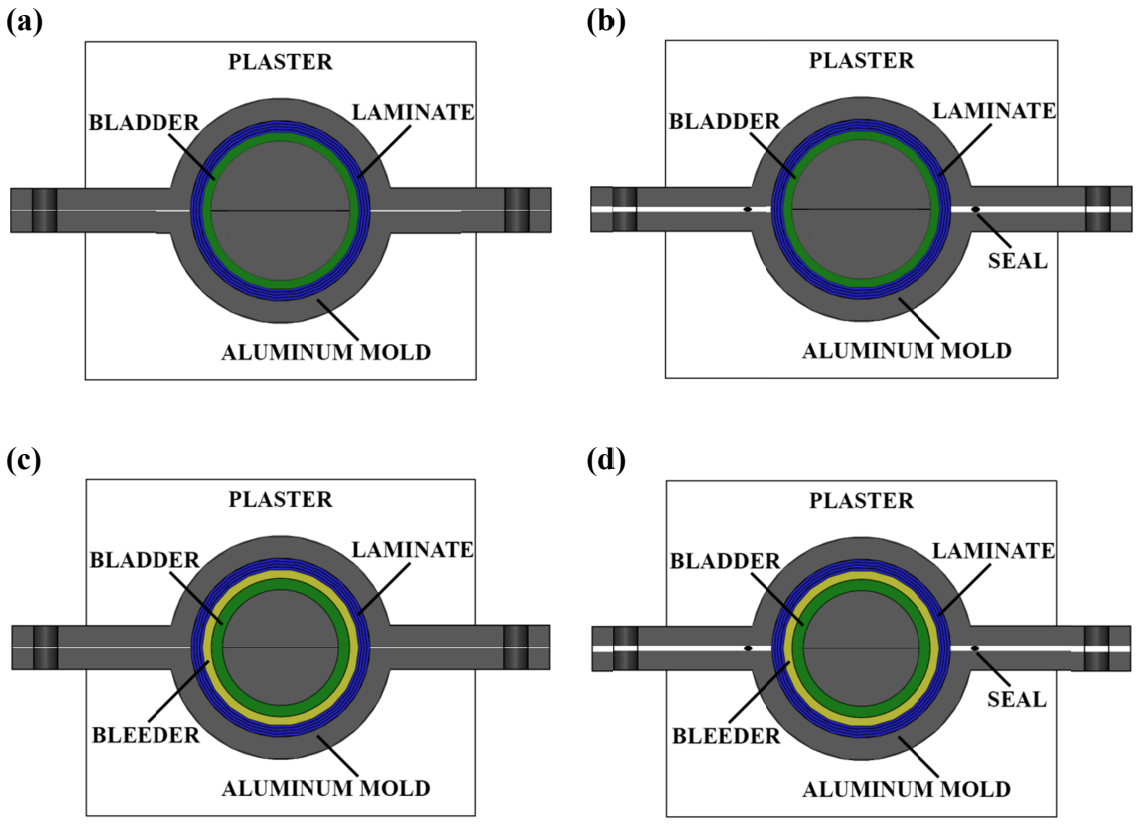

Figure 19- Schematics of the (a) I-, (b) S-, (c) B-, and (d) C-BACM mold configurations.

3.2.6 Sample Fabrication Process

Two 4-ply composite cylinders (OD=50.8mm and L=101.6mm) were manufactured at bladder pressures of 207 kPa (30 psi) and 483 kPa (70 psi) for each of the four mold configurations studied. This resulted in the manufacturing of a total of sixteen cylinders. The prepreg plies for each of these cylinders were conditioned at 99% relative humidity for 24hrs at 25°C (wet-conditioned). The wet-conditioning was expected to increase the moisture contained within the resin system. As a result, the diffusion of moisture vapor into any air voids present should increase, thus causing these voids to grow increasing laminate void content [18]. Having prepregs conditioned at such high humidity levels will allow for better comparisons to be drawn among the studied BACM manufacturing

configurations. After conditioning in the high humidity environment, the plies were laid-up by wrapping a single piece of prepreg material around an aluminum mandrel four times while allowing for an overlap of 6.4mm at the seam of the cylinders. It should be noted that this resulted in the reinforcing fibers to be oriented along the length and circumference of the cylinder. Following the manufacturing of the above sixteen cylinders, two additional cylinders will be made at bladder pressures of 207 kPa and 483 kPa from prepreg plies which were conditioned at 5% relative humidity for 24hrs at 25°C (dry-conditioned) using the BACM configuration found to be the most successful in reducing void content. Conditioning the prepreg in this way is expected to minimize the moisture contained within the prepreg at the time of manufacture. As a result, void growth due to nucleation is expected to be negligible and laminates with low void contents are expected to be produced [18].

During the lay-up, one thermocouple was placed between the second and third plies at each end of the cylinder and used for process control purposes. The cure cycle for the cylinders consisted of a 2°C/min ramp from 25°C to 127°C where they were held for three and a half hours. After the isothermal hold, the cylinders were cooled to 80°C and removed from the mold. In addition, the energy consumed during the manufacturing of the cylinders was recorded using a P3 International P4460 plug power meter to allow for the comparison of the total energy of each BACM configuration used. The typical cure cycles for the I-BACM, S-BACM, and B-BACM configurations are shown in Figure 20. It is evident from the figure that the temperature lag between the set-point and composite part is minimal. The average deviation from the set-point temperature for each of the complete cure cycles is approximately 3ºC with a maximum deviation of

5ºC, which indicates the process is thermally stable regardless of the BACM mold configuration used.

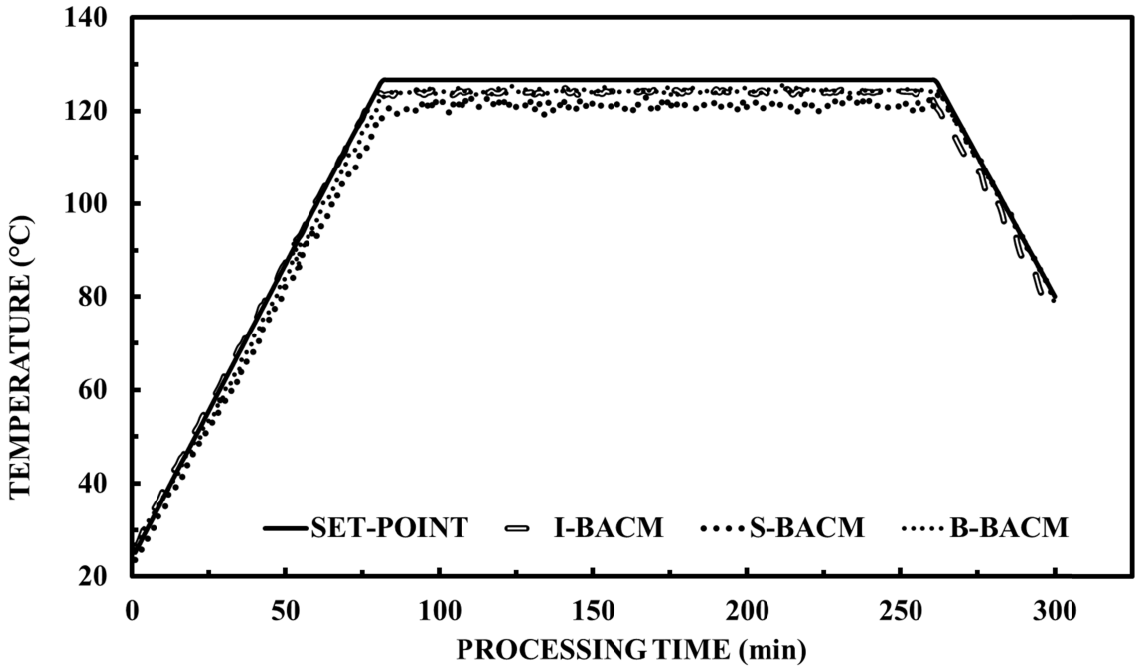

Figure 20- BACM cure cycle showing the effect the mold configurations had on cure profile temperature stability. The average temperature profiles shown for the sealed and bleeder configurations were recorded by thermocouples placed between the second and third plies, 6.4mm from each end of the lay-up.

3.2.7 CHARACTERIZATION OF FLEXURAL PROPERTIES

The flexural properties of the composite cylinders manufactured from the four mold configurations were determined by adopting test procedures for thin-walled, cylindrical laminates. Six 12.7mm wide ring samples were cut from the center of each cylinder, resulting in 12 ring specimens for each mold configuration. Four rings from each configuration was left whole and 8 were cut, as shown in Figure 21, to create flexure, void, and microscope samples.

The circumferential elastic modulus of the composite rings was determined, as in Chapter 2, by laterally compressing the ring specimens between two flat platens using a

Com-Ten® 705TN testing system. The rings were compressed at a rate of 2mm/min, as in Ref. [40], to ensure quasi-static loading. The platens compressed the rings until they had deflected 5.08mm (10% original diameter) at which point the test was terminated. Four uncut, whole ring specimens from each mold configuration were tested using this procedure. The circumferential elastic moduli of the rings were determined at a deflection of 2.50mm by using Eq. (5) as recommended by ASTM D2412-10a.

$$E = \frac{0.149PR^3}{I\delta}\left[1 + \frac{\delta}{4R}\right]^3 \tag{5}$$

The circumferential flexural strength of the laminates produced were determined by testing half ring segments in three-point bending as described in Ref. [41]. To ensure a span to depth ratio was chosen which minimized shear effects, a hot pressed laminate was first manufactured using prepreg plies, which had been dried at 5% relative humidity for 24hrs at 25°C to minimize void content. Following manufacturing, the flexure strength of the laminate as its span to depth ratio was varied was compared to the tensile strength of the laminate as shown in Figure 22. The figure shows the flexural strength of the laminate is constant across all of the span to depth ratio's examined and correlates very well with the tensile strength results. As such, the spans to depth ratio for all flexure tests were maintained at 40 to 1 as recommended by ASTM D790-10. Accordingly, the average span for the 207kPa and 483kPa specimen was 32.4mm (0.81mm thick) and 30.8mm (0.77mm thick) respectively. All curved specimens were placed concave side down on support pins to reduce the effect of geometric nonlinearities [42]. The ring segments were loaded at a rate of 2mm/min until an outer surface rupture occurred. This procedure was used to test twelve ring segment

specimens from each mold configuration. The high radius to thickness ratios for the ring segments ensured that the strength of the samples can be obtained without accounting for sample curvature (see Appendix C.2) [43]. Therefore, the circumferential flexural strength of the composite ring segments, expressed in Eq. (6) were calculated as recommended by ASTM D790-10.

$$\sigma_f = \frac{3PL}{2bd^2} \tag{6}$$

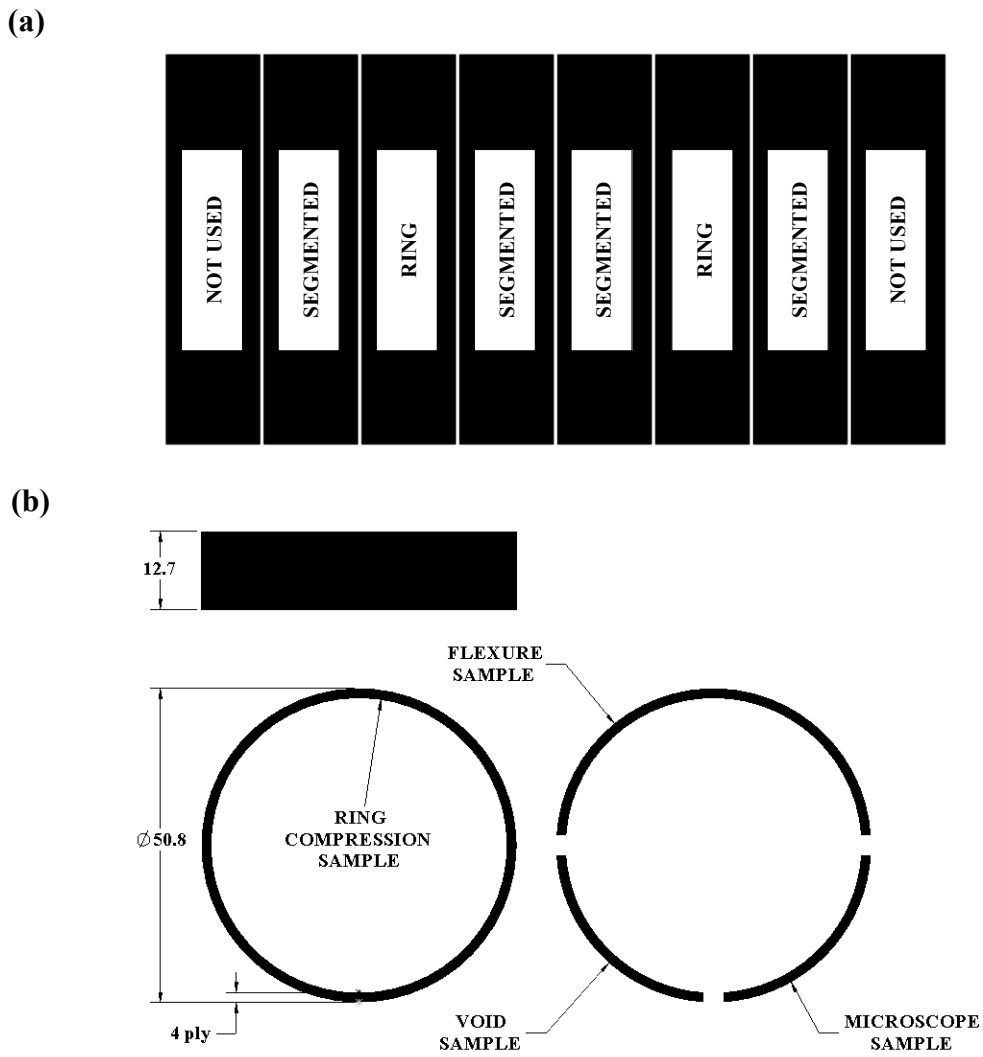

Figure 21- Schematic representation of the (a) rings cut from BACM processed cylinders and (b) how these ring specimens were cut to allow for the characterization of the laminates elastic modulus and flexural strength. Note: all dimensions are in mm.

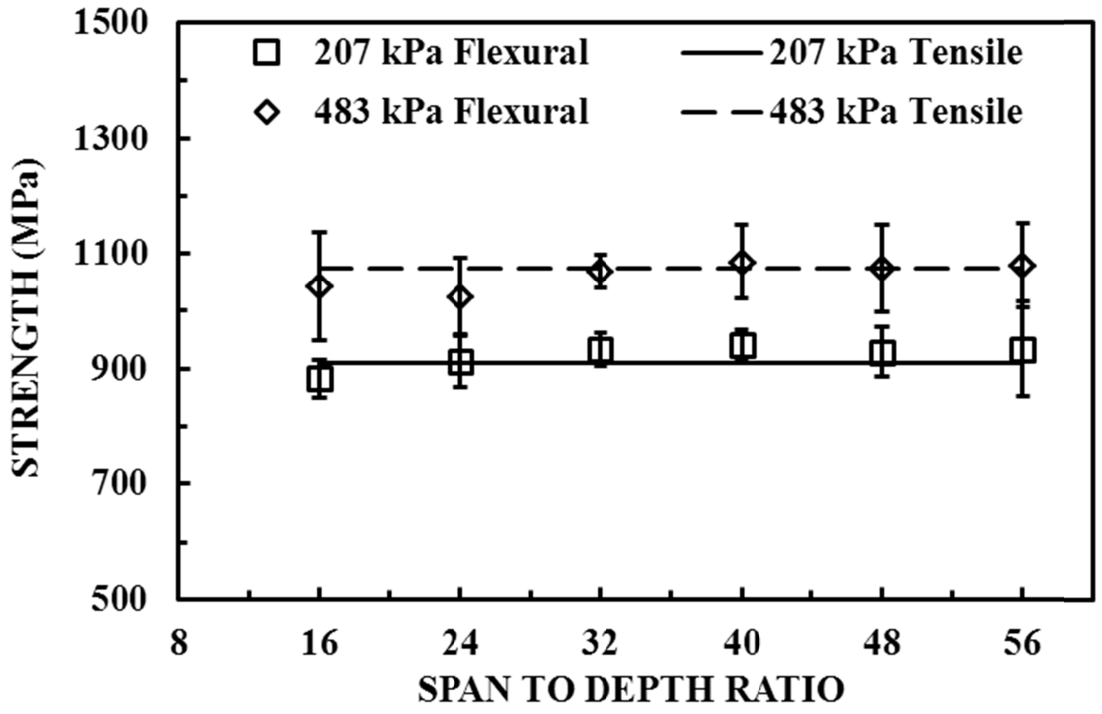

Figure 22- Effect of varying span to depth ratio on the flexural strength of TenCate® EX-1522/Plain Weave carbon fiber/epoxy prepreg. Note: Error bars represent the 95% confidence interval for n=5.

3.2.8 MEASUREMENT OF FIBER VOLUME AND VOID CONTENT

The composite industry oftentimes uses void content as a way to assess the relative quality of individual parts. Characterization of the void content via the measurement of composite density is a highly accurate technique and can be performed without sophisticated equipment and material specific calibration. However, the bulk composite density, constituents' densities and constituents' weight fractions must be accurately measured in order to properly use the density technique.

In this chapter, the effectiveness of different BACM mold configurations in reducing the void content of the composite cylinders were of interest. Hence, the density of each ring segment was found individually prior to mechanical testing to allow for a quantitative and accurate determination of the effects of voids on mechanical properties.

To this end, each sample used in testing was suspended in a solution of Cargill Labs 2.49 g/cc Heavy Liquid whose density was reduced with the addition of water until a suspension of the composite sample is achieved. The subsequent measurement of the solution density with a pycnometer allowed for the accurate measurement of the bulk density of each cured sample. The densities of the fibers and matrix were reported by TenCate®, the prepreg manufacture, to be 1.79 g/cc and 1.35 g/cc respectively. In addition to the densities, the weight fractions of the individual constituents were required to determine the bulk void content of the composite samples. Therefore, after mechanical testing, the fiber and matrix weight fractions of each composite sample were determined using the matrix digestion technique as recommended by ASTM D3171 Procedure B. The bulk void content of each sample was then found using Eq. (7).

$$V_v = 100 - \rho_{specimen}\left(\frac{W_{fiber}}{\rho_{fiber}} + \frac{W_{matrix}}{\rho_{matrix}}\right) \quad (7)$$

Using the bias uncertainty for each of the measured values and propagating them through the calculation shown in Eq. (7), the uncertainty of the void content values can be shown to be ±0.22% using the outlined procedure. This indicates that the accurate measurement of the composite density combined with the matrix digestion method is useful to characterize low void content levels (i.e., <1%).

In addition to the bulk void content, the size, location, and shape morphology of the voids present in the cylinders were examined using a Zeiss DSM-960A SEM. Six specimens from each of the mold configurations were embedded in a quick cure acrylic

resin and polished with grit sizes ranging from 15 μm to 1.9 μm using three successive steps. Afterwards, the samples were sputter coated with gold/palladium to prevent sample charging and cross-sectional images were acquired at 50x and 200x.

3.3 RESULTS AND DISCUSSION

3.3.1 ENERGY CONSUMPTION DURING MANUFACTURING

To reduce the environmental impact of manufacturing processes, companies are gradually moving towards introducing energy efficient, green manufacturing processes that focus on reducing operational waste and energy consumption [44, 59, 60]. In general, the energy efficiency of curing processes which use an autoclave or an oven are inferior compared to the molding processes that take place in closed or matching molds with shorter cycle times. Although autoclave or oven curing is commonly used to fabricate high-quality laminates, both suffer from reduced energy efficiency (i.e., large energy consumption and energy waste) due to the heating of a large thermal mass during the cure process. Hence, the energy efficiency of these processes would be improved if: (a) the thermal mass of the autoclave or oven could be reduced proportionate to the size of the cured composite; (b) the amount of heated gaseous medium around the cured part is minimized, and (c) unnecessary venting of heated gases to maintain a constant cure pressure is eliminated. In this chapter, changes were made to the I-BACM configuration to produce the three new BACM mold configurations as described earlier. The effect of these mold configurations on the energy efficiency of the process was of interest. This is an important consideration as an increase in energy consumption could increase manufacturing costs, and thus reduce the viability of the BACM process. In Figure 23, the energy consumed during the

manufacturing of the cylinders for each of the studied mold configurations is compared to the I-BACM configuration. The changes in the mold configurations were determined to not result in any appreciable increase in the energy consumed during the manufacturing of the cylinders. In fact, the average energy consumption of all the mold configurations was found to be 0.69±0.03 kW-h. If this result is compared to the energy consumption per part reported in Section 2.3.1, one finds that the parts manufactured in this chapter required 23% more energy (0.69 kW-h vs 0.56 kW-h). However, this is expected as the material system used in Chapter 2 (Newport® 321/7781) required a two hour hold at 121°C whereas the material system in this chapter (TenCate® EX-1522/plain weave) required a three and a half hour hold at 127°C.

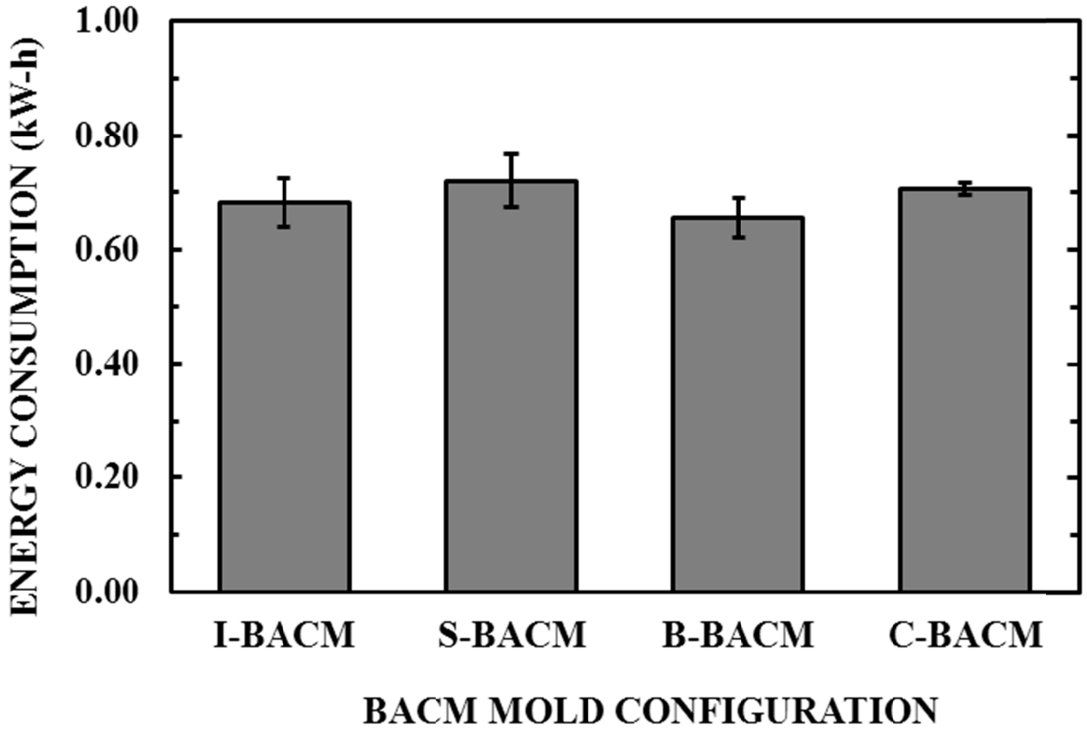

Figure 23- Variations in energy consumption by the BACM curing processes. The effect of changing the BACM mold configurations on the energy consumed was found to be insignificant. Note: Error bars represent the 95% confidence interval for n=4.

3.3.2 MOLD CONFIGURATION EFFECT ON FIBER VOLUME FRACTION

If analogous composite components are manufactured using somewhat different molding processes or mold configurations, the resulting fiber volume fractions and, thus, the mechanical properties are likely to vary. In the BACM process, these variations are a result of the use of different mold configurations, which facilitate or restrict resin outflow during curing. Accordingly, components cured with increased resin outflow will be expected to approach a theoretical maximum fiber volume fraction as determined by prepreg weave pattern, packing factor, or processing pressure. Conversely, if the resin outflow is restricted during curing, the fiber volume fraction may remain within the proximity of the prepregs' initial fiber content. Figure 24 illustrates the effect of each mold configuration on the fiber volume fraction obtained.

From the figure, the dependence of fiber volume fraction on mold configuration is clearly observed. The B- and C-BACM configurations resulted in average fiber volume fraction increases of approximately 3.5% when compared to the I-BACM configuration regardless of the studied processing pressures. These increases in fiber fractions implies that the bleeders used in both configurations were effective in increasing resin outflow through the thickness of the laminate. The S-BACM configuration was found to cause a slight reduction in the obtained fiber volume fraction (≈1.3%) when compared to the I-BACM configuration at each of the studied processing pressures. This came as a surprise because the seal in the S-BACM configuration was expected to have a significant effect on laminate resin outflow, which would in turn cause the obtained fiber volume fraction to be lower (≈5%) than that of the I-BACM configuration. Therefore, this minor reduction in fiber volume fraction seems to indicate that the resin

outflow from the laminate was not great enough to utilize the seal in the S-BACM configuration. These findings demonstrate that the fiber volume fractions of composite components can be affected and can therefore be tailored by the judicious selection of mold configuration.

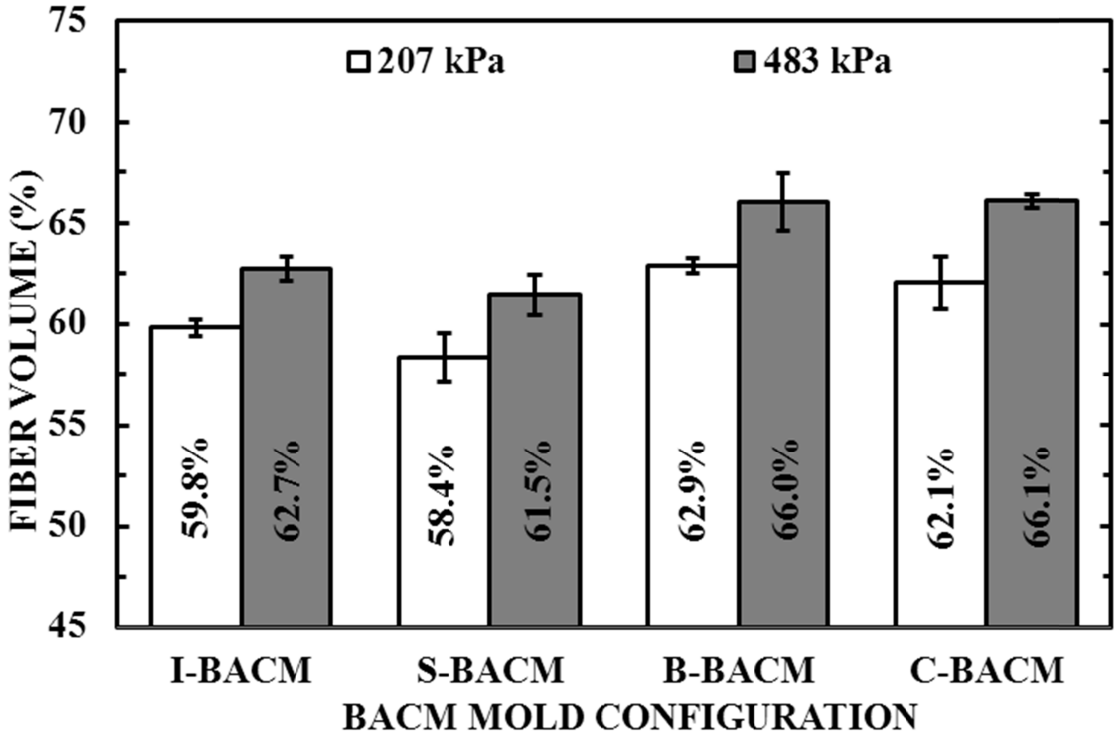

Figure 24- The effect of mold configuration on fiber volume fraction. Note: Error bars represent the 95% confidence interval for n=6.

3.3.3 WET-CONDITIONED LAMINATES RESULTS

3.3.3.1 Bulk Void Content in Wet-Conditioned Laminates

The average void contents of the samples obtained from each of the molding configurations are shown in Figure 25. It is immediately evident that the B-, and C-BACM mold configurations resulted in marked decreases in the void content when compared to the I-BACM configuration. The most significant change was observed in

parts manufactured at 483 kPa by the B-BACM configuration. For this case, the void content of the B-BACM configuration was reduced by 43% (from 6.1% to 3.5%) when compared to the I-BACM configuration. This reduction is thought to be caused by the shorter and less tortuous pathways open for the voids to escape the laminate [21, 58]. Similarly, the C-BACM configuration, which uses both the seal and the bleeder, showed a void content reduction of 36%.The primary void reduction mechanism of this configuration is believed to be the same as the B-BACM configuration, which explains the statistically identical fiber volume and void content results shown in Figure 24 and Figure 25 respectively. The S-BACM case was expected to result in a dramatic drop in the part void content due to an increase in internal resin pressure, induced by the seals' limiting resin outflow. However, as discussed in the previous section, it appears the seals were underutilized because the resin outflow from the laminate was not great enough for the seals' have an appreciable effect. This finding does not delegitimize the void suppression method (high resin pressure) used in the S-BACM configuration but instead highlights the need to tailor the manufacturing configuration to the prepreg used. For the prepreg (TenCate® EX-1522/plain weave) used in this chapter, the B-BACM configuration was found to be the most successful for suppressing void formation. However, if the prepreg had a higher initial resin content the resin flow would have been expected to be much greater which would have in turn increased the likelihood of the seals increasing resin pressure causing voids to be reduced/eliminated.

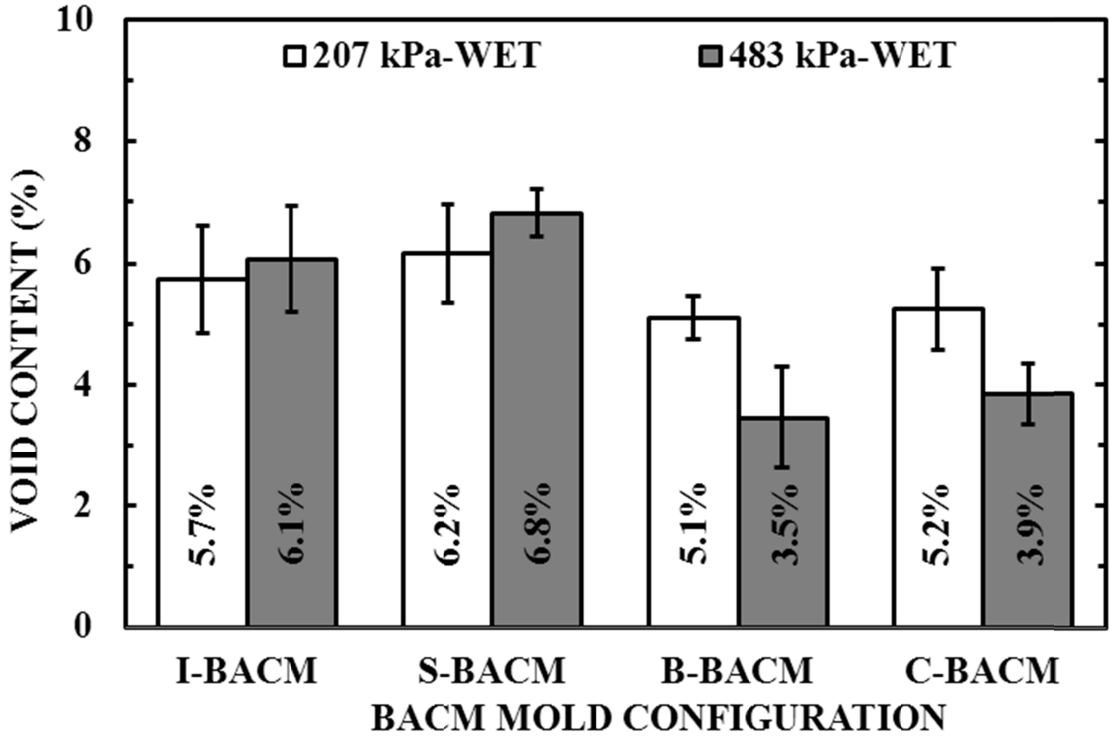

Figure 25- Void contents of the cylinders produced using each of the mold configurations. Note: Error bars represent the 95% confidence interval for n=6.

3.3.3.2 Wet-Conditioned Laminates Flexural Properties

The effectiveness of the BACM mold configurations in producing high-quality composite components can be assessed from their flexural properties. A comparison of flexural properties will result in the cumulative consideration of most process-induced effects such as degree of cure, fiber volume fraction, compaction, voids, and similar microstructural defects [61]. As a result, the intricacies of process-induced properties become evident. The circumferential elastic moduli obtained from the different BACM mold configurations are shown in Figure 26. As the fiber volume fraction was increased, the elastic moduli of the samples were found to increase from a minimum of 53.4 GPa to a maximum of 61.5 GPa indicating a clear upward trend regardless of the mold configuration used.

The failure strength of a laminate is reliant on its fiber volume fraction and the ability of the matrix to transfer an applied load to the fiber reinforcement. Therefore, the failure strength of composite laminates with minimal voids often increases with fiber volume fraction. The effect of fiber volume fraction on the average circumferential failure strength of the cylinders produced using the I-, S-, B- and C-BACM configurations are shown in Figure 27. The failure strengths are generally found to increase with fiber volume fraction from a minimum of 652 MPa to a maximum of 925 MPa. As with the elastic modulus, the mold configuration used was not found to cause a deviation from the general upward trend of the data. However, the presence of voids appeared to have a significant negative effect on the flexural strengths of the specimens.

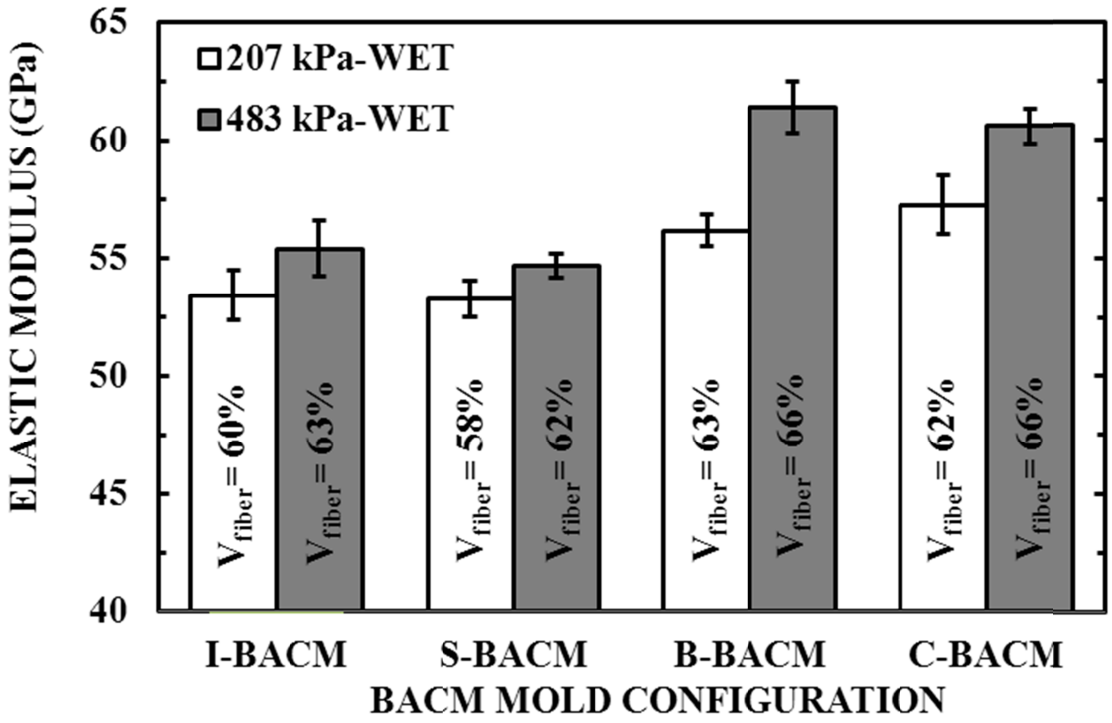

Figure 26- Mold configuration and fiber content effect on measured elastic modulus of the cylinders. Note: Error bars represent the 95% confidence interval for n=6.

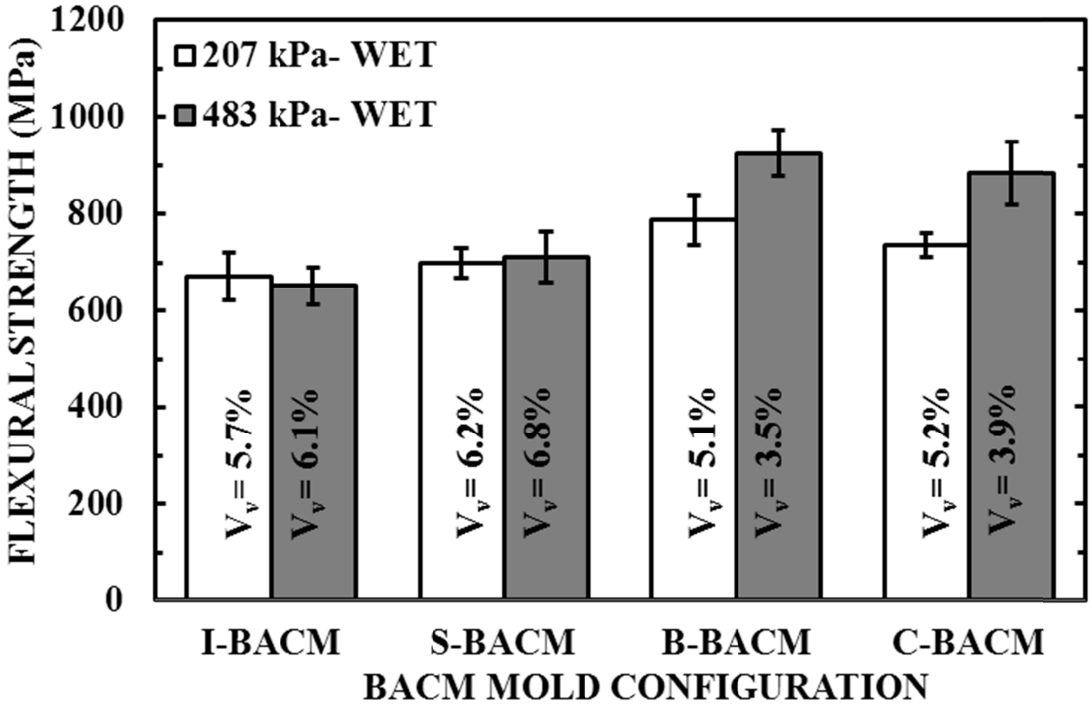

Figure 27- The failure strengths of the cylinders produced using each of the mold configurations. Note: Error bars represent the 95% confidence interval for n=6.

3.3.3.3 Wet-Conditioned Laminates Void Morphology

SEM images were taken from representative specimens of each mold configuration and processing pressure to determine the morphology of the voids present. In addition, these images were used to determine the type of voids that were most effectively removed by each of the three BACM configurations compared to the I-BACM configuration. Representative SEM images of the specimens processed at 207 kPa and 483 kPa are shown in Figure 28 and Figure 29 respectively.

The I-BACM configuration images, shown in Figure 28a and Figure 29a, are found to contain both intra- and inter-tow voids. The morphology of the inter-tow macro-voids (i.e. voids> 50μm) indicate they are most likely a result of air entrapped during the lay-up of the composite cylinders as well as the moisture present in the resin before manufacturing, while the inter-tow voids are believed to come from voids present in the

resin phase before lay-up [18, 22, 62, 63]. The S-BACM configuration images shown in Figure 28b and Figure 29b were found to contain voids in both the inter- and intra-tow regions with no appreciable difference in void morphology when compared to the I-BACM configuration. Thus, it appears this configuration was unable to develop an increase in resin pressure, which would cause the macro-voids to collapse. The B-BACM configuration images, shown in Figure 28c and Figure 29c, do not contain any discernible inter-/intra-tow micro-voids. However, occasional, larger macro voids are still present. The absence of micro-voids is explained by the supposition made earlier that shorter and less tortuous pathways are available to the voids to escape the laminate. The presence of remaining inter-tow macro-voids is explained by the fact that they are less mobile than the micro-voids due to their increased contact diameters [52, 58, 64]. It is interesting to note that the C-BACM configuration images, Figure 28d and Figure 29d, show no noticeable change in the void morphology when compared to the B-BACM configuration. This seems to indicate that the full effect of the bleeder is retained from the B-BACM configuration with no apparent benefit of the seal. A schematic representation of the way in which the resin and the voids it carries is believed to exit the I- and B-BACM configurations may be found in Figure 30. For the I-BACM configuration (Figure 30a), the resin is shown to move along the circumference of the laminate and to exit at the mold part line. Thus, an average void, assuming void distribution is homogeneous in the laminate, must travel approximately $0.5\pi R$. Conversely, an average void in the B-BACM configuration (Figure 30b) must only travel 0.5d. Thus, the effectiveness of the B-BACM configuration in removing voids is expected to remain constant regardless of part size.

(a)

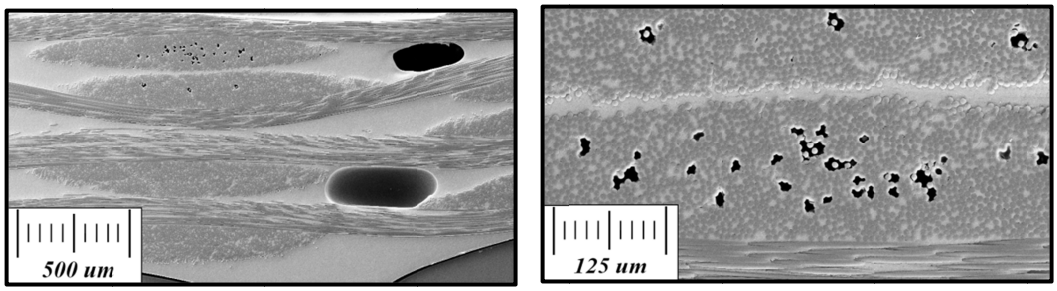

(b)

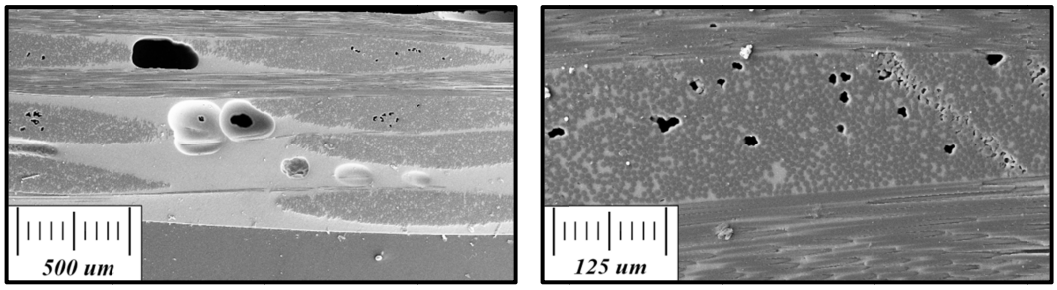

(c)

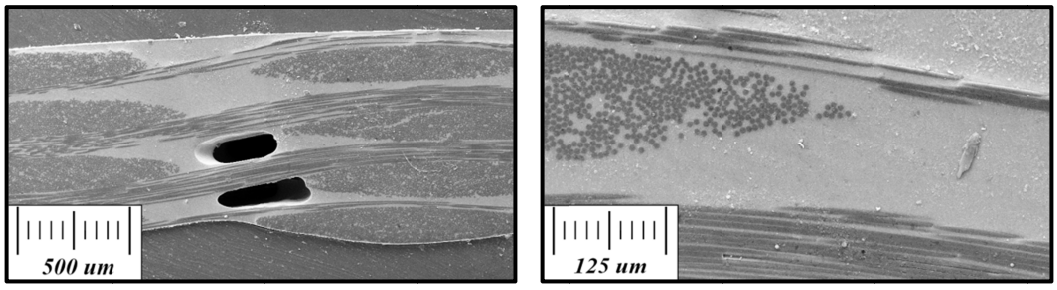

(d)

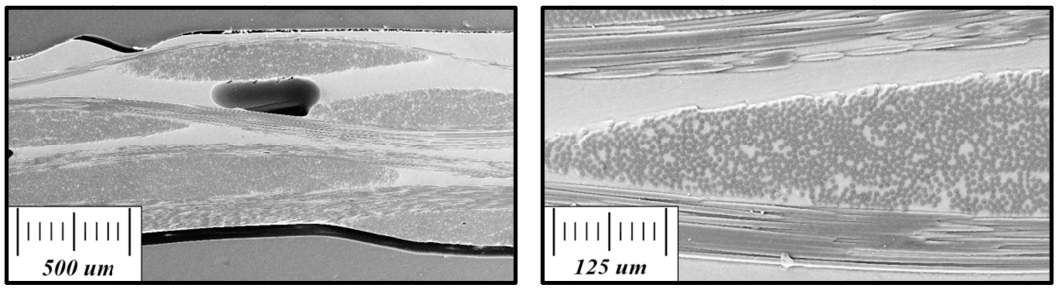

Figure 28- SEM images of the 207 kPa processed specimens manufactured by the (a) I-, (b) S-, (c) B- and (d) C-BACM mold configurations at 50x, and 200x.

(a)

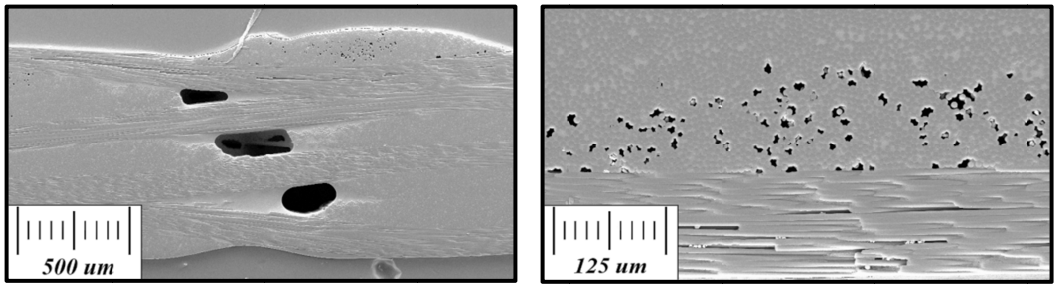

(b)

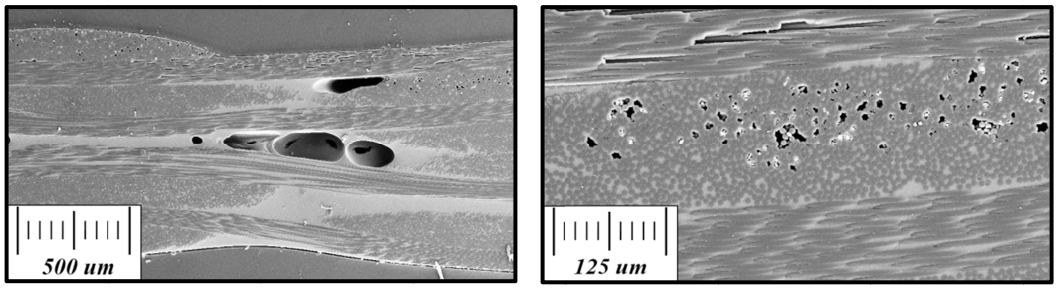

(c)

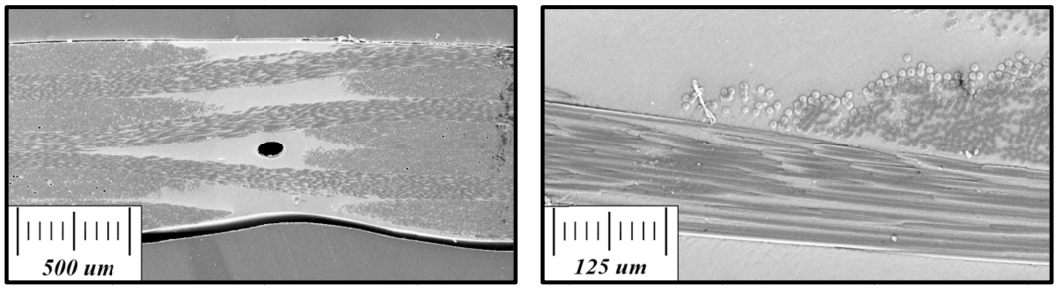

(d)

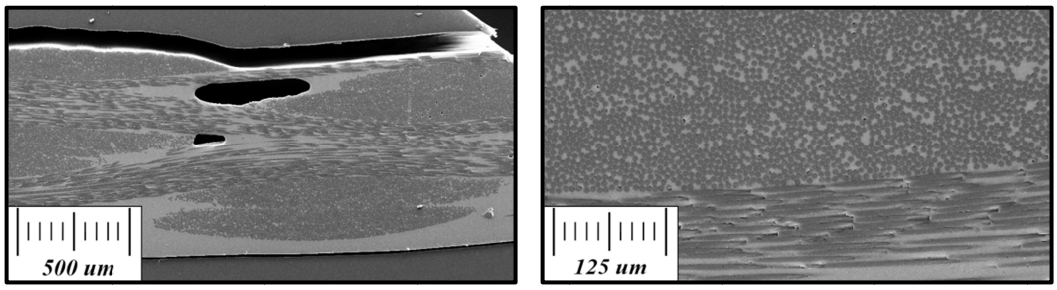

Figure 29- SEM images of the 483 kPa processed specimens manufactured by the (a) I-, (b) S-, (c) B- and (d) C-BACM mold configurations at 50x, and 200x.

(a)

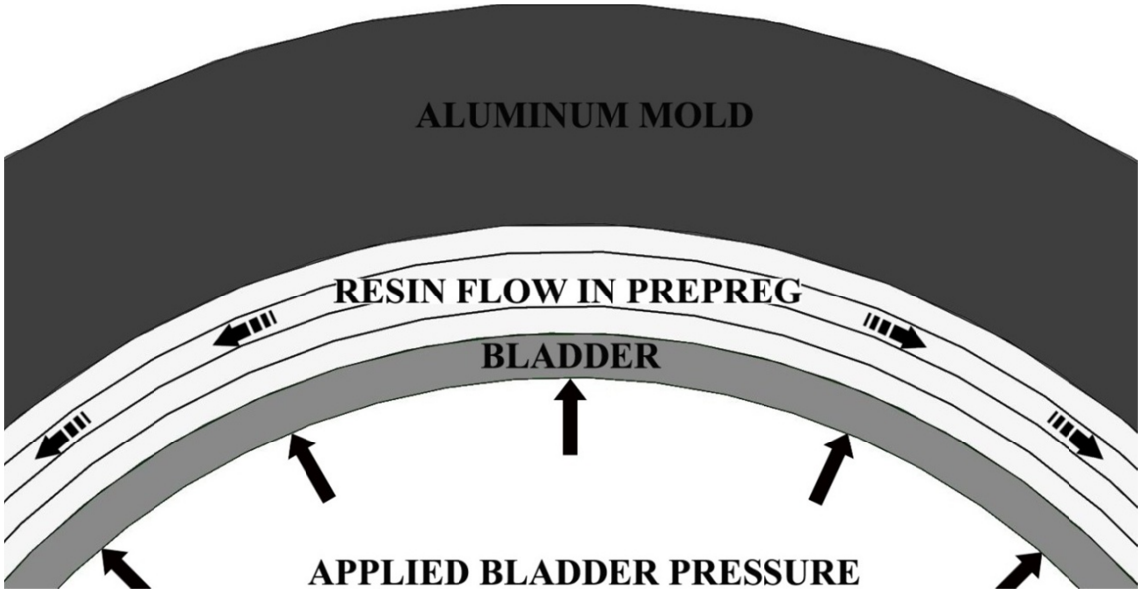

(b)

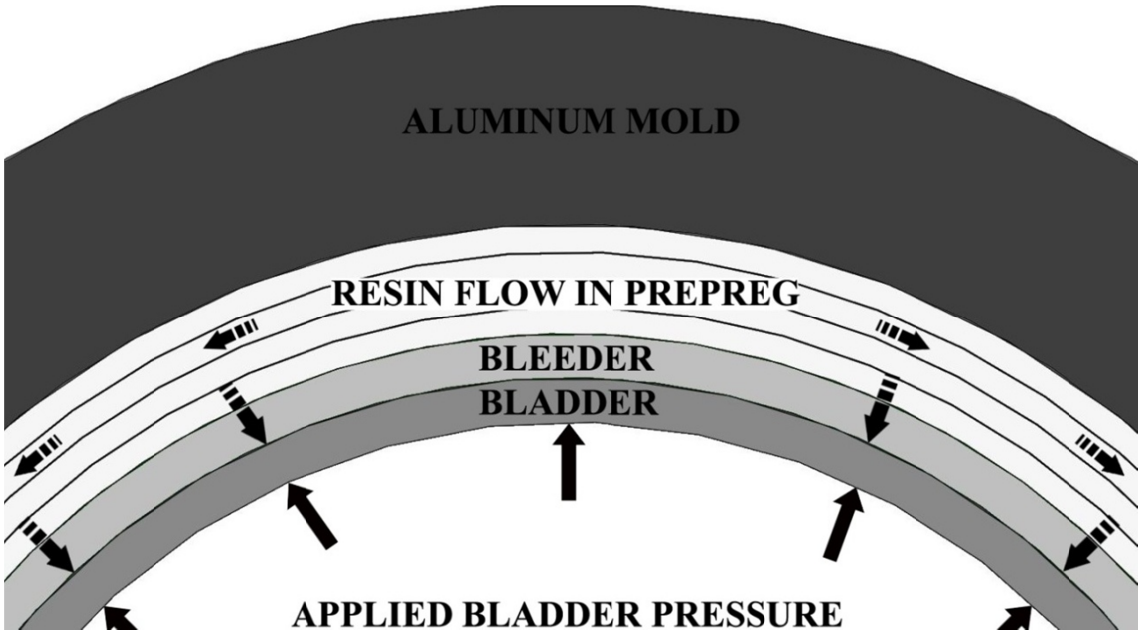

Figure 30- Schematic representations of the (a) I-BACM and (b) B-BACM configurations. The effect of the bleeder is shown in the (b) B-BACM configuration. In the I-BACM configuration, the absence of a bleeder leads to resin outflow along the circumference of the laminate. In the B-BACM configuration, the presence of bleeder leads to higher resin outflow and higher fiber volume fractions.

3.3.4 DRY-CONDITIONED LAMINATES RESULTS

The B-BACM configuration was found to be the most capable of removing voids and/or suppressing void formation in tubular laminates whose prepreg had been wet-conditioned as was shown in Section 3.3.3. Therefore, it was of interest to determine the minimum obtainable void content of the cylinders manufactured by the BACM technique if they were manufactured under ideal conditions, i.e. prepreg dried at 5% relative humidity for 24hrs at 25°C. In addition, it was of interest to compare these results to laminates conditioned in the same way manufactured using the hot press. To facilitate these determinations, two cylinders and flat laminates were manufactured at 207 kPa and 483 kPa using the B-BACM and hot-press manufacturing techniques after having been dried as outlined above.

3.3.4.1 Bulk Void Content in Dry-Conditioned Laminates

The average void contents of the samples obtained from the hot-press and B-BACM techniques are shown in Figure 31. From the figure, it is evident that the laminates whose constituent prepreg had been dried produced laminates with the lowest void contents for any particular processing technique or pressure. In addition, the figure indicates the B-BACM configuration produces cylinders whose quality is comparable to the hot-pressed laminates for all cases except for those manufactured at 483 kPa whose prepreg had been dried. For this case, the hot-press technique produced laminates with void contents of 1.3% whereas the B-BACM configuration produced cylinders with void contents of only 0.2%. This improvement over the pressed laminate is attributed to the shorter and less tortuous pathways open for the voids to escape the laminate made by the bleeder [21, 58].

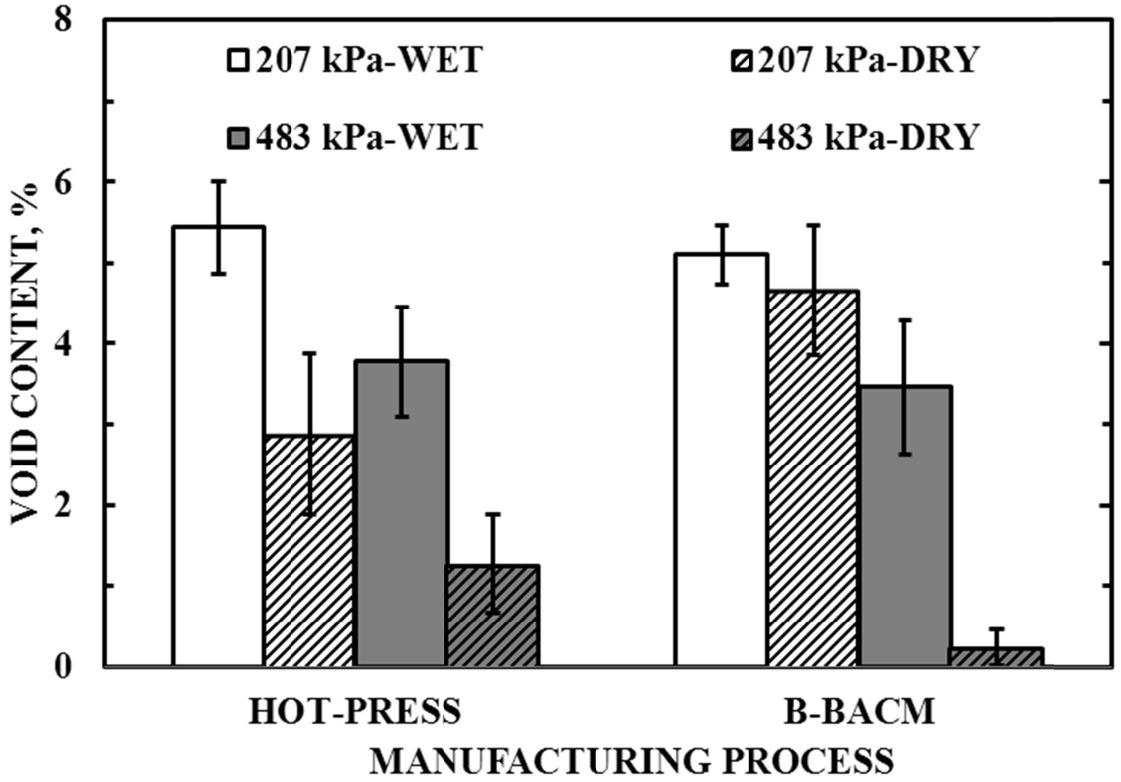

Figure 31- Void content of laminates using the hot-press and B-BACM manufacturing techniques. Note: Error bars represent the 95% confidence interval for n=6.

3.3.4.2 Dry-Conditioned Laminates Flexural Properties

The effectiveness of drying the prepreg in producing high-performance composite components can be assessed from their flexural properties. The in-plane and circumferential moduli of the hot-pressed and B-BACM samples are shown in Figure 32. As the fiber volume fraction was increased, the elastic moduli of the samples were found to increase from a minimum of 55.3 GPa to a maximum of 71.9 GPa indicating a clear upward trend independent of void content and manufacturing technique used. Results such as these are not surprising, because the elastic modulus of a composite is fiber dominated [19, 24, 25, 48].

The laminate fiber volume fraction and the efficiency of the matrix in transferring an applied load to the fiber reinforcement will generally dictate the failure strength of a laminate. Therefore, the failure strength of composite laminates is coupled with fiber volume and void content. For a laminate with minimal voids, failure strength is expected to increase. However, when voids are present this will not necessarily be the case. The flexural strength of the hot-pressed and B-BACM specimens are shown in Figure 33. The failure strengths are found to increase as void content is reduced. In fact, for the B-BACM laminates the failure strength was found to increase from 925 MPa to 1272 MPa when the void content was reduced from 3.5% to 0.2%. Further examination of the data seemingly indicates the negative effect of voids becomes more significant as fiber volume content is increased.

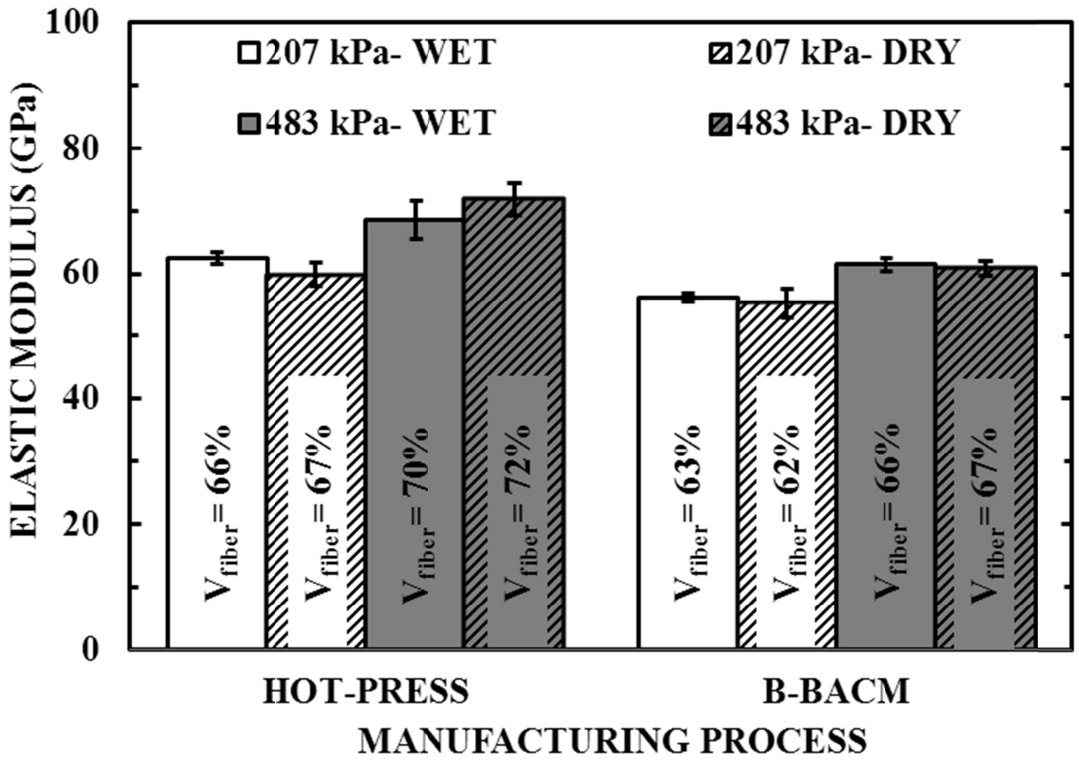

Figure 32- Manufacturing technique, preconditioning, and fiber volume content effect on measured elastic modulus. Note: Error bars represent the 95% confidence interval for n=6.

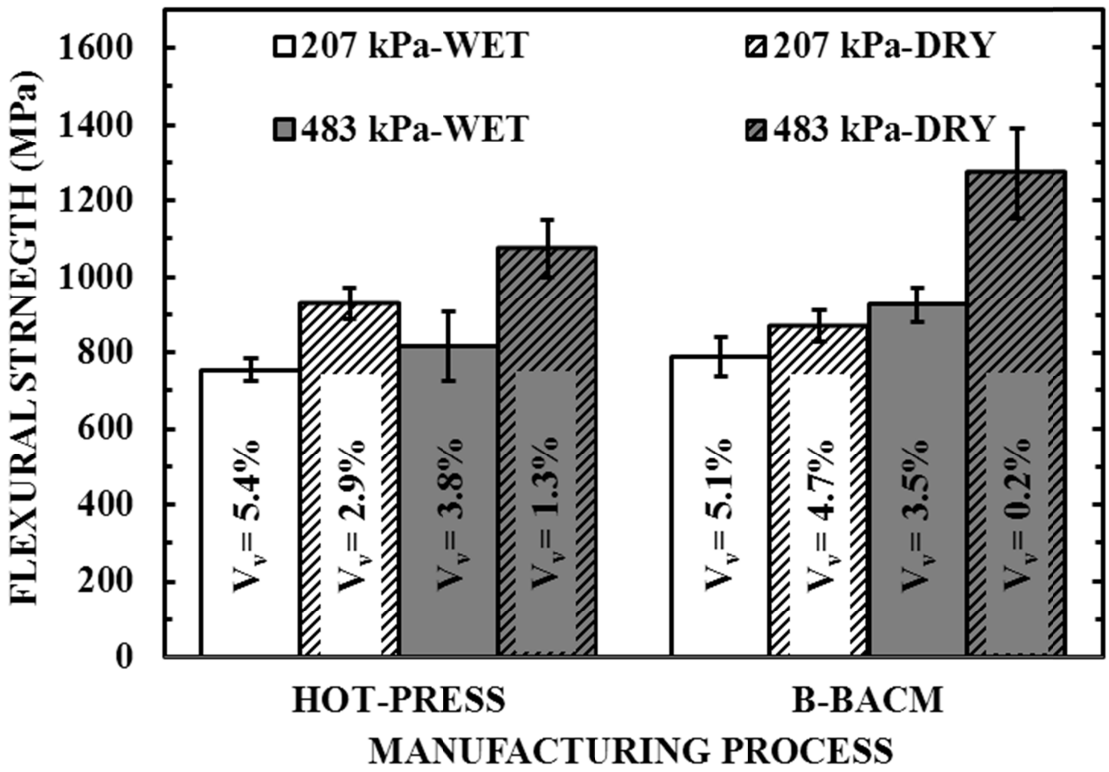

Figure 33- Manufacturing technique, preconditioning, and fiber volume content effect on flexural strength. Note: Error bars represent the 95% confidence interval for n=6.

3.3.4.3 Dry-Conditioned Laminates Void Morphology

SEM images of typical specimens were taken of the dry-conditioned B-BACM and hot-pressed laminates manufactured at 207 kPa and 483 kPa to determine how the void morphology of these laminates compared to those, which were wet-conditioned. Representative SEM images of the dry-conditioned specimens manufactured by the B-BACM and hot-press techniques are shown in Figure 34 and Figure 35 respectively.

The void morphology of the dry-conditioned B-BACM specimen processed at 207 kPa, shown in Figure 34a, is found to be somewhat similar to the wet-conditioned specimen in Figure 28c (voids located in the inter-tow regions). However, upon further examination the inter-tow voids in the dry-conditioned specimen are found to be smaller

than those observed in the wet-conditioned specimen. This observation appears to illustrate how the nucleation of moisture vapor during manufacturing can affect the final void content of a manufactured laminate. This apparent effect of moisture vapor nucleation is further observed when comparing the SEM images of the wet- and dry-conditioned B-BACM specimen processed at 483 kPa found in Figure 29c and Figure 34b. For these images, the voids found in the inter-tow regions of the wet-conditioned specimen are no longer observable in the dry-conditioned specimen. Seemingly, indicating that the voids found in the comparable wet-conditioned specimen was caused solely by moisture nucleation.

The voids in the dry-conditioned hot-pressed specimen processed at 207 kPa and 483 kPa, shown in Figure 35, are found to contain voids in both the inter- and intra-tow regions. In addition, the aspect ratio of the voids observed in the hot-pressed specimen in Figure 35 (≈4.5) are greater than the aspect ratios of the voids in the B-BACM specimen found in Figure 34 (≈1.5). This observation is explained by the fact that the B-BACM specimen fiber volume contents are less than the hot-pressed specimen, which indicates the width of the matrix rich region between plies is less in the hot-pressed specimen. Consequently, the likelihood of a void becoming located on the fiber-matrix interface is expected to increase with fiber volume content, illustrated in Figure 36. This is significant, given that the matrix transfers applied loads by shear to the fibers. Voids on the fiber-matrix interface reduce the shear area, effectively increasing the shear stress in the matrix, which can in turn result in early failure of composite components [27, 65-67]. This hypothesis may explain why the negative effect of voids

on flexural strength seemed to be greater in the laminates studied in this chapter, which had higher fiber volume contents. This hypothesis is explored in detail in Chapter 5.

(a)

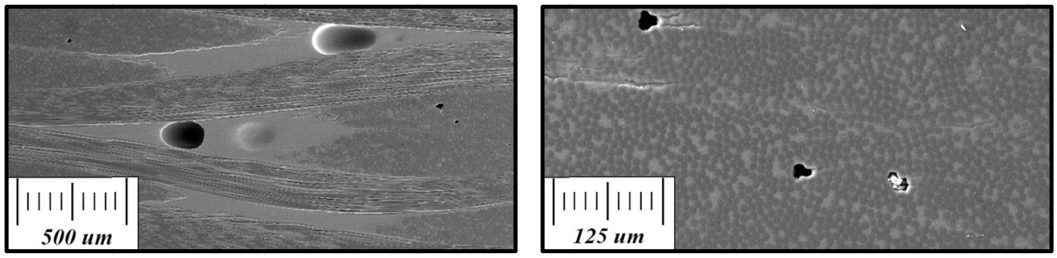

(b)

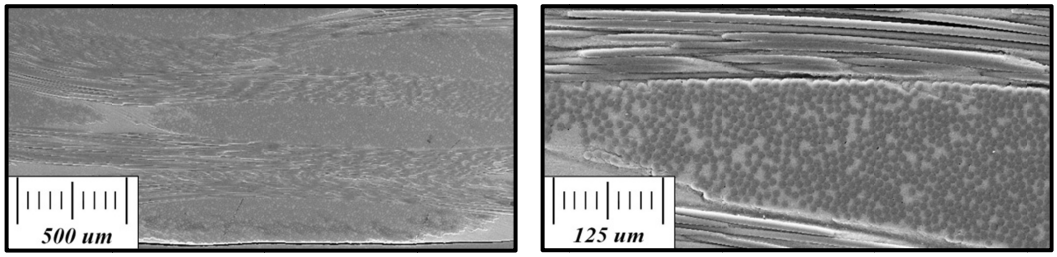

Figure 34- SEM images of the dry-conditioned B-BACM specimen processed at (a) 207 kPa and (b) 483 kPa at 50x, and 200x.

(a)

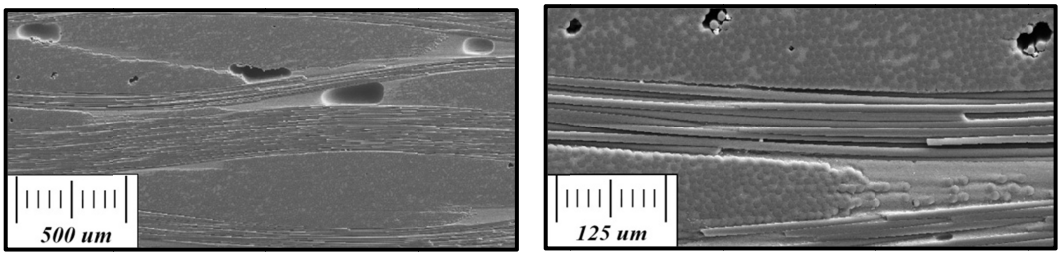

(b)

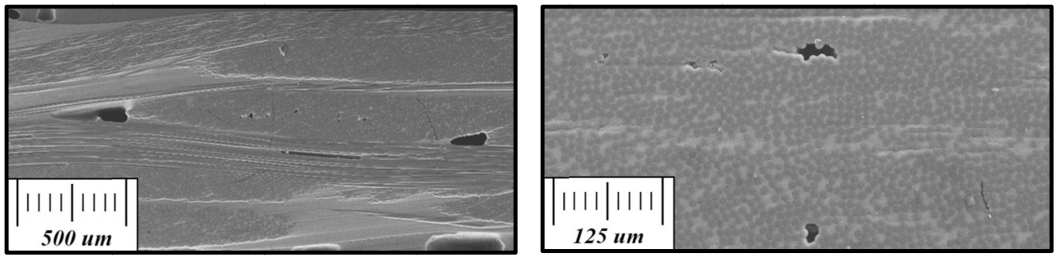

Figure 35- SEM images of the dry-conditioned hot-pressed specimen processed at (a) 207 kPa and (b) 483 kPa at 50x, and 200x.

(a)

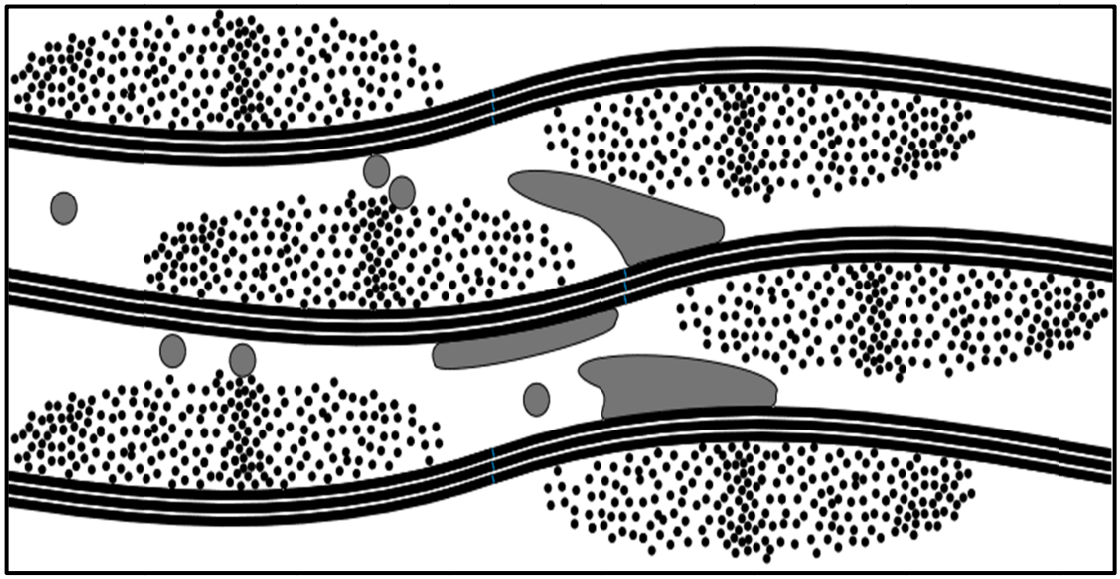

(b)

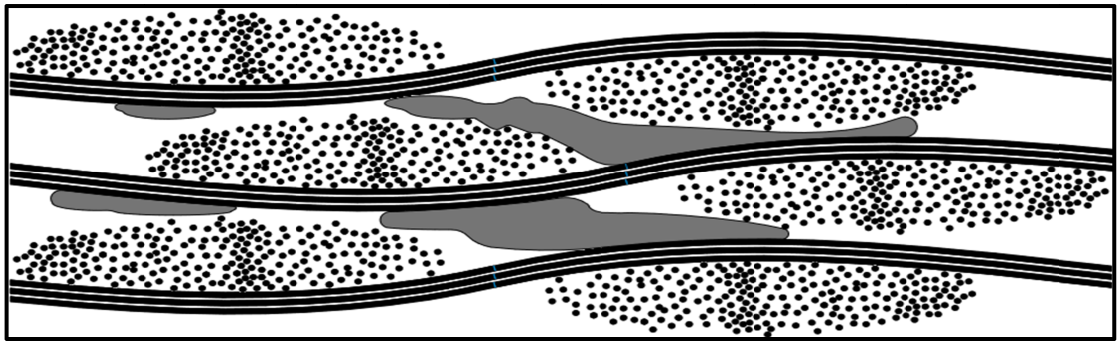

Figure 36- Hypothesized effect of increasing from (a) low to (b) high fiber volume content on the morphology of voids.

3.6 CONCLUSIONS

In this chapter, we have assessed the feasibility of adapting the I-BACM configuration using bleeders and seals to reduce void contents of composite cylinders manufactured at processing pressures of 207 kPa and 483 kPa. The effects of three mold configurations in reducing void contents, and on mechanical properties were reported. It was shown that the fiber volume contents of the cylinders could be increased from 62% to 67% by incorporating a bleeder in the mold. The void contents of the composite cylinders,

manufactured at 483 kPa using the B- and C-BACM variations, were reduced by as much 43% (6.1% to 3.5%) when compared to the I-BACM configuration. When the prepreg was dried, the void content of the cylinders manufactured at 483 kPa using the B-BACM configuration was found to be reduced to 0.2% (a 94% reduction). The morphology of voids present in specimen processed using each of the mold configurations were examined using a SEM. It was found that micro-voids were most effectively removed using mold configurations, which implemented a bleeder.

The mechanical properties of the components were found to increase as expected with fiber volume content. Voids were shown to affect the elastic moduli and failure strengths of the composite components very differently. The elastic moduli of the specimen were found increase in a linear fashion from 53 GPa to 61 GPa as fiber volume content was increase from 58% to 66%. Thus appearing to be unaffected by the presence of voids. The flexure strengths of the specimen were found to increase from 652 MPa to 1272 MPa as fiber volume content increased and void content decreased. In addition, the effect of voids on the flexure strengths appeared to become more significant with increasing fiber volume content. This phenomena is explored in detail in Chapter 5.

4. FORMATION OF VOIDS IN COMPOSITE LAMINATES: COUPLED EFFECT OF HUMIDITY EXPOSURE AND CURE PRESSURE

4.1 INTRODUCTION

Experimental studies available in literature have attempted to address the cause of void formation in composite laminates and have primarily focused on either the effect of curing pressure or moisture content [17-23]. The effect of processing pressure on void formation in laminates laid-up from a glass/epoxy prepreg and manufactured by autoclave/isostatic press was investigated by Boey and Lye [17]. They did this by varying the processing pressure from 100 kPa to 7000 kPa. They found that as the processing pressure was increased from 100kPa to 400 kPa the void content of the laminates dropped content dropped marginally from 38% to 35% [17]. They believed this was a result of the initial pressurization only serving to resist void growth. When the processing pressure was increased beyond 400 kPa void content was dramatically reduced to an asymptotic value below 3% [17].

Following the previous work, Grunenfelder and Nutt [21] explored what effect if any moisture dissolved in resin, caused by humidity exposure, would have on the formation of voids manufactured by both the vacuum-bag-only (VBO) and autoclave processes. They did this by exposing a carbon fiber/epoxy prepreg to 70%, 80%, and 90% relative humidity until moisture saturation occurred. Upon manufacturing they found the void contents of the laminates manufactured by the autoclave were seemingly unaffected by the presence of moisture. This result was attributed to the relatively high processing pressure of the autoclave (609 kPa) causing the moisture in the resin to remain in

solution during manufacturing preventing the formation of voids [21]. For the VBO laminates, which were manufactured at atmospheric pressure (101 kPa), they found moisture content would result in a parabolic void content increase. The above studies were completed while manufacturing laminates at either high or low pressure and have not addressed how moisture will effect void formation in the pressures between 101kPa and 609 kPa. In addition, these studies focused only on the effect of one parameter at a time, i.e. moisture content or pressure and did not considered if the humidity/moisture and pressure parameters are coupled. Therefore, it is of interest to explore the relationship between processing pressure and moisture content in the formation of voids and determine if the currently available models are able to cope with both at the same time.

Upon reviewing the models available in literature which attempt to explain void formation, one finds that they are predominantly centered around a diffusion-based void growth model proposed by Kardos et al. which predicts final average void diameter [18, 22]. This model is based on the assumptions that (i) voids are spherical, (ii) voids form due to moisture in the resin diffusing into air voids, (iii) voids occur in resin rich regions are not affected by fibers in the material. Because of these assumptions, the Kardos model predicts voids will grow, i.e. void content will increase, until the internal pressure of the void is equal to that of the surrounding resin. Therefore, according to Kardos et al. [18, 22], the final average diameter of a void present in the resin is a function of the resins' moisture content, temperature profile, processing time, and pressure profile.

As an extension to the Kardos model, Boey and Lye [17] suggested that by calculating the volume of the predicted void and using a characteristic volume element the void content of any particular laminate could be determined provided the processing conditions are known. This approach was used successfully by Grunenfelder and Nutt [21] for laminates manufactured by vacuum bag only (VBO) prepregs which were processed at different initial moisture contents and constant processing pressure. However, the approach has not been used in situation where the processing pressure is varied.

There are a number of shortcomings in the diffusion based void content prediction model suggested by Boey and Lye [17] which limits its ability to be used in its current state for all circumstances. The first is the moisture content in the resin, which is caused by the diffusion of environmental moisture into the resin, is modeled to occur instantly and is not time dependent. Thus, depending on the environmental humidity history of the storage location the model can either over or under predict the moisture content of the resin, which can drastically affect predicted void content. The second is the model assumes the resin pressure is equal to the applied pressure. Therefore, the model does not consider the effect of the fiber bed carrying a portion of the applied load [23, 68-72]. Finally, the model disregards the escape of voids from the laminate as a result of resin outflow, which can be significant [62, 73]. In this chapter, the combined effect of humidity exposure and processing pressure on void formation is explored experimentally. In addition, the void prediction model suggested by Boey and Lye [17] is improved to distinguish the difference between the applied and resin pressure, and to account for both fiber bed effects, and time dependent moisture absorption.

4.2 MATERIALS AND METHODS

4.2.1 FABRICATION PROCEDURE

The specimens in this chapter were fabricated from TenCate® BT250/7781, a glass/epoxy prepreg. Eight-ply laminates (L=152mm W=152mm) were manufactured by the hot-press technique using curing pressures of 69 kPa (10 psi), 207 kPa (30 psi), 345 kPa (50 psi), and 483 kPa (70 psi). To determine the effect of moisture on laminate void formation, the prepreg plies for each laminate were: (i) unconditioned (direct from storage), (ii) conditioned at 25% relative humidity and, (iii) conditioned at 99% relative humidity for 24hrs at 25°C to induce different initial levels of moisture. After conditioning, the plies were laid-up and the laminates were manufactured using the cure cycle shown in Figure 37, which consists of a 1°C/min ramp from 25°C to 121°C, a two-hour isothermal hold at 121°C, and a 5°C/min ramp down to 60°C.

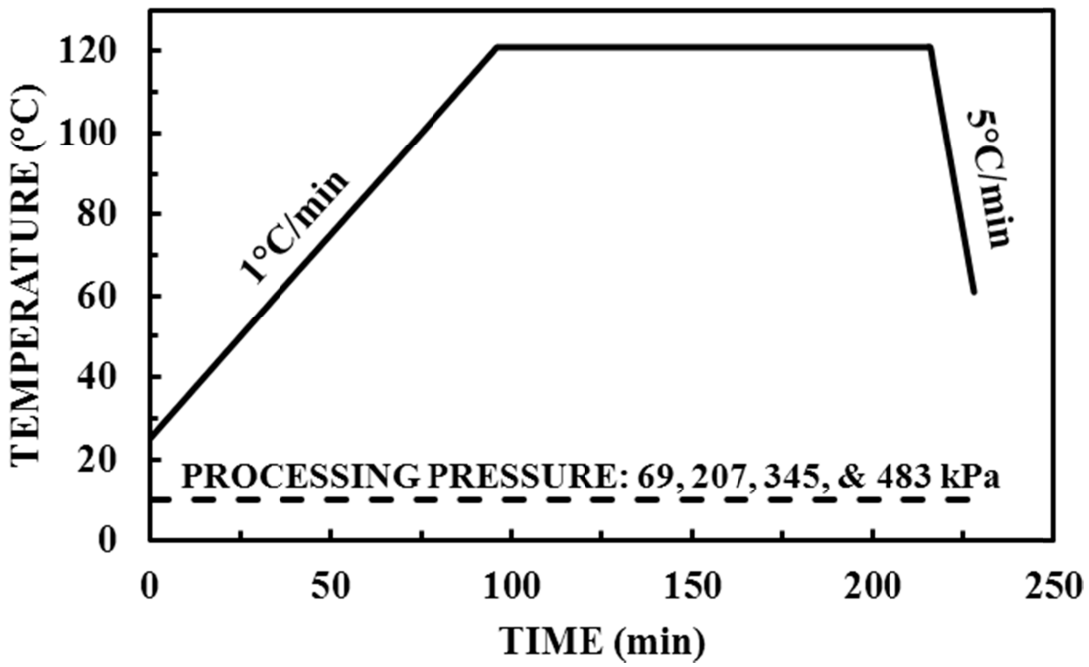

Figure 37- Temperature cure profile used to manufacture the laminates in this chapter.

4.2.2 MOISTURE CONTENT

The moisture contents of the laminates in this chapter were determined using a Computrac Vapor Pro® moisture analyzer. The analyzer functions by circulating a dry carrier gas across a heated sample and measuring the relative humidity of the outflowing gas. Combining the humidity data, gas flow rate, and sensor temperature, allows for the moisture transmission rate from the sample to be determined. Integrating this data with time allows the total moisture mass of the sample to be found. For this work, the gas flow rate was set to 75 mL/min, the samples were heated to 121°C, and the moisture content measured until the moisture transmission rate decreased below 0.5 µg/s. Figure 38 and Figure 39 show how the moisture in a typical prepreg sample is transmitted during the experiment outlined above.

The time-dependent moisture content of the prepregs was determined by exposing prepreg strips (L=31.8mm W=25.4mm) to environments of 99%, 45%, and 25% relative humidity at 25°C and recording their moisture contents with time until moisture saturation occurred. Using the measured time-dependent moisture contents, the 1-D Fickian moisture diffusion model [74],

$$G = 1 - \exp\left[-7.3\left(\frac{Dt}{2h^2}\right)^{0.75}\right], \tag{8}$$

$$M_c = G(M_m - M_i) + M_i, \tag{9}$$

was fit to the data. Thus allowing, the diffusivity and the saturation moisture contents of the three humidity levels to be determined. In addition, the use of these parameters

allows the transient moisture content of the prepregs to be predicted assuming the environmental humidity level and exposure time are known.

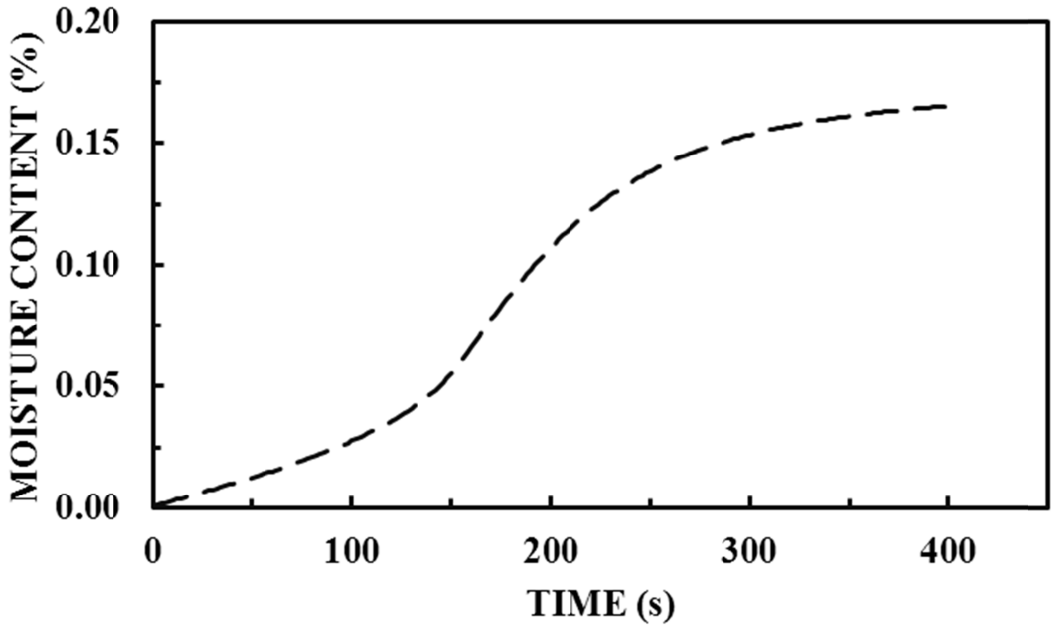

Figure 38- Total moisture transmission of a representative prepreg specimen.

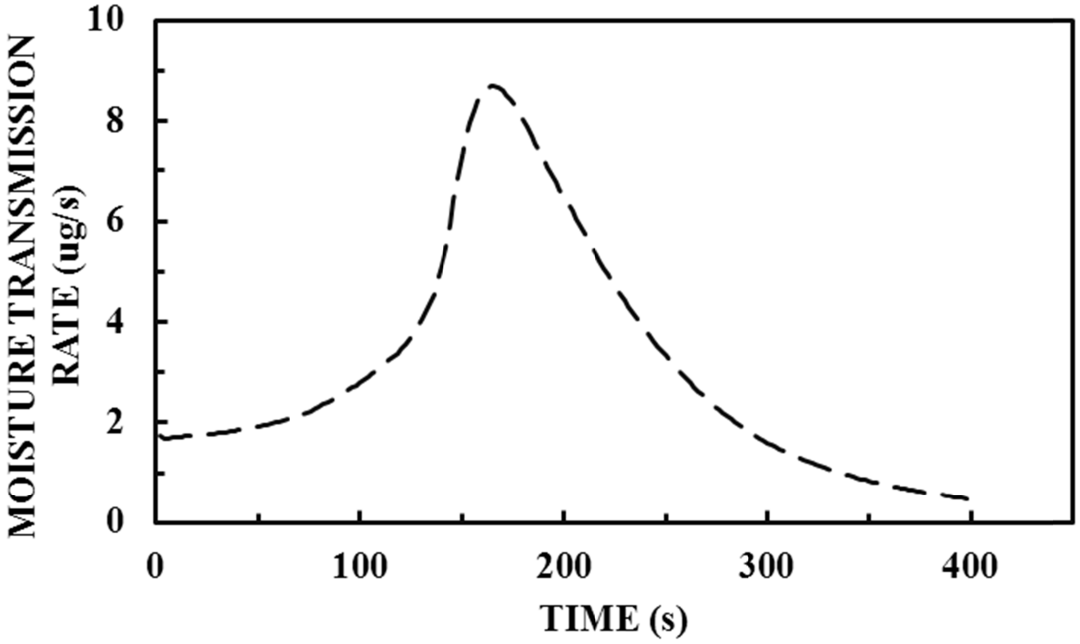

Figure 39- Time dependent moisture transmission rate of a representative prepreg specimen.

4.2.3 VOID CONTENT MEASUREMENT

From each manufactured laminate, eight rectangular specimen (L=31.8mm W=12.7mm) were cut to allow for the void contents to be determined using the technique outlined in ASTM D2734-09, which is capable of resolving void contents to within ±0.22% [51]. Thus, each composite specimen's density ($\rho_{specimen}$) was determined by suspending each in a solution of Cargill Labs 2.49g/cc Heavy Liquid that had been diluted by water. Similarly, the matrix density (ρm) was determined by suspending void free matrix specimens in a water/glycerol solution. The subsequent measurement of the solution density, using a fluid pycnometer, allowed for the accurate measurement of the bulk density of each specimen. The fiber reinforcement density (ρf) was alternatively determined by the use of a helium pycnometer. From these experiments, the densities of the matrix and fiber reinforcement were found to be 1.224 g/cc and 2.635 g/cc respectively. Next, the weight fractions of the matrix and fiber for each specimen were found using the burn-off method described by ASTM D2584-08. Then, using the constituent densities and weight fractions, the void contents of the specimens were calculated using Eq. (10).

$$V_v = 100 - \rho_{specimen}\left(\frac{W_{fiber}}{\rho_{fiber}} + \frac{W_{matrix}}{\rho_{matrix}}\right) \quad (10)$$

4.3 RESULTS AND DISCUSSION

4.3.1 MOISTURE DIFFUSION IN UNCURED PREPREGS

The moisture content of TenCate® BT250/7781 for different humidity environments with the progression of time and the 1-D Fickian model fit is shown in Figure 40. It is

found that the diffusion of moisture into and out of the prepreg is Fickian with a diffusivity of 4.01E-2mm^2/h indicating that moisture can be easily exchanged between the studied material and its environment. For example, the prepreg used in this chapter reached the saturation moisture contents for each of the three humidity environments studied after just 10 hours of exposure. The saturation moisture contents varied significantly and were found to be 0.35%, 0.15%, and 0.11% by weight when exposed to 99%, 45%, and 25% relative humidities respectively and agree well with the results reported elsewhere [21, 75]. The above findings illustrate the importance of not only carefully controlling the manufacturing environment but also the storage environment of prepregs. This is due to the relatively high diffusivity of the prepreg resin, in which short exposure to a varying humidity environment can result in significant moisture absorption. Since resin moisture content can have a drastic impact on the quality of a composite component, any void content prediction model should incorporate a transient moisture content prediction capability [17, 21, 62].

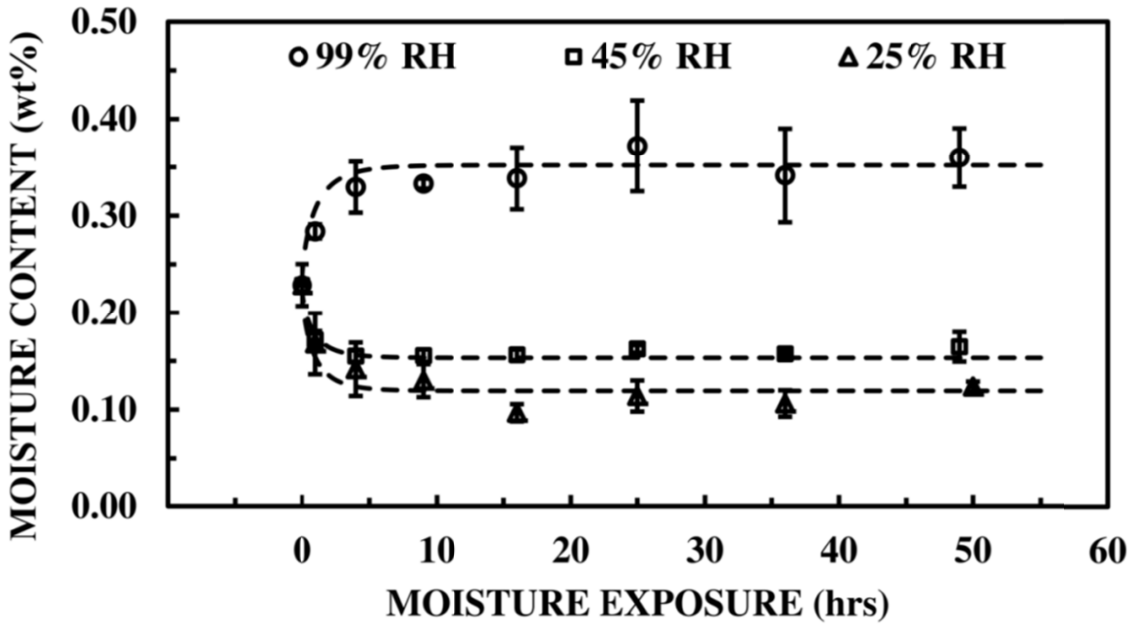

Figure 40- Moisture content of TenCate® BT250/7781 exposed to humidity environments of 99%, 45%, and 25% relative humidity at 25°C until saturation was reached. The fit of the Fickian 1-D diffusion model, i.e. Eq. (9), is also shown. Note: Error bars represent the 95% confidence interval for n=3.

4.3.2 HUMIDITY AND PRESSURE EFFECT ON VOID FORMATION

The effect of exposing the laminates to different environmental humidities as well as the effect of increasing cure pressure is presented in Figure 41. From the figure, it becomes obvious that the presence of moisture in the laminate before processing is of chief importance. For example, the void contents for the laminates processed at 69 kPa were found to increase from 2.79% to 4.94% as the initial moisture content of the laminate increased from 0.11% to 0.35%. This finding was not surprising and is explained by the higher moisture content found in the laminates diffusing into the voids which is vaporized during curing resulting in an exponential increase of void pressure with temperature during processing which cause the voids to grow [17, 18, 21, 22, 33].

However, as the processing pressure was increased for all humidity cases the void contents for each laminate were found to approach an asymptotic void content of

approximately 1.6%. This was unexpected as the model suggested by Boey and Lye [17] and used by Grunenfelder and Nutt [21] infers that void content will decrease to 0% as processing pressure is increased. Thus, it is believed a yet unreported physical phenomenon has been observed. Examination of the SEM micrographs, shown in Figure 42, seems to give clear evidence as to the cause of the observed phenomenon. The fiber tows appear to be becoming increasingly packed as processing pressure/fiber volume content is increased. This packed structure is thought to be carrying a portion of the applied consolidation load and limiting the pressure developed in the resin [23, 68-72]. In addition to carrying the applied load, this packed microstructure reduces the permeability of the fiber bed resulting in the less mobile macro-voids becoming trapped in the laminate [45, 52, 53, 64, 76, 77].

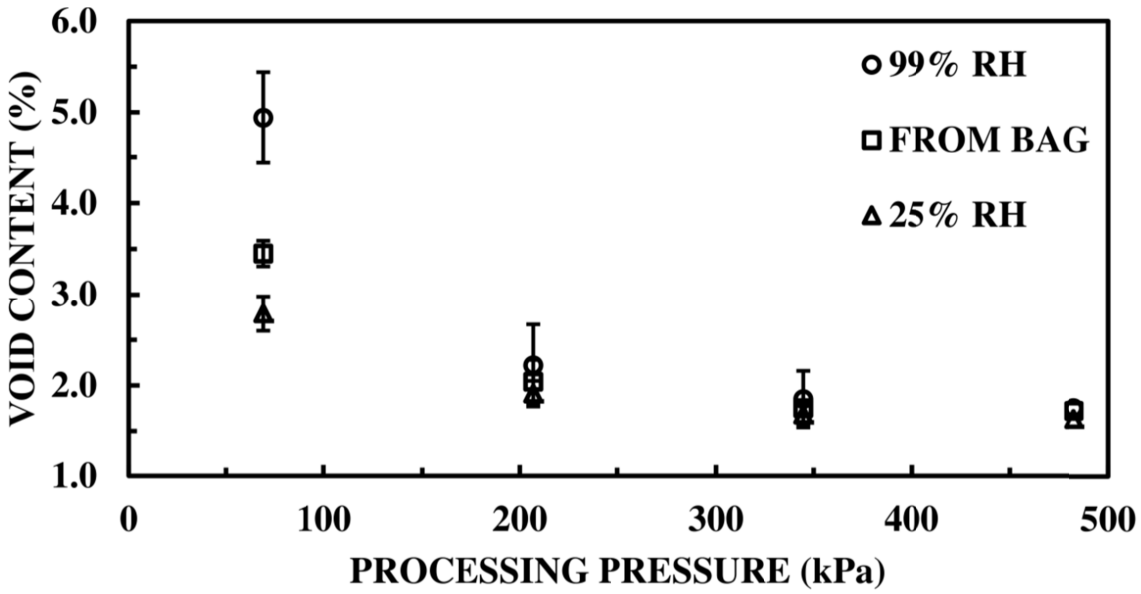

Figure 41- Effect of humidity environment and processing pressure on the formation of voids. Note: Error bars represent the 95% confidence interval for n=8.

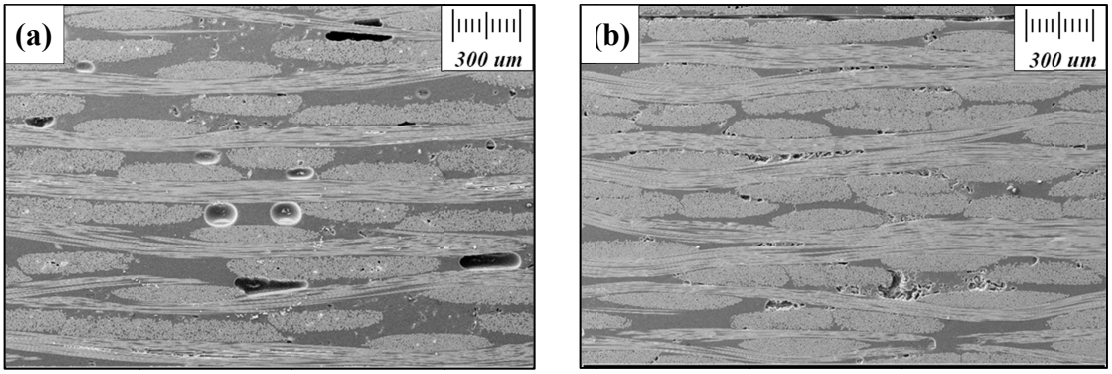

Figure 42- Fiber bundle hierarchy of laminates manufactured at (a) 69 kPa and (b) 483 kPa whose prepreg plies were conditioned at 25% RH for 24 hrs.

4.4 PROPOSED MODEL

4.4.1 MODEL DEVELOPMENT

As a result of the above findings and due to the seemingly incomplete nature of the model used by Grunenfelder and Nutt [21] an analytical model was developed to predict final laminate void content as a function of processing pressure and time-dependent resin moisture content. The model is based on the diffusion void growth model of Kardos et al., which assumes voids grow due to the diffusion of moisture from the surrounding resin [18, 22]. Thus, temperature and pressure are the driving forces behind the diffusion process and will determine whether discrete voids grow or are reduced in size [16-18, 22, 34, 45]. Void growth is expected to occur when the internal void pressure exceeds that of the surrounding resin. Thus, a pure air void is likely to collapse under an applied pressure but it is important to note that the internal pressure of a void with moisture will increase exponentially with temperature making void growth much more likely to occur [17-19, 22, 33]. Therefore, higher processing temperatures and lower processing pressures will facilitate the growth of voids.

To simplify the void growth analysis, Kardos et al. [18, 22] assumed that void growth occurs in a pseudo-homogenous medium which resembles the mass diffusion bubble growth [78]. The details of the analysis and a complete list of the assumptions made are presented elsewhere [18, 22]. The equation governing the final void diameter is

$$d_v = \frac{4R_g T\sqrt{D\,t}(S\,RH^2 - C_{sat})}{M_{H_2O}\,P_g} \tag{11}$$

where the coefficient of resin solubility is obtained from a parabolic fit to the saturation moisture content vs. relative humidity [18, 21, 22, 75]. Boey and Lye [17] suggested that final void content, V_v, could be determined via converting the void diameters predicted by Eq. (11) into void volumes and dividing them by characteristic volume element as shown in Eq. (12).

$$V_v = \frac{\pi}{6V_m}\left(\frac{4R_g T\sqrt{D\,t}(S\,RH^2 - C_{sat})}{M_{H_2O}\,P_g}\right)^3 \tag{12}$$

It is important to note that the term "*S RH*^{2}", in Eq.'s (11) & (12), gives the saturation moisture content for an environment maintained at a constant humidity state and does not account for variable humidity exposure [18, 21, 22]. Therefore, the incorporation of Eq. (9) into the moisture content term in Eq.'s (11) & (12) would allow for a more versatile model. In addition, the pressure term in the above equations assume the applied pressure is the same as the resin pressure in the laminate, which is not necessarily valid as the resin pressure can be much less [23, 68-72]. Furthermore, because of the potential for high fiber volume fractions, the fiber bed permeability is reduced causing the macro-voids becoming trapped in the laminate resulting in an

asymptotic minimum void content [45, 52, 53, 64, 76, 77]. Considering the experimental data as well as the above discussion, it is suggested that the void prediction model should be updated as,

$$V_v = \left(\frac{A_v * M_c + B_v}{P_g^{(1-P_R)}}\right)^3 + V_{min} \quad (13)$$

where the constant terms in Eq. (12) have been condensed into two variables, A_v & B_v, and two new terms, the pressure reduction coefficient, P_R, and the manufacturing processes asymptotic minimum void content, V_{min}, have been added.

4.4.2 MODEL FIT TO EXPERIMENTAL DATA

The fit of Eq. (12) to the experimental data is shown in Figure 43. It is interesting to note that the fit of the model used by Grunenfelder and Nutt [21] appears to be very good. However, this high quality fit only occurs if the experimental data is examined at the four pressure levels independently. If all the data is considered as a whole, the model is unable to accurately predict the void content of the laminates at any point indicating that the effect of humidity exposure and cure pressure on void formation is indeed coupled. The fit of Eq. (13) to the experimental data is shown in Figure 44 and the parameters used to obtain the fit are found in Table 1. The model proposed in Eq. (13) is found to accurately predict how the final void content of the laminates vary with humidity/pressure which Eq. (12) was unable to do. The fit of the model shows that the resin pressure does not necessarily increase proportionally with processing pressure. This conclusion is supported by the fact that the pressure reduction coefficient, P_R, in Table 1 is found to be 0.055 indicating that the resin pressure is reduced by as much as 12% at a processing pressure of 483 kPa, which diminishes its ability to cause voids to

collapse. In addition, an asymptotic void content of 1.64% is indicated by the model, which correlates well with the experimental data.

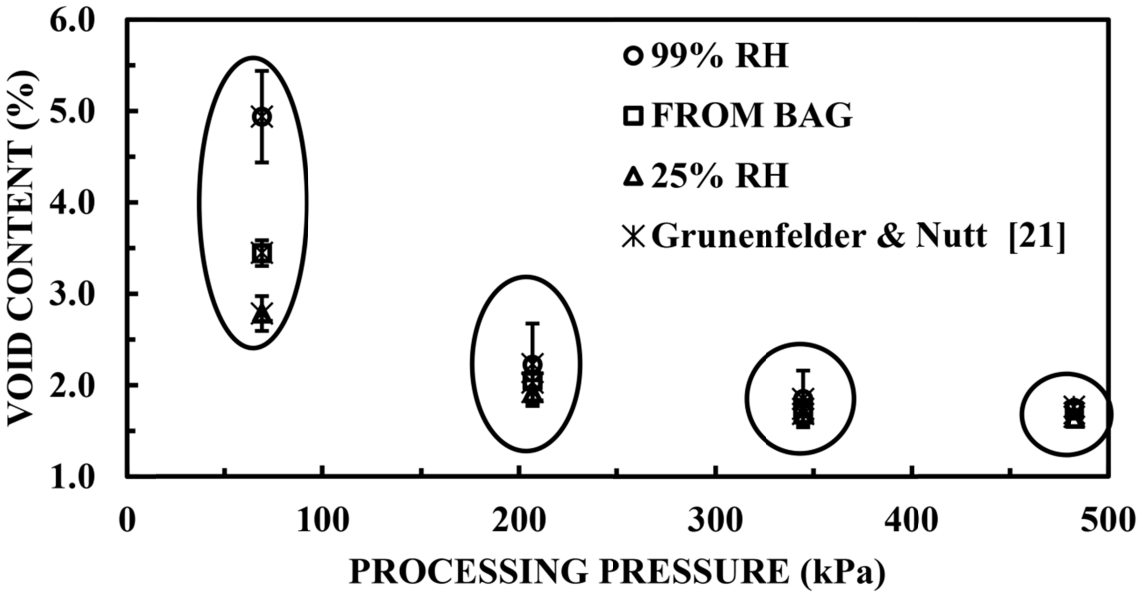

Figure 43- Fit of the model Grunenfelder and Nutt [21] used, Eq. (12), when fit to the data points at each cure pressure separately along. Note: The model was unable to be fit to the entire data set. Note: Error bars represent the 95% confidence interval for n=8.

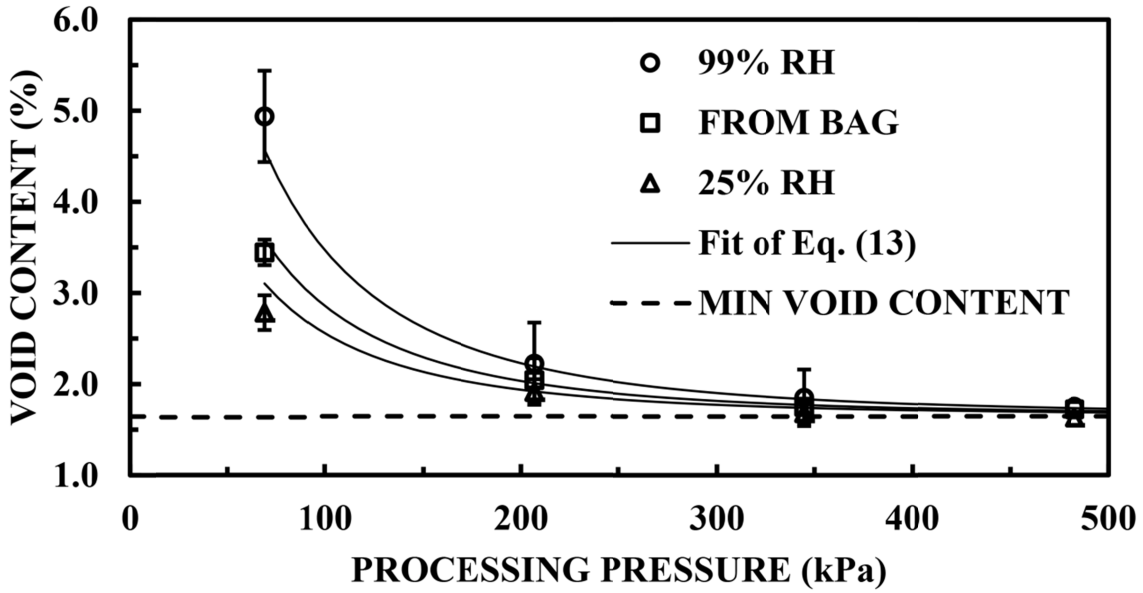

Figure 44- Fit of the model proposed in this chapter, Eq. (13), to the complete data set. Note: The model is capable of predicting void contents at all pressure/humidity levels and the error bars represent the 95% confidence interval for n=8.

Table 1: Fitting parameters of Eq. (13) for the experimental data.

P_R	V_{min}	A_v	B_v
0.055	1.64	3.16	1.32

4.4.3 MODEL VALIDATION

The proposed model, Eq. (13), was found capable of accurately predicting the void contents of the laminates used in its development. Nevertheless, further validation of the model was required. Therefore, two additional eight-ply laminates were manufactured after having their prepreg plies cycled through one of the two humidity cycles shown in Figure 45. During each of the humidity cycles, the moisture content of the prepregs were measured every two hours, as shown in Figure 46, and compared to the moisture content predicted by the 1-D Fickian model using the diffusivity and saturation moisture contents previously discussed. The comparison shows the utility of using the Fickian model to predict the transient moisture content of a laminate as it is exposed to a known humidity environment. Indicating, the moisture content of a prepreg at the time of manufacturing can be predicted if the humidity level and time of exposure is known. Therefore, the incorporation of the Fickian model into a void prediction model makes it much more versatile. At the end of the humidity exposure cycles, the laminates were laid-up and processed at a pressure of 69 kPa using the same cure cycle as the previous nine laminates. Using both the final predicted and measured moisture contents, the two laminates void contents were predicted by Eq. (13) using the parameters in Table 1. The void content predictions using these moisture contents are compared to the measured void contents of the validation laminates in Table 2. It is shown that the void contents predicted by the using either the predicted or measured moisture contents lie within the uncertainty of the measured void content.

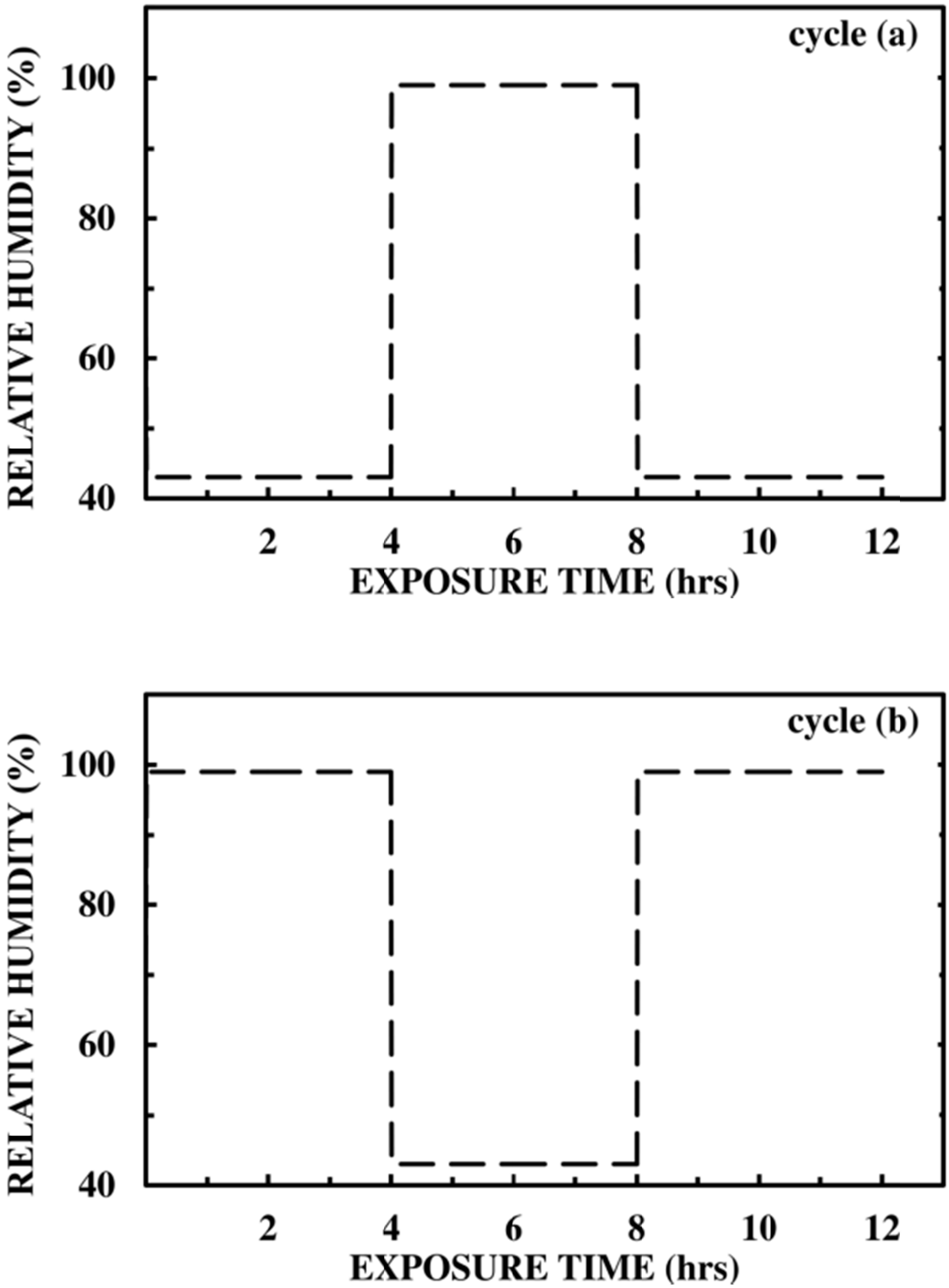

Figure 45- The two humidity exposure cycles of the prepreg plies which composed the laminates used to verify the proposed model. Note: The temperature at the time of the exposure cycles was 25°C.

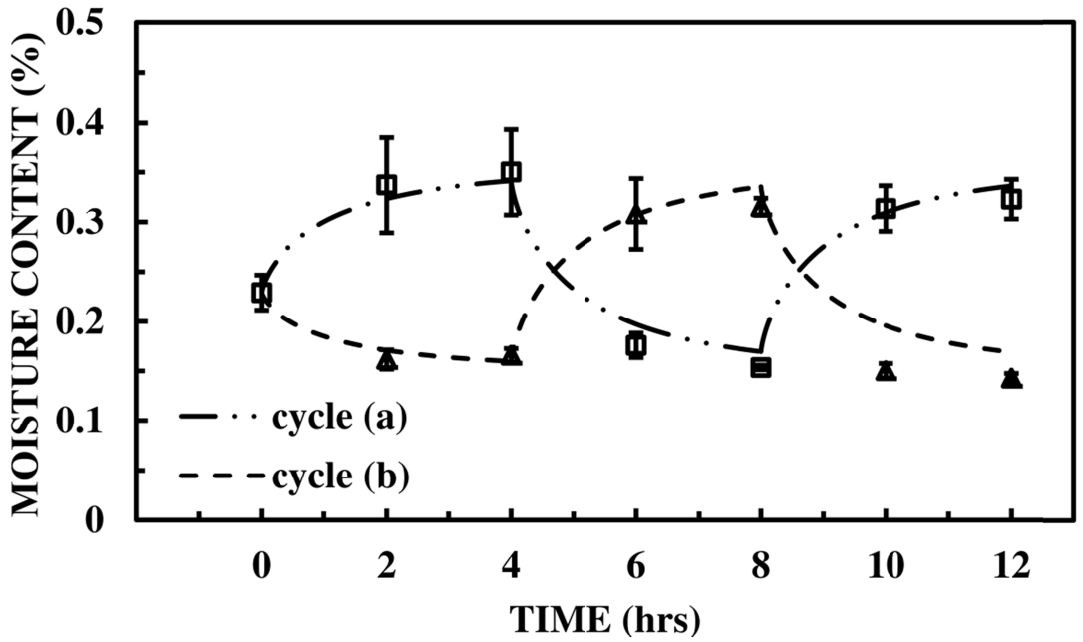

Figure 46- Moisture content of the prepreg plies composing the verification laminates during their humidity cycles shown with the predicted moisture content using Eq. (9). Note: Error bars represent the 95% confidence interval for n=3.

Table 2: Predicted void contents compared to the actual void content of the laminates exposed to separate humidity cycles.

Humidity Cycle	Predicted Void% Using M_c from		Experimentally Determined Void%
	Fickian Model	Measured	
(a)	3.10	2.92	3.27±0.42
(b)	4.75	4.58	4.65±0.69

4.5 CONCLUSIONS

The motivation behind this work was to determine the coupled effect of humidity exposure and cure pressure on void formation in laminates fabricated from a glass/epoxy prepreg and manufactured by hot-press. The moisture content of the prepreg plies were found to vary depending on the environments relative humidity and the time of exposure. The diffusion of moisture into and out of the prepreg was observed to behave as predicted by 1-D Fickian diffusion. In addition, the diffusivity was found to be 4.01E-2mm^2/h indicating that a prepreg ply subjected to environmental

humidity would rapidly approach its saturation moisture content for that humidity level. In this chapters experiments, moisture saturation occurred after 10 hrs for all humidity levels studied. This is important because the maximum observed void content occurred in the laminates whose pregreg plies had been exposed to high humidity conditions regardless of processing pressure. Conversely, the lowest void contents were observed in those laminates whose prepreg plies had been dried in a low humidity environment. Thus, the relative humidity in which laminates fabricated from prepreg are prepared and their moisture content at the time of manufacturing is significant.

The void contents in the laminates manufactured for this chapter were found to reduce to an asymptotic void content of 1.64% as processing pressure was increased regardless of initial laminate moisture content. This phenomenon was explained by the structure of the fiber bed as processing pressure/fiber volume fraction was increased. Namely, as fiber volume fraction was increased the fiber tows were observed to have an increasingly ordered microstructure. Due to this, the fiber bed began to carry an increasingly larger proportion of the applied load and its permeability was reduced. Thus, the resin pressure is becoming reduced and the less mobile macrovoids are trapped in the laminate.

Due to the coupled effect of humidity exposure and cure pressure on the formation of and final content of voids in the laminates, an improvement to the void content prediction model proposed by Boey and Lye [17] is proposed. The modified model incorporated the 1-D Fickian moisture diffusion model, a pressure reduction term, and an asymptotic void content. The model was found to be capable of predicting the void contents of two independent laminates to within experimental uncertainty.

5. MECHANICAL PROPERTIES OF COMPOSITE LAMINATES: COUPLED EFFECT OF MICROVOIDS AND FIBER CONTENT

5.1 INTRODUCTION

One of the most common manufacturing defects found in composite materials are voids, which are known to adversely affect the mechanical properties of composite laminates [19, 24, 25]. The general consensus among composite researchers is that voids act as crack initiation planes and, if located on the fiber-matrix interface, limits the ability of the matrix to transfer applied loads to the fiber reinforcement [17, 26-30]. Therefore, as one would expect the failure strength of a composite is significantly affected by the presence of voids but the in-plane elastic modulus is not because it is primarily dependent on fiber property [28-30]. Judd and Wright [14] conducted an exhaustive survey of twenty-four articles and found that depending on the article the flexural, tensile, compressive, and interlaminar shear strengths will be reduced by at least 3% for each volume percent of voids present in the composite. However, one of the most startling results from Judd and Wright [14] is they show in some cases reductions as high as 30% occur for each volume percent of voids. Peculiarities such as these are widely reported in the available literature and tend to explain why the aerospace industry's current rule of thumb is to only accept structural composite components that contain less than 1% voids and nonstructural components with less than 5% [17, 19, 31, 32].

Upon review of the experimental studies available in literature to distinguish the effect of voids on the various failure strengths of composite materials, one finds they have all

focused on void content alone and have by default assumed the effect of fiber volume content to be insignificant [15, 19, 24, 25, 31-35]. For example, Almeida and Neto [31] examined the effect of voids on the flexural strength of woven carbon/epoxy laminates. Four laminates were manufactured with void contents ranging from 1% to 6%, by controlling static resin pressure during manufacturing, while maintaining a fiber volume fraction of approximately 61%. Subsequent flexural testing of the laminates found the flexural strengths to be reduced by as much as 16% at the void content of 6%. They suggested this reduction was caused by matrix fractures occurring at voids lying on the fiber-matrix interface [31]. In addition, they proposed that for their material a critical void content of 3% must be surpassed before voids will begin to significantly affect the strength of a composite component. More recently, Chambers et al. [15] studied how the flexural strength of unidirectional carbon fiber laminates are affected by the presence of voids. They achieved void contents ranging from 2% to 3% by manufacturing laminates at vacuum levels of 70%, 80%, 90%, 95%, and 100% of the manufacturer's recommended vacuum pressure. Later flexural testing, found that laminates manufactured with 3% void content were reduced by 20% which conflicts directly with the 3% critical void content concept put forth by Almeida and Neto [31]. Because of this glaring discrepancy, Chambers et al. [15] concluded the critical void concept was too simplistic and that void morphology most likely drives the reduction in flexural strength [15].

A study by Wisnom et al. [36] investigated the effect of void morphology on the interlaminar shear strength (ILSS) of carbon/epoxy laminates by varying the aspect ratio of the voids in the laminates from 1-4 while maintaining a constant fiber volume

content. The voids were created and controlled by embedding PTFE monofilaments of various lengths into the laminates during manufacturing. Results from the flexural testing of these laminates found that their interlaminar shear strengths was reduced by as much as 25% and scaled directly with void aspect ratio.

Upon reviewing the models available in literature which attempt to explain the various effects of voids on the failure strength of composite laminates, one finds a number of models [24, 31, 32]. These models tend to suggest the presence of voids will result in either an exponential or a linear decrease in the failure strength of composite components. One of the most effective models currently used to explain failure strength reduction with increasing void content was originally developed for porous ceramic cubes by Ryshkewitch [79]. In this model, the extent of a voids effect is governed by a property reduction coefficient which was at the time of its development was believed to be constant [79]. This supposition was later disproven, first by Knudsen [80] and later by Brown et al. [81] who showed that void content alone could not fully explain the failure strength reduction in ceramic cubes. In their paper, it was concluded that void morphology and orientation were just as important as the void content of the studied specimen. The model was first applied to composites by Ghiorse [32] who found it could accurately predict the strength of a composite laminate if the reduction coefficient was first found empirically. Since its first use for composites, a number of researchers have successfully used it to explain observed reductions in failure strength [19, 31, 33, 82] .

There are a number of shortcomings in the model as presented by Ghiorse [32] for use in composites. The first is that at its core it is an empirical model that relies on an

exhaustive experimental investigation of the composite component in question to determine the appropriate reduction coefficient value. If the constituents of the component are altered in any way, the coefficient must once again be determined making the models use potentially impractical due to the high cost of the required experimental investigations [19, 31, 32, 83]. Second, the model does not consider the void morphological effects on the failure strength of the component as Brown et al. [81], Chambers et al. [15], and Wisnom et al. [36] observed. In this chapter, the influence of void content on the tensile properties of composite laminates with increasing fiber volume and void contents is explored. This was achieved by manufacturing laminates with four different fiber volume contents and three void contents. From these laminates, a relationship is found between fiber volume content and the effect of voids on the tensile strength of composite components. Due to this discovered relationship, the empirical model as presented by Ghiorse [32] is enhanced allowing the effect of voids to be determined analytically without requiring significant experimental investigations.

5.2 MATERIALS AND METHODS

5.2.1 FABRICATION PROCEDURE

All the specimens in this chapter were fabricated from TenCate® BT250/7781, a balanced eight-harness glass/epoxy prepreg. Eight-ply laminates (L=152mm W=152mm) were manufactured by the hot-press technique using curing pressures of 69 kPa (10 psi), 207 kPa (30 psi), 345 kPa (50 psi), and 483 kPa (70 psi). The prepreg plies for each laminate were: (i) unconditioned (direct from storage), (ii) conditioned at 25% and, (iii) conditioned at 99% relative humidity for 24hrs at 25°C to induce three

different void content levels and a constant fiber volume content for each of the processing pressures. After conditioning, the plies were laid-up and the laminates were manufactured using the cure cycle shown in Figure 47. This cycle consists of a 1°C/min ramp from 25°C to 121°C, a two-hour isothermal hold at 121°C, and a 5°C/min ramp down to 60°C at which point the laminate was removed from the press.

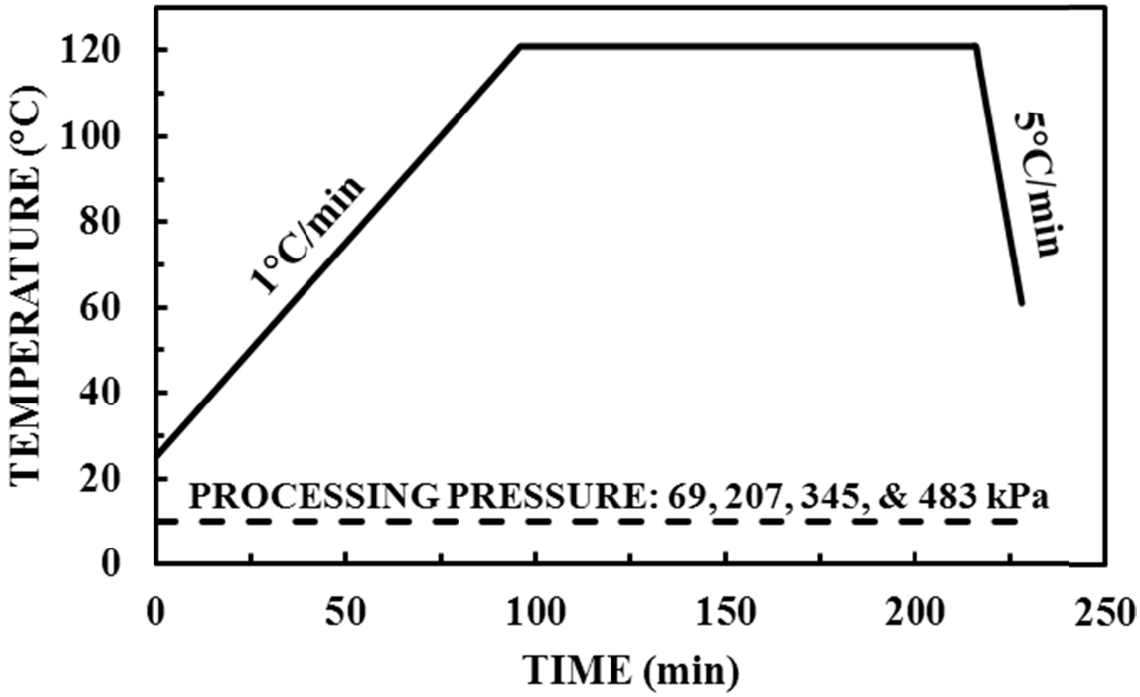

Figure 47- Cure profile used to manufacture the laminates in this chapter. Note: Three laminates were manufactured at 69 kPa, 207 kPa, 345 kPa, and 483 kPa producing a total of 12 laminates.

5.2.2 VOID AND FIBER VOLUME CONTENT MEASUREMENT

From each manufactured laminate, eight rectangular specimen (L=31.8mm W=12.7mm) were cut to allow for the void contents to be determined using the technique outlined in ASTM D2734-09, which is capable of resolving void contents to within ±0.22% [51]. Thus, each composite specimen's density was determined by suspending each in a solution of Cargill Labs 2.49g/cc Heavy Liquid that had been

diluted by water. Similarly, the matrix density was determined by suspending void free matrix specimens in a water/glycerol solution. The subsequent measurement of the solution density, using a fluid pycnometer, allowed for the accurate measurement of the bulk density of each specimen. The fiber reinforcement density was alternatively determined by the use of a helium pycnometer. From these experiments, the densities of the matrix and fiber reinforcement were found to be 1.224 g/cc and 2.635 g/cc respectively. Next, the weight fraction of the matrix and fiber for each specimen was found using the burn-off method described by ASTM D2584-08. Then, using the constituent densities and weight fractions, the void contents of the specimens were calculated using Eq. (14).

$$V_v = 100 - \rho_{specimen}\left(\frac{W_{fiber}}{\rho_{fiber}} + \frac{W_{matrix}}{\rho_{matrix}}\right) \quad (14)$$

In addition to the bulk void content, the morphology of the voids present in the laminates was examined using a Zeiss NEON FEG-SEM. Four specimens from each of the twelve laminates were embedded in a quick cure acrylic resin and polished with grit sizes ranging from 15 μm to 1.9 μm using three successive steps. Afterwards, the samples were sputter coated with gold/palladium to prevent sample charging and cross-sectional images were acquired at 75x.

5.2.3 CHARACTERIZATION OF LAMINATE TENSILE PROPERTIES

To determine the effect of voids on composite components, the tensile modulus and strength of this chapters composite laminates were determined. This was accomplished by cutting sixteen rectangular tensile test specimens with the reinforcing fibers oriented

along the length and width of the specimen, using an IsoMet precision diamond saw from each of the twelve manufactured laminates. This resulted in 192 specimens available to be tested. To each of these specimens, composite tabs were attached to insure no grip damage occurred during testing. The specimen geometry and configuration used is shown in Figure 48.

The tensile tests were performed by a MTS 810 servo hydraulic material test system at 25°C and at a constant crosshead rate of 2mm/min as specified by ASTM D3039M-08. The strain data was obtained through an extensometer with a gage length of 25.4mm and the force data through a 100kN load cell. The tensile strength and modulus of the tested specimen were determined using Eq.'s (15) and (16) respectively,

$$\sigma_T = \frac{P_{max}}{A} \tag{15}$$

$$E = \frac{\Delta\sigma}{\Delta\varepsilon} \tag{16}$$

The tensile strength reductions of the specimens due to void content were determined using Eq. (17) [79].

$$\sigma_T = \sigma_{f0\%} e^{-BV_V} \tag{17}$$

In Eq. (17), the parameter of interest is the strength reduction coefficient "*B*". To determine how this parameter varied as fiber volume content was changed, Eq. (17) was fit to the experimentally determined tensile strengths of the laminates with comparable

fiber volume content as void content was increased by minimizing the sum of the squared residuals.

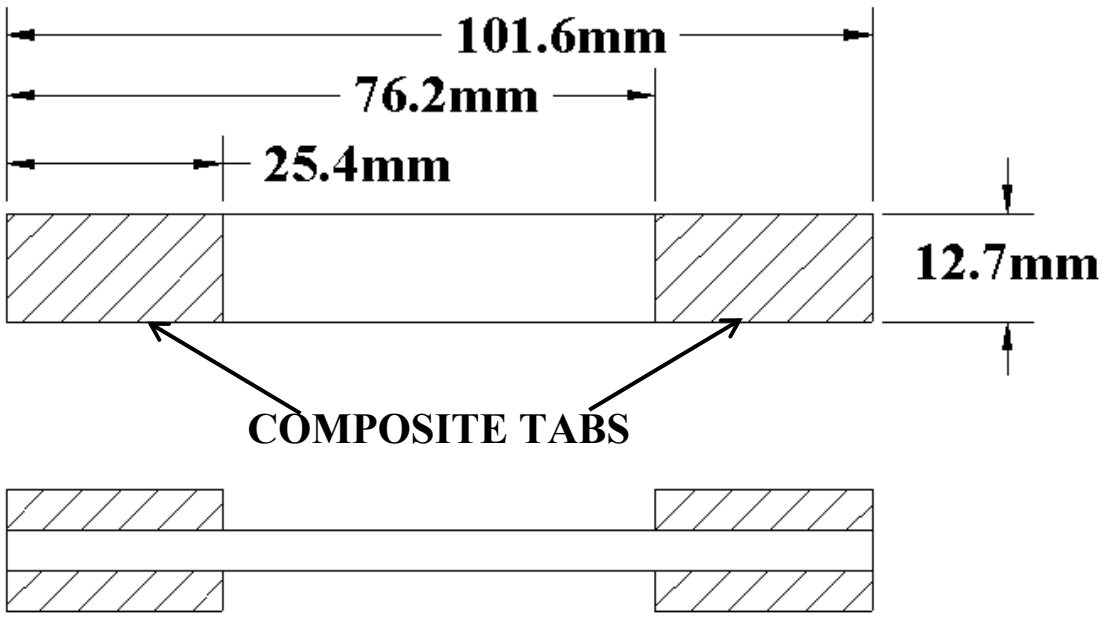

Figure 48- Tensile test specimen geometry used to determine the effect of voids.

5.3 RESULTS AND DISCUSSION

5.3.1 PROCESSING CONDITIONS EFFECT

The effect of exposing the laminates to different environmental humidities as well as the effect of increasing cure pressure on the formation of voids is presented Figure 49. From the figure, it is obvious that the humidity conditions in which the laminates were exposed before processing was of paramount importance. For example, the void contents for the laminates processed at 69 kPa were found to increase from 2.79% to 4.94% with increasing environmental humidity exposure. This finding was not surprising and is explained by the diffusion of moisture into or out of the laminates when humidity conditions are changed as discussed in Chapter 4. Thus, higher humidity

levels create higher laminate moisture contents. This moisture diffuses into any voids present in the laminate and is vaporized during curing resulting in an exponential increase of void pressure with temperature during processing which cause voids to grow [17, 18, 21, 22, 33]. The void growth is subdued, however, as processing pressure is increased as indicated by the figure. Regardless, because of humidity conditioning different void contents were created for each of the three laminates manufactured at each of this chapters four processing pressures. Thus, if the fiber volume contents of the three laminates cured at each processing pressure is constant the proposed coupled effect of voids with fiber volume content on mechanical properties can be shown. The effect of processing pressure on the fiber volume content of the laminates produced is shown in Figure 50. From the figure, the fiber volume contents of the laminates are found to increase from 45% to 57% with increasing applied pressure. In addition, each data point shown is composed of a total of twenty-four specimen obtained from the three laminates manufactured at each cure pressure. The fiber volume content variation between laminates included in each data point, as indicated by the error bars, was found to be minimal. Thus, the effect of voids on the mechanical properties of the laminates as void and fiber volume content is increased can be determined.

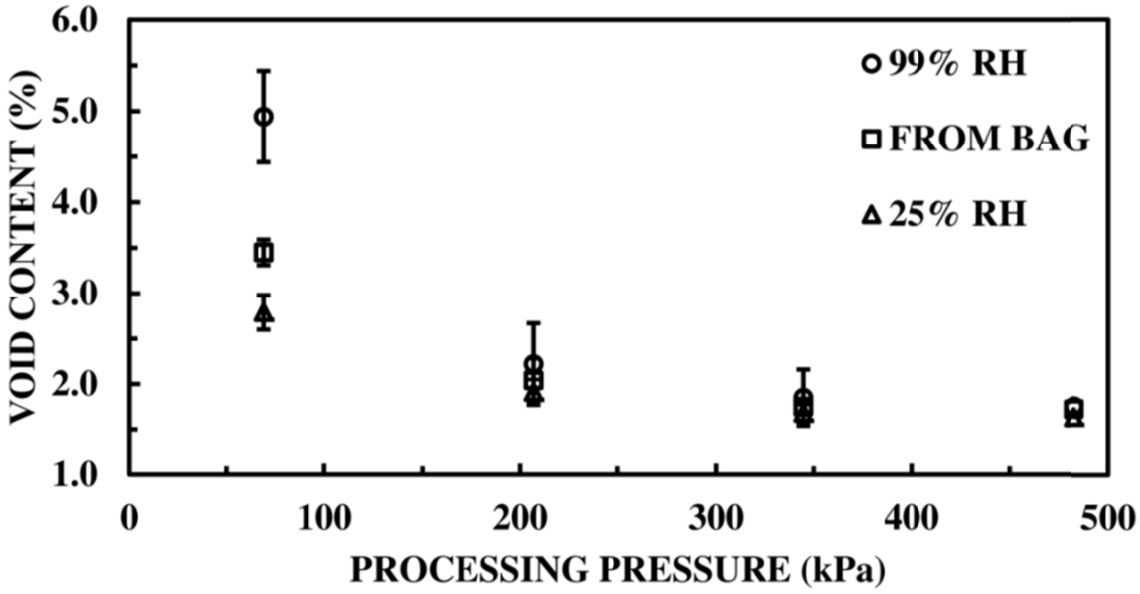

Figure 49- Effect of humidity environment and processing pressure on the formation of voids. Note: Error bars represent the 95% confidence interval for n=8.

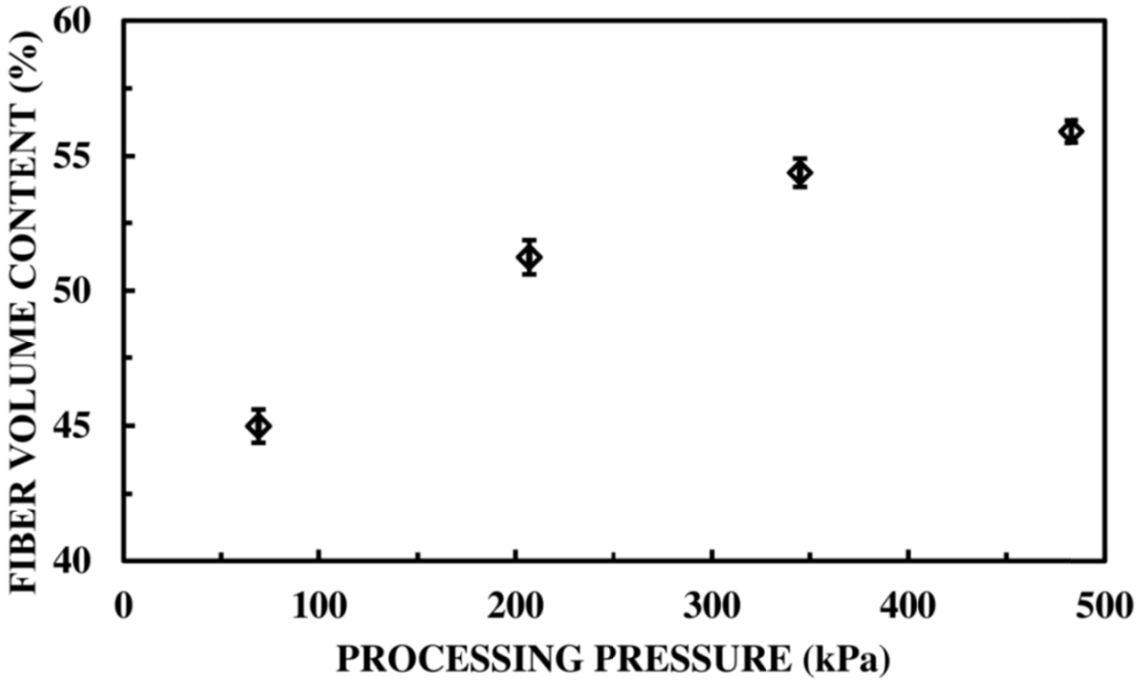

Figure 50- Effect of cure pressure on the fiber volume content of the manufactured laminates. Note: Error bars represent the 95% confidence interval for n=8.

5.3.2 TENSILE PROPERTIES OF LAMINATES

As has been shown in Chapter 4, cure pressure and laminate humidity exposure before manufacturing has a significant effect on void content. Void and laminate fiber volume content are known to influence laminate mechanical properties [15, 20, 28-30, 49, 65]. The extent of the voids influence on the tensile modulus of this chapters laminates as fiber volume content is increased is shown in Figure 51. From the figure, the tensile modulus of the laminates are found to steadily increase from 22.8 to 29.5 GPa as fiber volume content is increased from 45% to 57%. In addition, the presence of voids is found to not have a statistically significant effect on tensile modulus. These results are not surprising as the modulus of an aerospace grade composite along the fiber direction is primarily dependent on the fiber property and not that of the matrix [28-30]. In fact, Harper et. al [29] reported void contents as high as 5% did not affect the tensile modulus of a graphite/epoxy composite whose fibers were oriented along direction of testing.

The tensile strengths of the laminates were, unlike the tensile modulus, found to be significantly affected by the presence of voids as shown in Figure 52. Results such as these come as no surprise as they have been widely reported [14, 15, 24, 30-33]. However, it does appear the reduction in strength from the low to high void contents for each of the four fiber volume contents is nearly constant. Despite the fact, the difference between the high and low void contents is reduced from 2.1% to 0.2% as the fiber volume content is increased. Thus, the fiber volume content seems to affect the extent to which voids will degrade the strength of composite components.

This supposition is confirmed when Eq. (17) is fit to the experimental data in Figure 52 and the strength reduction coefficient "*B*" from the fit is plotted vs fiber volume content as shown in Figure 53. It is clearly shown, that for the laminates in this chapter, "*B*" increases linearly from 0.03 to 0.24 as fiber volume content increases from 45% to 57%. It is hypothesized that this phenomena is related to the changing morphology of the voids in the laminates as fiber volume content was increased.

This hypothesis was qualitatively confirmed when the voids of specimen obtained from each laminate was observed using a SEM, examples of which are shown in Figure 54. In this figure, the voids are found to become more and more elongated as fiber volume content is increased. This is explained by the fact that as the fiber volume content increases the width of the matrix rich region between plies is decreased. Thus, the likelihood of a void becoming located on the fiber-matrix interface increases. This is significant, given that the matrix transfers applied loads by shear to the fibers. Voids on the fiber-matrix interface reduce the shear area, effectively increasing the shear stress in the matrix, which can in turn result in early failure of composite components [27, 36, 65-67]. In addition, the presence of the void on the fiber-matrix interface increases the likelihood of it becoming squeezed between plies and becoming elongated. The extent to which the voids are elongated as fiber volume content is increased was determined by measuring their aspect ratios as shown in Figure 55.

In this figure, the voids aspect ratios are found to range from 1.46 to 4.25 depending on fiber volume content. In addition, the ratios are shown to increase linearly as the fiber volume content is increased from 51% to 57%. Therefore, it is proposed that the model as used by Ghiorse [32] and defined by Eq. (17) can be improved by making the

strength reduction coefficient a function of fiber volume content as shown in Eq. (18). Thus, allowing the morphological effects of voids to be accounted for.

$$\sigma_T = \sigma_{f0\%} e^{-B[V_{fiber}]\, V_V} \tag{18}$$

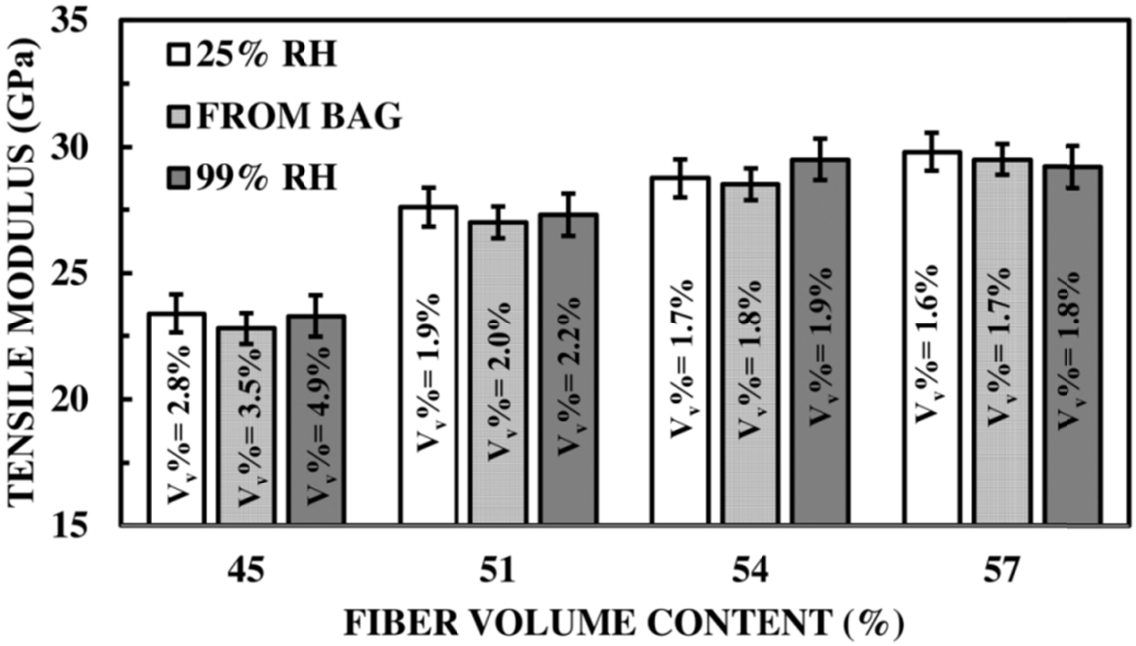

Figure 51- Tensile modulus of the specimen as void and laminate fiber volume content is increased. Note: Error bars represent the 95% confidence interval for n=16.

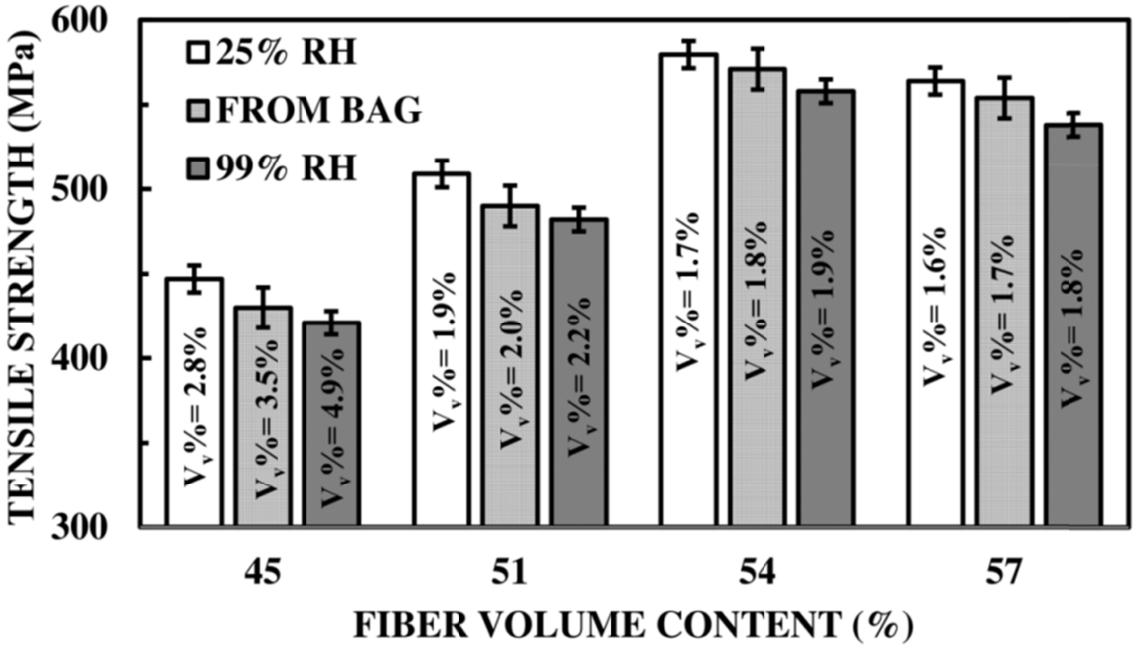

Figure 52- Tensile strength of the specimen as void and laminate fiber volume content is increased. Note: Error bars represent the 95% confidence interval for n=16.

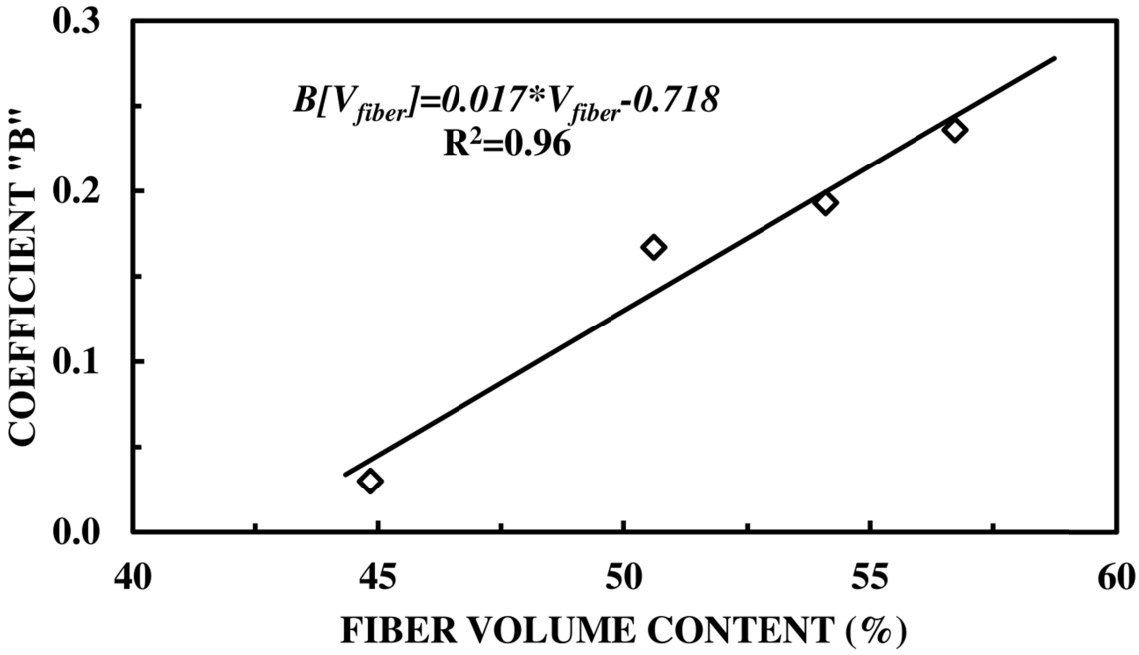

Figure 53- Variation of the strength reduction coefficient as fiber volume content is changed.

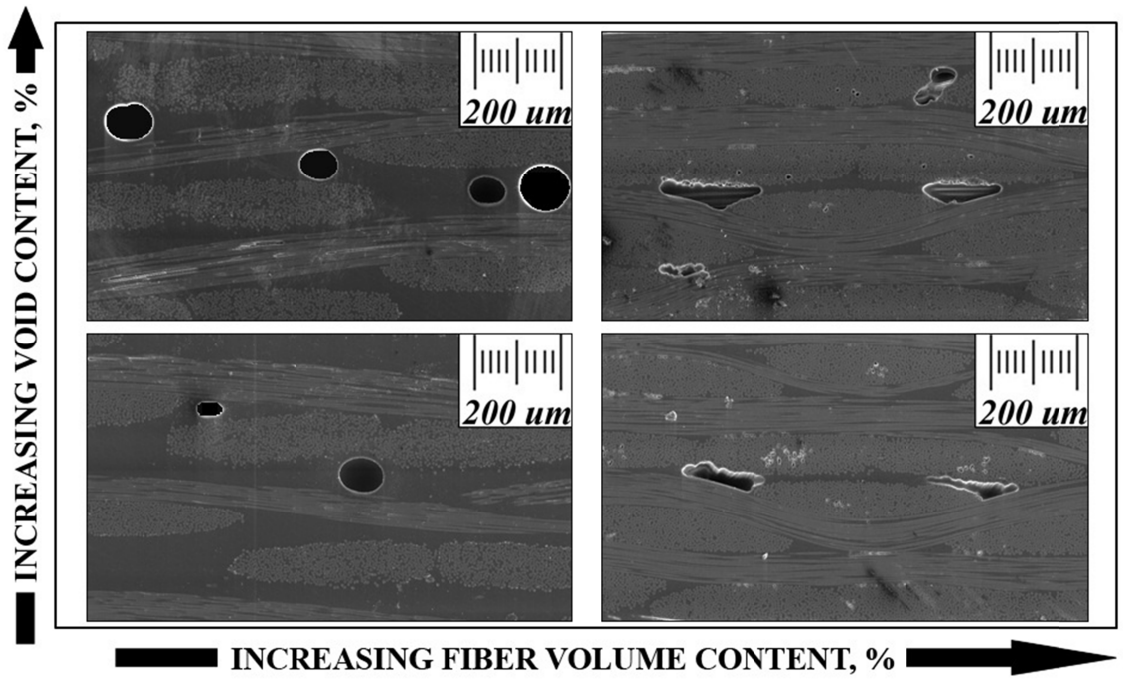

Figure 54- SEM images taken at 75x that show the morphologies and locations of voids in specimen as fiber volume contents are increased.

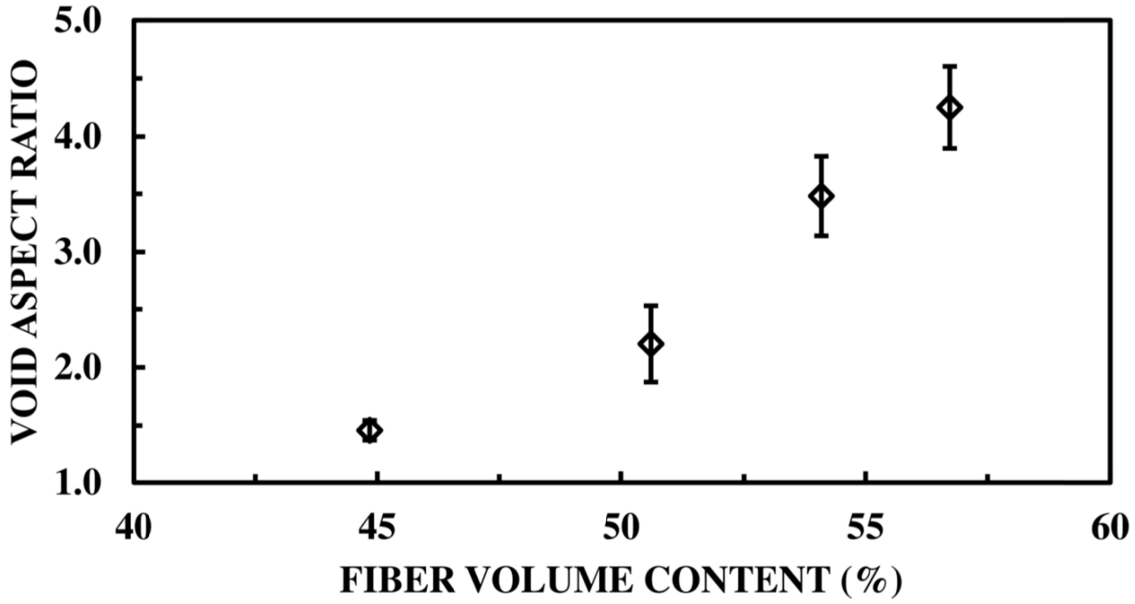

Figure 55- Effect of increasing laminate fiber volume content on the aspect ratio of voids. Note: Error bars represent the 95% confidence interval for n=5.

5.4 CONCLUSIONS

The influence of void content on the tensile properties of glass/epoxy composite laminates with increasing fiber volume and void contents was explored. It was found that the presence of voids had no effect on the tensile modulus of the laminates. However, their tensile strengths were significantly affected. It was found that as fiber volume content was increased the detrimental effects of voids became progressively more significant. This phenomenon was attributed to the increased occurrence of voids becoming located on the fiber-matrix interface and their changing morphology as the laminates fiber volume contents were increased. A modified strength reduction model was proposed which accounts for this coupled effect of the void and fiber volume content. This chapter's findings suggest that as fiber volume content is increased the elimination of voids in composite components become increasingly important.

6. CONCLUSIONS AND RECOMMENDATIONS

6.1 CONCLUSIONS

In this dissertation, a new fabrication method for the production of hollow composite components and the effect of voids on the mechanical properties of composite were presented. The major conclusions that can be drawn from the studies contained herein may be grouped as follows:

- **Development of an advanced composite manufacturing process (BACM):**

A new, cost-effective manufacturing process, Bladder Assisted Composite Manufacturing (BACM) was presented in Chapter 2. The BACM process was found to be capable of fabricating hollow, geometrically complex structural composite components using a variety of prepreg material. Unlike conventional oven or autoclave curing, the heating of the composite to be cured is provided by hot air circulated inside of a pressurized bladder. The process was shown to produce composite cylinders; (i) in a more energy efficient manner when compared to traditional cure processes with an external heat source and (ii) with void fractions and flexural properties comparable to hot pressed components.

- **Assessment and analysis of void suppression/removal techniques in the BACM process:**

In Chapter 3, the feasibility of adapting the I-BACM configuration (as introduced in Chapter 2) to produce composite cylinders with multiple fiber volume fractions, and

low void contents was studied. The effects of three mold configurations in varying the fiber volume fractions, reducing void contents, and on mechanical properties were reported. It was shown that fiber volume contents could be varied from 51% to 58% by sealing or incorporating a bleeder in the mold while maintaining a constant processing pressure of 483kPa. The void contents of the composite cylinders, manufactured using the three BACM variations, were reduced by at least 35.71% (2.24% to 1.44%) when compared to the I-BACM configuration. In fact, the sealed configuration resulted in the average laminate void content being reduced by 68.75% (2.24% to 0.70%).

- **Moisture content in an unprocessed prepreg and cure pressure are identified to be the driving factors in void formation in the studied prepreg materials:**

The motivation behind Chapter 4 was to determine the coupled effect of humidity exposure and cure pressure on void formation in laminates fabricated from a glass/epoxy prepreg manufactured by hot-press. The moisture content of the prepreg plies were found to vary depending on environmental relative humidity and the time of exposure. This is important, because for each of the four processing pressures studied the void content was reported to be at a maximum when the prepreg was exposed to high humidity and minimum when exposed to low humidity. In addition, the void contents were found to reduce to an asymptotic value of 1.64% as processing pressure was increased. This was attributed to the fiber bed carrying a greater portion of the applied load as processing pressure/fiber volume fraction was increased. Due to this, the fiber bed began to carry an increasingly larger proportion of the applied load and its permeability was reduced. Thus, the resin pressure was reduced and the less mobile macrovoids became trapped in the laminate. Due to the coupled effect of humidity

exposure and cure pressure on the formation of and final content of voids an improvement to the void content prediction model proposed by Boey and Lye [17] was proposed.

- **Mechanical property degradation due to moisture induced voids is shown to be highly correlated with fiber volume content:**

In Chapter 5, the influence of void content on the tensile properties of glass/epoxy composite laminates with increasing fiber volume and void contents was explored. It was found that the presence of voids had no appreciable effect on the tensile modulus of the laminates. However, their tensile strengths were significantly affected. It was found that as fiber volume content was increased the detrimental effects of voids became progressively more significant. This phenomenon was attributed to the increased occurrence of voids becoming located on the fiber-matrix interface and their changing morphology as the laminates fiber volume contents were increased. A modified strength reduction model was proposed which accounts for this coupled effect of the void and fiber volume content. The findings suggest that as fiber volume content is increased the elimination of voids in composite components become increasingly more important.

6.2 RECOMMENDATIONS FOR FUTURE WORK

The various studies presented in this dissertation are open for further development. One area that can be further developed is the BACM manufacturing process described in Chapter's 2 and 3. In the current work, the BACM process has been used to manufacture composite cylinders. It would be advantageous, to further develop the process so that it could be used to manufacture composite structures with integral iso-

and ortho-grid reinforcement as well as to increase the size of the parts being produced. These capabilities would increase the usefulness and attractiveness of the process for the automotive, marine, and aerospace industries.

A second area available for further work is void formation/effects discussed in Chapter's 4 and 5. Understanding how voids are formed during manufacturing and their effect on the performance of composite components can be used to develop manufacturing/design guidelines for composites. As a result, structural composite components cost could be reduced and their use become more widespread. In order to accomplish this goal, the following is recommended for future work:

- Study how susceptible common uncured pregreg resin systems are to absorbing moisture.

- Investigate how the parameters of the void formation model presented in Chapter 4 vary with fabric weave and manufacturing process.

- Study the effects of voids in composite components with fiber volume contents below 45% and above 57%.

REFERENCES

[1] M.G. Bader. 2002. "Selection of composite materials and manufacturing routes for cost-effective performance," *Composites Part A: Applied Science and Manufacturing.* 33(7): 913-934.

[2] M. Lossie and H. Van Brussel. 1994. "Design principles in filament winding," *Composites Manufacturing.* 5(1): 5-13.

[3] J.F. Davalos, H.A. Salim, P. Qiao, R. Lopez-Anido and E.J. Barbero. 1996. "Analysis and design of pultruded FRP shapes under bending," *Composites Part B: Engineering.* 27(3–4): 295-305.

[4] U. Lehmann and W. Michaeli. 1998. "Cores lead to an automated production of hollow composite parts in resin transfer moulding," *Composites Part A: Applied Science and Manufacturing.* 29(7): 803-810.

[5] H. Ghiasi, L. Lessard, D. Pasini and M. Thouin. 2010. "Optimum Structural and Manufacturing Design of a Braided Hollow Composite Part," *Applied Composite Materials.* 17(2): 159-173.

[6] A. Salomi, A. Greco, F. Felline, O. Manni and A. Maffezzoli. 2007. "A preliminary study on bladder-assisted rotomolding of thermoplastic polymer composites," *Advances in Polymer Technology.* 26(1): 21-32.

[7] I.C. Visconti and A. Langella. 1992. "Analytical modelling of pressure bag technology," *Composites Manufacturing.* 3(1): 3-6.

[8] B.J. Trimble. 1992. "Method of Making Composite Cycle Frame Components," *United States Patent Office.* US5624519, USA

[9] D. Rebard. 2004. "Bladder Molding with Latex in the Recreational Industry Lessons Learned," *49th International SAMPE Symposium and Exhibition.* SAMPE, Long Beach, CA, USA.

[10] R.F.J. McCarthy, G.H. Haines and R.A. Newley. 1994. "Polymer composite applications to aerospace equipment," *Composites Manufacturing.* 5(2): 83-93.

[11] L.W. Davies, R.J. Day, D. Bond, A. Nesbitt, J. Ellis and E. Gardon. 2007. "Effect of cure cycle heat transfer rates on the physical and mechanical properties of an epoxy matrix composite," *Composites Science and Technology.* 67(9): 1892-1899.

[12] H.H. Hodgkin and N. Rabu. 2000. "A New Development in High-Speed Composite Fabrication for Aerospace, Automotive, and Marine Applications," *45th International SAMPE Symposium and Exhibition.* Society for the Advancement of Material and Process Engineering, Long Beach, CA, USA.

[13] M.G. Bader and N. Noble. 2004. "A Comparison of the Costs of Manufacture of a Laminated Composite Component by Conventional Autoclave and a Novel Non-Autoclave Process," *25th International SAMPE-EUROPE.* Society for the Advancement of Material and Process Engineering, Paris, France.

[14] N.C.W. Judd and W.W. Wright. 1978. "Voids and their effects on the mechanical properties of composites-An appraisal," *SAMPE Quarterly.* 14(10-14.

[15] A.R. Chambers, J.S. Earl, C.A. Squires and M.A. Suhot. 2006. "The effect of voids on the flexural fatigue performance of unidirectional carbon fibre composites developed for wind turbine applications," *International Journal of Fatigue.* 28(10): 1389-1398.

[16] K.A. Olivero, H.J. Barraza, E.A. O'Rear and M.C. Altan. 2002. "Effect of Injection Rate and Post-Fill Cure Pressure on Properties of Resin Transfer Molded Disks," *Journal of Composite Materials.* 36(16): 2011-2028.

[17] F.Y.C. Boey and S.W. Lye. 1992. "Void reduction in autoclave processing of thermoset composites: Part 1: High pressure effects on void reduction," *Composites.* 23(4): 261-265.

[18] J.L. Kardos, R. Dave and M.P. Dudukovic. 1988. "Voids in Composites," *Manufacturing Science of Composites,* T. G. Gutowski, ASME, Atlanta, GA USA.

[19] L. Liu, B.-M. Zhang, D.-F. Wang and Z.-J. Wu. 2006. "Effects of cure cycles on void content and mechanical properties of composite laminates," *Composite Structures.* 73(3): 303-309.

[20] J. Varna, R. Joffe, L.A. Berglund and T.S. Lundström. 1995. "Effect of voids on failure mechanisms in RTM laminates," *Composites Science and Technology.* 53(2): 241-249.

[21] L.K. Grunenfelder and S.R. Nutt. 2010. "Void formation in composite prepregs – Effect of dissolved moisture," *Composites Science and Technology.* 70(16): 2304-2309.

[22] J. Kardos, M. Duduković and R. Dave. 1986. "Void growth and resin transport during processing of thermosetting matrix composites," *Epoxy Resins and Composites IV,* 80, K. Dušek, Springer Berlin / Heidelberg

[23] A.C. Loos and G.S. Springer. 1983. "Curing of Epoxy Matrix Composites," *Journal of Composite Materials.* 17(2): 135-169.

[24] P.O. Hagstrand, F. Bonjour and J.A.E. Månson. 2005. "The influence of void content on the structural flexural performance of unidirectional glass fibre reinforced polypropylene composites," *Composites Part A: Applied Science and Manufacturing.* 36(5): 705-714.

[25] E.M. Lenoe. 1970. "Effect of Voids on Mechanical Properties of Graphite Fiber Composites," U. S. D. o. t. Navy, U.S. Naval Air Systems Command, Washington D.C.

[26] J.L. Thomason. 1995. "The interface region in glass fibre-reinforced epoxy resin composites: 2. Water absorption, voids and the interface," *Composites.* 26(7): 477-485.

[27] B.K. Larson and L.T. Drzal. 1994. "Glass fibre sizing/matrix interphase formation in liquid composite moulding: effects on fibre/matrix adhesion and mechanical properties," *Composites.* 25(7): 711-721.

[28] H. Huang and R. Talreja. 2005. "Effects of void geometry on elastic properties of unidirectional fiber reinforced composites," *Composites Science and Technology.* 65(13): 1964-1981.

[29] B.D. Harper, G.H. Staab and R.S. Chen. 1987. "A Note on the Effects of Voids Upon the Hygral and Mechanical Properties of AS4/3502 Graphite/Epoxy," *Journal of Composite Materials.* 21(3): 280-289.

[30] P. Olivier, J.P. Cottu and B. Ferret. 1995. "Effects of cure cycle pressure and voids on some mechanical properties of carbon/epoxy laminates," *Composites.* 26(7): 509-515.

[31] S.F.M. de Almeida and Z.d.S.N. Neto. 1994. "Effect of void content on the strength of composite laminates," *Composite Structures.* 28(2): 139-148.

[32] Ghiorse, Sr. 1993. "Effect of Void Content on the Mechanical Properties of Carbon/Epoxy Laminates," *SAMPE QUARTERLY.* 24(2): 54-59.

[33] L. Liu, B.-M. Zhang, Z.-J. Wu and D.-F. Wang. 2005. "Effects of Cure Pressure Induced Voids on the Mechanical Strength of Carbon/Epoxy Laminates," *Journal of Materials Science and Technology.* 21(1): 87-90.

[34] T. Naganuma, K. Naito, J. Kyono and Y. Kagawa. 2009. "Influence of prepreg conditions on the void occurrence and tensile properties of woven glass fiber-reinforced polyimide composites," *Composites Science and Technology.* 69(14): 2428-2433.

[35] A. Spaggiari and N. O'Dowd. 2012. "The influence of void morphology and loading conditions on deformation and failure of porous polymers: A combined finite-element and analysis of variance study," *Computational Materials Science.* 64(0): 41-46.

[36] M.R. Wisnom, T. Reynolds and N. Gwilliam. 1996. "Reduction in interlaminar shear strength by discrete and distributed voids," *Composites Science and Technology.* 56(1): 93-101.

[37] J. Tomblin, Y.N. McKenna and K.S. Raju. 2001. "B-Basis Design Allowables for Epoxy-Based Prepreg Newport E-Glass Fabric 7781/NB321," AGATE, National Institute for Aviation Research, Washington D.C.

[38] J. Tomblin, L. Salah and Y.C. Ng. 2001. "Determination of Temperature/Moisture Sensitive Composite Properties," U. S. D. o. Transportation, Office of Aviation Research, Washington D.C.

[39] J. Karni and E.Y. Karni. 1995. "Gypsum in construction: origin and properties," *Materials and Structures.* 28(2): 92-100.

[40] N.K. Gupta and H. Abbas. 2000. "Lateral collapse of composite cylindrical tubes between flat platens," *International Journal of Impact Engineering.* 24(4): 329-346.

[41] S.P. Prosen, S. Karpe, M.A. Kinna, C. Mueller, H.A. Perry and F.R. Barnet. 1963. "Compression, Fatigue, and Stress Studies on NOL Ring Specimens," *Symposium for Filament Wound Reinforced Plastics.* ASTM International, Naval Ordnance Laboratory White Oak, Silver Spring, MD USA.

[42] R.M. Guedes and A. Sá. 2008. "Numerical analysis of singly curved shallow composite panels under three-point bend load," *Composite Structures.* 83(2): 212-220.

[43] B.J. Wilson and J.F. Quereau. 1928. "A Simple Method of Determining Stress in Curved Flexural Members," *Circular No. 16.* University of Illinois, Urbana

[44] G. Azzone and G. Noci. 1998. "Identifying effective PMSs for the deployment of "green" manufacturing strategies," *International Journal of Operations & Production Management.* 18(4): 308-335.

[45] Y.K. Hamidi, L. Aktas and M.C. Altan. 2005. "Effect of packing on void morphology in resin transfer molded E-glass/epoxy composites," *Polymer Composites.* 26(5): 614-627.

[46] C.E. Browning. 1986. "Processing Science of Graphite/Epoxy Composites," *Chemical Engineering Progress.* 82(6): 41-44.

[47] F.Y.C. Boey and S.W. Lye. 1990. "Optimized Curing Process for an Autoclave Cured Fibre Reinforced Composite," *2nd NTI/NUS Symposium- Material Processing Technology.* Singapore, Singapore.

[48] N.L. Hancox. 1975. "The compression strength of unidirectional carbon fibre reinforced plastic," *Journal of Materials Science.* 10(2): 234-242.

[49] J.-M. Tang, W.I. Lee and G.S. Springer. 1987. "Effects of Cure Pressure on Resin Flow, Voids, and Mechanical Properties," *Journal of Composite Materials.* 21(5): 421-440.

[50] L.G. Stringer. 1989. "Optimization of the wet lay-up/vacuum bag process for the fabrication of carbon fibre epoxy composites with high fibre fraction and low void content," *Composites.* 20(5): 441-452.

[51] J.P. Anderson and M.C. Altan. 2012. "Properties of Composite Cylinders Fabricated by Bladder Assisted Composite Manufacturing (BACM)," *Journal of Engineering Materials and Technology.* 134(4): 044501.

[52] H.J. Barraza, Y.K. Hamidi, L. Aktas, E.A. O'Rear and M.C. Altan. 2004. "Porosity Reduction in the High-Speed Processing of Glass-Fiber Composites by Resin Transfer Molding (RTM)," *Journal of Composite Materials.* 38(3): 195-226.

[53] N. Patel, V. Rohatgi and L.J. Lee. 1995. "Micro scale flow behavior and void formation mechanism during impregnation through a unidirectional stitched fiberglass mat," *Polymer Engineering & Science.* 35(10): 837-851.

[54] R.B. Deo, J.H. Starnes and R.C. Holzwarth. 2001. "Low-Cost Composite Materials and Structures for Aircraft Applications," *RTO AVT Specialists' Meeting on "Low Cost Composite Structures",* RTO/NATO, Loen, Norway.

[55] J. Muric-Nesic, P. Compston and Z.H. Stachurski. 2011. "On the void reduction mechanisms in vibration assisted consolidation of fibre reinforced polymer composites," *Composites Part A: Applied Science and Manufacturing.* 42(3): 320-327.

[56] M. Sumikawa, Y. Shindo, T. Takeda, F. Narita, S. Takano and K. Sanada. 2005. "Analysis of Mode I Interlaminar Fracture and Damage Behavior of GFRP Woven Laminates at Cryogenic Temperatures," *Journal of Composite Materials.* 39(22): 2053-2066.

[57] P. McMullen. 1984. "Fibre/resin composites for aircraft primary structures: a short history, 1936–1984," *Composites.* 15(3): 222-230.

[58] Y.K. Hamidi and M.C. Altan. 2003. "Spatial variation of void morphology in resin transfer molded E-glass/epoxy composites," *Journal of Materials Science Letters.* 22(24): 1813-1816.

[59] G. Azzone and R. Manzini. 1994. "Measuring strategic environmental performance," *Business Strategy and the Environment.* 3(1): 1-14.

[60] R.A. Clarke, R.N. Stavins, J.L. Greeno, J.L. Bavaria, F. Cairncross, D.C. Esty, B. Smart, J. Piet, R.P. Wells, R. Gray, K. Fischer and J. Schot. 1994. "The Challenge of Going Green," *Harvard Business Review*. Harvard Business Publishing,

[61] A.A. Kafi, K. Magniez and B.L. Fox. 2011. "Effect of manufacturing process on the flexural, fracture toughness, and thermo-mechanical properties of bio-composites," *Composites Part A: Applied Science and Manufacturing*. 42(8): 993-999.

[62] T. Centea and P. Hubert. 2011. "Measuring the impregnation of an out-of-autoclave prepreg by micro-CT," *Composites Science and Technology*. 71(5): 593-599.

[63] D.H.J.A. Lukaszewicz and K.D. Potter. 2011. "The internal structure and conformation of prepreg with respect to reliable automated processing," *Composites Part A: Applied Science and Manufacturing*. 42(3): 283-292.

[64] B. Blackmore, D. Li and J. Gao. 2001. "Detachment of Bubbles in Slit Microchannels by Shearing Flow," *Journal of Colloid and Interface Science*. 241(2): 514-520.

[65] F.M. Zhao and N. Takeda. 2000. "Effect of interfacial adhesion and statistical fiber strength on tensile strength of unidirectional glass fiber/epoxy composites. Part I: experiment results," *Composites Part A: Applied Science and Manufacturing*. 31(11): 1203-1214.

[66] C. Kim and S.R. White. 1996. "The Continuous Curing Process for Thermoset Polymer Composites. Part 2: Experimental Results for a Graphite/Epoxy Laminate," *Journal of Composite Materials*. 30(5): 627-647.

[67] H.J. Barraza, K. Olivero, Y. Hamidi, E.A. O'Rear and M.C. Altan. 2002. "Elastomeric sizings for glass fibers and their role in fiber wetting and adhesion in resin transfer molded composites," *Composite Interfaces*. 9(6): 477-507.

[68] T.G. Gutowski, T. Morigaki and Zhong Cai. 1987. "The Consolidation of Laminate Composites," *Journal of Composite Materials*. 21(2): 172-188.

[69] T.G. Gutowski and G. Dillon. 1992. "The Elastic Deformation of Lubricated Carbon Fiber Bundles: Comparison of Theory and Experiments," *Journal of Composite Materials*. 26(16): 2330-2347.

[70] R. Dave, J.L. Kardos and M.P. Duduković. 1987. "A model for resin flow during composite processing: Part 1-General mathematical development," *Polymer Composites*. 8(1): 29-38.

[71] R. Dave, J.L. Kardos and M.P. Duduković. 1987. "A model for resin flow during composite processing: Part 2-Numerical analysis for unidirectional graphite/epoxy laminates," *Polymer Composites.* 8(2): 123-132.

[72] R. Davé. 1990. "A Unified Approach to Modeling Resin Flow During Composite Processing," *Journal of Composite Materials.* 24(1): 22-41.

[73] N. Patel and L.J. Lee. 1995. "Effects of fiber mat architecture on void formation and removal in liquid composite molding," *Polymer Composites.* 16(5): 386-399.

[74] C.-H. Shen and G.S. Springer. 1976. "Moisture Absorption and Desorption of Composite Materials," *Journal of Composite Materials.* 10(1): 2-20.

[75] R.A. Brand, G.G. Brown and E.L. McKague. 1983. "Processing Science of Epoxy Resin Composites," M. L. A. F. W. A. Laboratories, Air Force Systems Command, Wright-Patterson AFB

[76] T.S. Lundström. 1997. "Measurement of void collapse during resin transfer moulding," *Composites Part A: Applied Science and Manufacturing.* 28(3): 201-214.

[77] Y.K. Hamidi, L. Aktas and M.C. Altan. 2005. "Three-dimensional features of void morphology in resin transfer molded composites," *Composites Science and Technology.* 65(7–8): 1306-1320.

[78] J.R. Wood and M.G. Bader. 1994. "Void control for polymer-matrix composites (1): Theoretical and experimental methods for determining the growth and collapse of gas bubbles," *Composites Manufacturing.* 5(3): 139-147.

[79] E. Ryshkewitch. 1953. "Compression Strength of Porous Sintered Alumina and Zirconia," *Journal of the American Ceramic Society.* 36(2): 65-68.

[80] F.P. Knudsen. 1959. "Dependence of Mechanical Strength of Brittle Polycrystalline Specimens on Porosity and Grain Size," *Journal of the American Ceramic Society.* 42(8): 376-387.

[81] S.D. Brown, R.B. Biddulph and P.D. Wilcox. 1964. "A Strength–Porosity Relation Involving Different Pore Geometry and Orientation," *Journal of the American Ceramic Society.* 47(7): 320-322.

[82] Zhan-Sheng Guo, Ling Liu, Bo-Ming Zhang and Shanyi Du. 2009. "Critical Void Content for Thermoset Composite Laminates," *Journal of Composite Materials.* 43(17): 1775-1790.

[83] E. Stephen, O. Steve and R. Carl. 2012. "Industry Perspectives on Composite Structural Certification and Design," *53rd AIAA/ASME/ASCE/AHS/ASC Structures, Structural Dynamics and Materials Conference
20th AIAA/ASME/AHS Adaptive Structures Conference
14th AIAA,* American Institute of Aeronautics and Astronautics

[84] A.C. Ugural and S.K. Fenster. 2003. "Advanced Strength and Applied Elasticity," Prentice Hall

APPENDIX A: BACM PROCESS CONTROLLER

A.1: BACM CONTROL SCHEME

The control of the BACM process is achieved thru the use of a custom controller written using Visual Basic 6. The controller allows for the ramp rate, final hold temperature, hold time, proportional gain and allowable temperature gradient in the part to set by the user. The heating element, which is used to cure the part, is controlled using pulse width modulation (PWM). The pulse duration (i.e. % duty cycle) is determined by multiplying the proportional gain by the difference between the set point and average laminate temperature. If the longitudinal temperature gradient in the laminate, as determined by two embedded thermocouples, exceeds the set allowable, the air valve is opened to induce airflow inside the bladder. This flow serves to removes temperature gradients formed by localized heating within the bladder and helps to achieve thermal uniformity. After the completion of the cure cycle, the air valve is kept open constantly to facilitate cooling of the mold/part. The decision flow chart of the controller is shown in Figure 56. In addition to process control, the controller records the part temperature and bladder pressure at a rate of 10 Hz throughout the course of the curing cycle. Thus, allowing for the full documentation of each parts cure cycle.

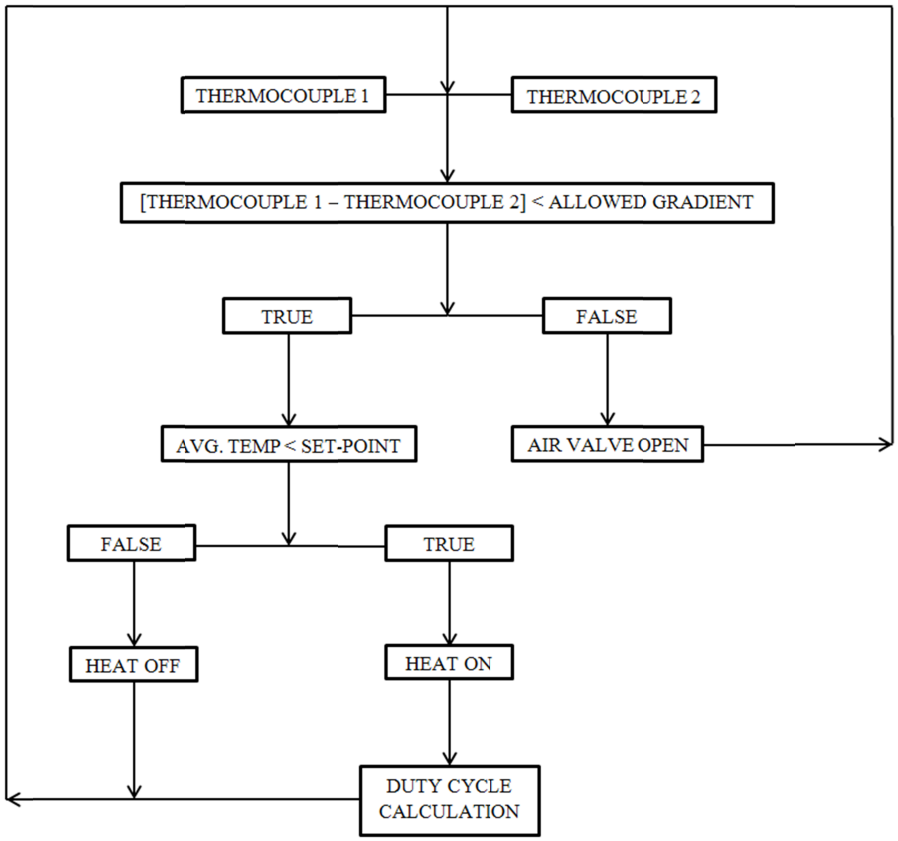

Figure 56- The BACM process controllers' decision flow chart.

A.2: BACM CONTROLLER VB6 CODE

```
'LabJack channel assignments
   'FIO0- OPEN
   'FIO1- OPEN
   'FIO2-HEATING ELEMENT
   'FIO3-AIR VALVE
   'FI04-THERMOCOUPLE #1 INPUT
   'FI05-PRESSURE SENSOR
   'FI06-CURRENT SENSOR
   'FI07-THERMOCOUPLE #2 INPUT
   'SDA-OPEN
   'SCL-OPEN
   'DAC0-OPEN
   'DAC1-OPEN

   'RR-Ramp rate
   'CT-Cure Temperature
```

```
    'HT-Hold Time
    'TC-Temp. C
    'TF-Temp. F
    'ST-Starting Temperature
    'CT1-Control Temperature 1
    'CT2-Control Temperature 2
    'ACT-Average Control Temperature
    'CTD-Control Temperature Delta
    'SPT-Set-Point Temperature
    'CTI-Cycle Time
    'PP-Process Pause
    'AD-Allowable Temp. Delta
    'AV-Air Valve On
    'TI-Cycle Time input
    'D-Difference between ACT and SPT
    'ETC-Estimated Time To Completion
    'Cu-CURRENT
    'KWH-POWER CONSUMPTION IN KILOWATT HOURS
    'Pressure-Pressure in psi

Dim lngError As Long
Dim lngHandle As Long
Dim lngIOType As Long
Dim lngChannel As Long
Dim dblDriverVersion As Double
Dim strError As String * 256
Dim dblAIN4 As Double
Dim dblAIN7 As Double
Dim dblInternal As Double
Dim ainResolution As Double
Dim TCVolts As Double
Dim TCVolts1 As Double
Dim pTCTempK As Double
Dim pTCTempK1 As Double
Dim offSetVoltage As Double
Dim TCType As Long
Dim D As Double
Dim Vo1 As Long
Dim Vi1 As Long
Dim Ao2 As Long
```

```
Dim Vo2 As Long
Dim PWR As Long

Private Sub AV_Click()
   LJ_ERROR_stdcall = eDO(lngHandle, 3, 1)
      AO.Visible = True
   End Sub
Private Sub Check1_Click()
        If  Check1 = 1 Then
                Check1.Enabled = False
                LogFormCSV.Show
        Else
                Check1.Enabled = True
        End If
End Sub

Private Sub Command1_Click()
        REAL_TIME.DoVerb [(-2)]
 End Sub

Private Sub Check4_Click()
        If Check4 = 1 Then
                Check4.Enabled = False
                curep.Enabled = False
                curep = "##.#"
        FormPressure.Show
        Else
                curep.Enabled = True
                curep = ""
                Check4.Enabled = True
        End If
End Sub

Private Sub Form_Load()
        lngError = OpenLabJack(LJ_dtU3, LJ_ctUSB, "1", 1, lngHandle)
        dblDriverVersion = GetDriverVersion()
         txtDriverVersion = Str(dblDriverVersion)
         lngError = eGet(lngHandle, LJ_ioGET_AIN, 30, dblInternal, 0)
        TC = dblInternal - 273.15
         TF = TC * 1.8 + 32
```

```
        ST = Format(TF, "###.#")
        lngError = ePut(lngHandle, LJ_ioPIN_CONFIGURATION_RESET, 0, 0, 0)
        lngError = eDO(lngHandle, 2, 0)
        lngError = eDO(lngHandle, 3, 0)
        ainResolution = 17
        lngError = eGet(lngHandle, LJ_ioPUT_ANALOG_ENABLE_BIT, 4, 1, 0)
        lngError = eGet(lngHandle, LJ_ioPUT_ANALOG_ENABLE_BIT, 5, 1, 0)
        lngError = eGet(lngHandle, LJ_ioPUT_ANALOG_ENABLE_BIT, 6, 1, 0)
        lngError = eGet(lngHandle, LJ_ioPUT_ANALOG_ENABLE_BIT, 7, 1, 0)
        lngError = eGet(lngHandle, LJ_ioPUT_CONFIG, LJ_chAIN_RESOLUTION,
        ainResolution, 0)
        TIMER.Enabled = False
End Sub

Private Sub Abort_CLICK()
        POWER1 = 0
        Call LogFormCSV.StopIt
        LogFormCSV.hourstxbx.Text = 0
        LogFormCSV.minutes.Text = 0
        LogFormCSV.Text1.Text = 0
        LogFormCSV.Label1 = LogFormCSV.hourstxbx.Text & ":" &
        LogFormCSV.minutes.Text & ":" & LogFormCSV.Text1.Text 'output to label
        hours minutes seconds
        LogFormCSV.Timer1.Enabled = FalsE
        TIMER.Enabled = False
        Timer1.Enabled = False
        Timer3.Enabled = False
        START1.Text = ""
        CTI = 0
        LJ_ERROR_stdcall = eDO(lngHandle, 2, 0)
        LJ_ERROR_stdcall = eDO(lngHandle, 3, 0)
End Sub

Private Sub Form_QueryUnload(Cancel As Integer, UnloadMode As Integer)
        LJ_ERROR_stdcall = eDO(lngHandle, 2, 0)
        LJ_ERROR_stdcall = eDO(lngHandle, 3, 0)
        If LogFormCSV.opentxt = open Then
                Call LogFormCSV.StopIt
                Unload (LogFormCSV)
        End If
```

```
End Sub

Private Sub initialtemp_Click()
        ST = ACT
End Sub

Private Sub PP_Click()
        LogFormCSV.Timer1.Enabled = False
        Pause1.Text = Pause
        TIMER.Enabled = False
        Timer3.Enabled = False
End Sub

Private Sub Timer3_Timer()
      If CTI > 300 Then
            Timer3.Enabled = False
      Else
            Timer3.Enabled = True
      End If
Interval = 60000

Dim InputCol(5) As Variant
Dim InputRow(200) As Variant
InputCol(1) = CTI.Caption
InputCol(2) = CT1.Caption
InputCol(3) = CT2.Caption
InputCol(4) = ACT.Caption
InputCol(5) = SPT.Caption
Set xlBook = REAL_TIME.object
Dim Nm As Integer
REAL_TIME.DoVerb vbOLEShow 'or OLE1.DoVerb vbOLEUIActivate
   Nm = 1
      50:
      ar = A & Nm
         If xlBook.Worksheets(DATA).Range(ar).Value <>  Then
                  Nm = Nm + 1
                  GoTo 50
         Else
                  ar = A & Nm
                  BR = B & Nm
```

```
                CR = C & Nm
                DR = D & Nm
                ER = E & Nm
        End If
          xlBook.Worksheets(Data).Range(ar).Value = InputCol(1)
          xlBook.Worksheets(Data).Range(BR).Value = InputCol(2)
          xlBook.Worksheets(Data).Range(CR).Value = InputCol(3)
          xlBook.Worksheets(Data).Range(DR).Value = InputCol(4)
          xlBook.Worksheets(Data).Range(ER).Value = InputCol(5)
          Set xlBook = Nothing

Private Sub Start_Click()
        START1.Text = Start
          If Check1 = 1 Then
                Call LogFormCSV.gostart
                If LogFormCSV.FileNameTX =  Or LogFormCSV.Vin =  Then Exit Sub
                LogFormCSV.Timer1 = True
                TIMER.Enabled = True
                Timer1.Enabled = True
                Timer3.Enabled = True
          Else
                TIMER.Enabled = True
                Timer1.Enabled = True
                Timer3.Enabled = True
End If

Private Sub TIMER_Timer()
          TIMER.Interval = 600
          Z = 1 / 60000
          T = Z * Val(TIMER.Interval)
          CTII = Val(CTI) + T
          CTI = Format(CTII, ###.##)
          If Val(RR.Text) = 0 Then
                RR = 3
          Else
          End If
          ec = (2 * (Val(CT) - Val(ST)) / Val(RR) + Val(HT)) - Val(CTI)
          ETC = Format(ec, ###.##)
          If Val(AD.Text) = 0 Then
                 AD = 10
```

```
        Else
        End If
        If Val(CT.Text) = 0 Then
                CT = 250
        Else
        End If
        If Val(HT.Text) = 0 Then
                HT = 120
        Else
        End If
        If Val(ST) = 0 Then
                ST = 70
        Else
        End If
        If Check2 = 1 Then
                CTD = 0
                ACT = Val(CT2)
        Else
                If Check3 = 1 Then
                        CTD = 0
                        ACT = Val(CT1)
                Else
                        CTD = Val(CT1) - Val(CT2)
                        ACT = (Val(CT1) + Val(CT2)) / 2
                End If
         End If
If CTD < Val(AD.Text) Then
        If ACT < Val(SPT) Then
                EO.Visible = True
        Else
                EO.Visible = False
        End If
Else
        LJ_ERROR_stdcall = eDO(lngHandle, 2, 0)
End If
If ACT > Val(SPT) Then
        EO.Visible = False
        LJ_ERROR_stdcall = eDO(lngHandle, 2, 0)
Else
End If
```

```
If CTD >= Val(AD.Text) Then
        AO.Visible = True
        TIMER.Enabled = False
        LJ_ERROR_stdcall = eDO(lngHandle, 3, 1)
Else
        AO.Visible = False
        TIMER.Enabled = True
        LJ_ERROR_stdcall = eDO(lngHandle, 3, 0)
End If
If CTI > (Val(CT.Text) - Val(ST)) / Val(RR.Text) + Val(HT.Text) Then
        If SPT < ACT Then
                AO.Visible = True
                LJ_ERROR_stdcall = eDO(lngHandle, 3, 1)
        Else
                AO.Visible = False
                LJ_ERROR_stdcall = eDO(lngHandle, 3, 0)
        End If
Else
End If
If CTI <= (Val(CT.Text) - Val(ST)) / Val(RR.Text) Then
        SPT = Val(CTI) * Val(RR.Text) + Val(ST)
        Label5.Visible = False
        Label6.Visible = False
Else
        SPT = CT
        Label5.Visible = True
End If
If CTI > (Val(CT.Text) - Val(ST)) / Val(RR.Text) + Val(HT.Text) Then
        SPT = ((Val(CT.Text) - Val(ST)) / Val(RR.Text) + Val(HT.Text) - Val(CTI)) *
        Val(RR.Text) + Val(CT.Text)
        Label6.Visible = True
Else
End If
If SPT < ST - 0.1 Then
        REAL_TIME.DoVerb [(-2)]
        TIMER.Enabled = False
        Timer1.Enabled = False
        Timer3.Enabled = False
        CTI = 0
        LJ_ERROR_stdcall = eDO(lngHandle, 2, 0)
```

```
        LJ_ERROR_stdcall = eDO(lngHandle, 3, 0)
  Else
  End If
If ACT > CT * 1.5 Then
        TIMER.Enabled = False
        Timer1.Enabled = False
        Timer3.Enabled = False
        CTI = 0
        LJ_ERROR_stdcall = eDO(lngHandle, 2, 0)
        LJ_ERROR_stdcall = eDO(lngHandle, 3, 0)
Else
End If
End Sub

Private Sub Timer1_Timer()
        Timer1.Interval = 100
        Dim TEMP1(9) As Variant
        Dim TEMP2(9) As Variant
        Dim PRESS1(9) As Variant
For Q = 0 To 9
        lngError = eGet(lngHandle, LJ_ioGET_AIN, 4, dblAIN4, 0)
        C1C = dblAIN4 * 98.927
        C1f = Val(C1C * 1.8 + 32)
        lngError = eGet(lngHandle, LJ_ioGET_AIN, 7, dblAIN7, 0)
        C2C = dblAIN7 * 98.927
        C2F = Val(C2C * 1.8 + 32)
        lngError = eGet(lngHandle, LJ_ioGET_AIN, 5, dblain5, 0)
        PRESS = 32.5 * dblain5 - 32.5 'old sensor 169.25 * dblain5 - 14.765
        TEMP1(Q) = C1f
        TEMP2(Q) = C2F
        PRESS1(Q) = PRESS
Next Q
        WW = (TEMP1(1) + TEMP1(2) + TEMP1(3) + TEMP1(4) + TEMP1(0) +
        TEMP1(5) + TEMP1(6) + TEMP1(7) + TEMP1(8) + TEMP1(9)) / 10
        SS = (TEMP2(1) + TEMP2(2) + TEMP2(3) + TEMP2(4) + TEMP2(0) +
        TEMP2(5) + TEMP2(6) + TEMP2(7) + TEMP2(8) + TEMP2(9)) / 10
        ZZ = (PRESS1(1) + PRESS1(2) + PRESS1(3) + PRESS1(4) + PRESS1(0) +
        PRESS1(5) + PRESS1(6) + PRESS1(7) + PRESS1(8) + PRESS1(9)) / 10
        CT1 = Format(WW, ###.#)
        CT2 = Format(SS, ###.#)
```

```
        Pressure = Format(ZZ, ###)
If CTD < Val(AD.Text) Then
        If ACT < Val(SPT) Then
                Y = Val(100) * Val(TI.Text) / Val(100)
                X = Val(100) - Y
                If Val(TI.Text) <= 0 Then
                        LJ_ERROR_stdcall = eDO(lngHandle, 2, 0)
                Else
                        For i = 0 To Y
                                LJ_ERROR_stdcall = eDO(lngHandle, 2, 1)
                        Next i
                End If
                         If Val(TI.Text) >= 100 Then
                                LJ_ERROR_stdcall = eDO(lngHandle, 2, 1)
                        Else
                                For j = 0 To X
                                        LJ_ERROR_stdcall = eDO(lngHandle, 2, 0)
                                Next j
                         End If
        Else
                LJ_ERROR_stdcall = eDO(lngHandle, 2, 0)
        End If
Else
        LJ_ERROR_stdcall = eDO(lngHandle, 2, 0)
End If
  D = Val(SPT) - Val(ACT)

If Val(CycleM.Text) * D < 0 Then
        TI = 0
Else
        If Val(CycleM.Text) * D > 100 Then
                TI = 100
        Else
                T = Val(CycleM.Text) * D
                TI = Format(T, ###)
          End If
End If
End Sub
Private Sub Timer2_Timer()
If Check1 = 1 Then
```

```
        lngError = eGet(lngHandle, LJ_ioGET_AIN, 6, dblain6, 0)
        Cu = Format(dblain6 * 87.381 - 51.765, ##.###)
        Vin = LogFormCSV.Vin
        If START1.Text = "START" Then
                SSS = Vin * Cu / 1000 'Instantaneous Power
                p = SSS * (2 / 3600)
                POWER1 = Val(POWER1) + p 'Cumulative Power
                 kwh = Format(POWER1, ##.####)
                LogFormCSV.kwh = kwh
        Else
        End If
Else
End If
End Sub
```

APPENDIX B: VOID CONTENT

B.1: DERIVATION OF ASTM D2734

The constituents of a composite material may be represented as fraction of the whole as in Eq. (19).

$$V_v + V_{fiber} + V_{matrix} = 1 \tag{19}$$

Where "V_{fiber}" and "V_{matrix}" are defined as follows in Eq.'s (20) & (23).

$$V_{fiber} = \frac{Vol._{fiber}}{Vol._{specimen}} = \frac{\frac{F_{mass}}{\rho_{fiber}}}{\frac{S_{mass}}{\rho_{specimen}}} = \frac{F_{mass}\,\rho_{specimen}}{S_{mass}\,\rho_{fiber}} \tag{20}$$

Where,

$$W_{fiber} = \frac{F_{mass}}{S_{mass}} \tag{21}$$

Thus, Eq. (20) becomes,

$$V_{fiber} = \frac{\rho_{specimen} W_{fiber}}{\rho_{fiber}} \tag{22}$$

Similarly, the matrix fraction of a composite material can be shown to be,

$$V_{matrix} = \frac{\rho_{specimen} W_{matrix}}{\rho_{matrix}} \tag{23}$$

Substitution of Eq.'s (22) & (23) into Eq. (19) yields,

$$V_v + \frac{\rho_{specimen} W_{fiber}}{\rho_{fiber}} + \frac{\rho_{specimen} W_{matrix}}{\rho_{matrix}} = 1 \quad (24)$$

The rearrangement of terms gives

$$V_v = 1 - \rho_{specimen}\left(\frac{W_{fiber}}{\rho_{fiber}} + \frac{W_{matrix}}{\rho_{matrix}}\right) \quad (25)$$

Multiplying Eq. (25) by 100 gives the void content as a percentage as shown in Eq. (26).

$$V_v = 100 - \rho_{specimen}\left(\frac{W_{fiber}}{\rho_{fiber}} + \frac{W_{matrix}}{\rho_{matrix}}\right) \quad (26)$$

B.2: VOID CONTENT UNCERTAINTY

The densities of the specimen and matrix were calculated using Eq. (27).

$$\rho_{specimen} = \rho_{matrix} = \frac{M_{fluid}}{V_{cup}} \quad (27)$$

The uncertainty associated with the calculated values of "$\rho_{specimen}$" and "ρ_{matrix}" can be found by using Eq. (28) where "$U_{Msol.}$" and "$U_{Vcup.}$" are the uncertainties associated with each parameter.

$$U_{\rho_{specimen}} = U_{\rho_{matrix}} = \sqrt{\left(\frac{1}{V_{cup}} U_{M_{fluid}}\right)^2 + \left(\frac{M_{fluid}}{V_{cup}^2} U_{V_{cup.}}\right)^2} \quad (28)$$

The weight fractions of the fibers "$\%W_f$" and matrix "$\%W_m$" were determined using Eq. (29) where "$_I$" represents either fiber or matrix.

$$\%W_{fiber} = \%W_{matrix} = \frac{M_I}{S_{mass}} \times 100 \tag{29}$$

As with the density, the calculated weight fractions uncertainties were found. The uncertainties for each of these parameters were calculated using Eq. (30) where "U_{Imass}" and "U_{Smass}" are the uncertainties of each measured quantity.

$$U_{\%W_{fiber}} = U_{\%W_{matrix}} = \sqrt{\left(\frac{100}{S_{mass}} \times U_{I_{mass}}\right)^2 + \left(\frac{100 \times I_{mass}}{S_{mass}^2} \times U_{S_{mass}}\right)^2} \tag{30}$$

Using the uncertainties calculated in Eq.'s (28) & (30), the uncertainty for the void volume content was calculated using .

$$U_{\%V_v} = \sqrt{\begin{aligned}&\left[\left(\frac{\%W_{fiber}}{\rho_{fiber}} + \frac{\%W_{matrix}}{\rho_{matrix}}\right) \times U_{\rho_{specimen}}\right]^2 + \left(\frac{\rho_{specimen}}{\rho_{fiber}} \times U_{\%W_{fiber}}\right)^2 + \\ &\left(\frac{\rho_{specimen}}{\rho_{matrix}} \times U_{\%W_{matrix}}\right)^2 + \left(\frac{\%W_{fiber} \times \rho_{specimen}}{\rho_{fiber}^2} \times U_{\rho_{fiber}}\right)^2 + \\ &\left(\frac{\%W_{matrix} \times \rho_{specimen}}{\rho_{matrix}^2} \times U_{\rho_{matrix}}\right)^2\end{aligned}} \tag{31}$$

B.2.1: SAMPLE UNCERTAINTY CALCULATION

Sample calculations are made using the equations in the previous sections. The relevant values used for each calculation can be found in Table 3.

Table 3: Values used for Uncertainty Calculations

Parameter	Value	Uncertainty of Measurement
M_{fluid}	159.488	±0.001 g
M_{fluid} Matrix	101.828	
S_{mass}	0.5690	±0.0001 g
F_{mass}	.3996	
M_{mass}	0.1694	
V_{cup}	83.2 cc	0.1 cc
ρ_{fiber}	2.637 g/cc	±0.009 g/cc

Using the values from Table 3, each of the variables value and uncertainties were calculated. The results are listed in Table 4.

Table 4: Calculated Uncertainty Values

Parameter	Calculated Value	Uncertainty of Calculation
$P_{specimen}$	1.917 g/cc	±0.002 g/cc
ρ_{matrix}	1.224 g/cc	
$\%W_{fiber}$	70.23 %	±0.02 %
$\%W_{matrix}$	29.77 %	
$\%V_v$	2.31 %	±0.22 %

APPENDIX C: RING FLEXURAL PROPERTIES

C.1: RING FLEXURAL MODULUS

The most approachable technique to determine the flexural modulus of a linearly elastic ring is to use Castigliano's second theorem which is shown in Eq. (32) [40].

$$\delta = \frac{dU}{dP} \tag{32}$$

Where, "δ" is the maximum vertical deflection, "P" is the applied load, and "U" is the total elastic strain energy as defined in Eq. (33).

$$U = U_{flex.} + U_{shear} + U_{circum.} \tag{33}$$

With "$U_{flex.}$", "U_{shear}", and "$U_{circum.}$" being the flexural, shear, and circumferential strain energies respectively. A free-body diagram of the lateral compression of cylindrical ring is shown below in Figure 57.

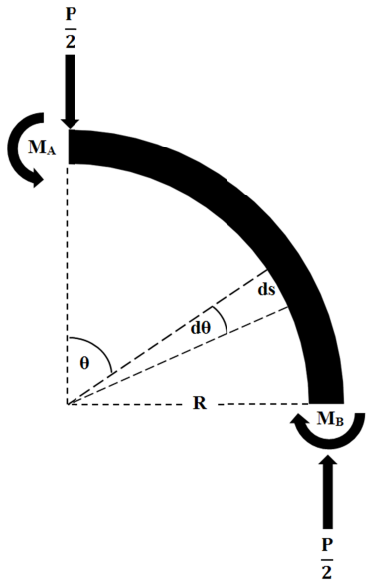

Figure 57- Free-body diagram of a cylindrical ring that is laterally compressed.

C.1.1: FLEXURAL STRAIN ENERGY

The flexural strain energy of a bar in bending is shown in Eq. (34).

$$U_{flex.} = \int \frac{M^2}{2EI}\, ds = \int \frac{6M^2}{Ewt^3} ds \tag{34}$$

The "M", "E", "d", "b", and "ds" terms are the bending moment at angle θ, materials elastic modulus, width of the ring, thickness of the ring, and differential arc element respectively. The differential arc element is defined in Eq. (35).

$$ds = Rd\theta \tag{35}$$

In the above equation, the "D" and "dθ" represents the cylinder diameter and differential angle respectively. The moment "M" is defined at angle θ as shown in Eq. (36).

$$M = M_A - \frac{PR}{2}\sin\theta \tag{36}$$

The moment "M_A" is the moment at the top of the cylinder and "P" is the load applied to crush the cylinder. The substitution of Eq.'s (35) and (36) into Eq. (34) yields the following.

$$U_{flex.} = \frac{24R}{Ebd^3}\int_0^{\frac{\pi}{2}} \left(M_A - \frac{PR}{2}\sin\theta\right)^2 d\theta = \frac{3R}{2Ebd^3}\left(P^2R^2\pi + 8{M_A}^2\pi - 16M_APR\right) \tag{37}$$

The moment "M_A" can be found by using the principle of minimum strain energy. Thus, taking the partial derivative of "$U_{flex.}$" with respect to "M_A", setting it equal to zero and solving for "M_A" yields Eq. (38).

$$M_A = \frac{PR}{\pi} \tag{38}$$

Substitution of the above into Eq. (37) yields the final form of the flexural component of the strain energy as shown in Eq. (39) below.

$$U_{flex.} = \frac{0.893R^3P^2}{Ebd^3} \tag{39}$$

C.1.2: SHEAR STRAIN ENERGY

The shear strain energy written in terms of the shear stress "q" and shear modulus "G" and assuming the laminate is transversely isotropic, can be calculated using Eq. (40).

$$U_{shear} = w\iint \frac{q^2}{2G}\,ds\,dy \tag{40}$$

The shear stress is given by Eq. (41) and the shear modulus is given by Eq. (42).

$$q = \frac{6P\cos\theta}{bd^3}\left(\frac{t^2}{4} - y^2\right) \tag{41}$$

$$G = \frac{E}{2(1+\nu)} \tag{42}$$

The substitution of Eq.'s (35), (41) and (42) into Eq. (40) yields the final form of the strain energy equation.

$$U_{shear} = \iint_{-\frac{t}{2}}^{\frac{t}{2}} \frac{18P^2}{Gbd^6}\cos^2\theta\left(\frac{t^2}{4} - y^2\right)^2 ds\, dy = \frac{3P^2R}{5bdG}\int_0^{\frac{\pi}{2}} \cos^2\theta\, d\theta$$
$$= \frac{3\pi P^2 R(1+\upsilon)}{10bdE} \tag{43}$$

C.1.3: CIRCUMFERENTIAL DEFORMATION STRAIN ENERGY

The circumferential strain energy is related to the axial force "F", cross-sectional area "A", and elastic modulus "E" as shown in Eq. (44).

$$U_{circum.} = \int \frac{F^2}{2EA}\, ds = \int_0^{\frac{\pi}{2}} \int \frac{RP^2 \sin^2\theta}{2bdE} d\theta = \frac{RP^2\pi}{8bdE} \tag{44}$$

Combining the final "$U_{flex.}$", "U_{shear}", and "$U_{circum.}$" terms into Eq. (33) gives the total strain energy for a laterally collapsing cylinder as the following.

$$U = \frac{0.893R^3P^2}{Ebd^3} + \frac{3\pi P^2 R(1+\nu)}{10bdE} + \frac{RP^2\pi}{8bdE} \tag{45}$$

Applying Castigliano's theorem (i.e. Eq. (32) the deflection of the cylinder can be found using Eq. (46)).

$$\delta = \frac{1}{Ebd}\left[\frac{1.786R^3P}{d^2} + \frac{3\pi PR(1+\upsilon)}{5} + \frac{RP\pi}{4}\right] \tag{46}$$

Rearranging Eq. (46) allows for the elastic modulus "E" to be solved directly as shown in Eq. (47).

$$E = \frac{1}{\delta b d}\left[\frac{1.786R^3P}{d^2} + 1.89PR(1+\upsilon) + 0.785RP\right] \quad (47)$$

Eq. (47) shows that the shear and circumferential strain energies become insignificant in cases where the radius to thickness ratio is high. For the cylinders studied, this ratio is sufficiently large. Therefore, the shear and circumferential strain energies in Eq. (47) were neglected. A comparison between Eq. (2) without the correction factor recommended by the ASTM standard and Eq. (47) is shown below in Table 5.

Table 5: Comparison of Equations used for Calculating the Elastic Moduli of Composite Rings

Parameters \ Equations	#2	#47
Radius (mm)	25.4	25.4
Thickness (mm)	0.864	0.864
Load (N)	21.13	21.13
Length (mm)	12.83	12.83
Deflection (mm)	5.08	5.08
Calculated Elastic Modulus	29.45	29.54

C.2: RING FLEXURAL STRENGTH

As stated in the characterization section of the report, the flexural strength of the ring segments can be approximated by the straight beam theory if the radius to depth ratio is sufficiently high. In this appendix, the elastic solution of a curved beam in bending will be derived [84]. The results of which will be compared to straight beam theory for different radius to depth ratio's and an acceptable range will be identified. A free body diagram of the curved beam in bending, stress element, and the variables used for the derivation is shown in Figure 58.

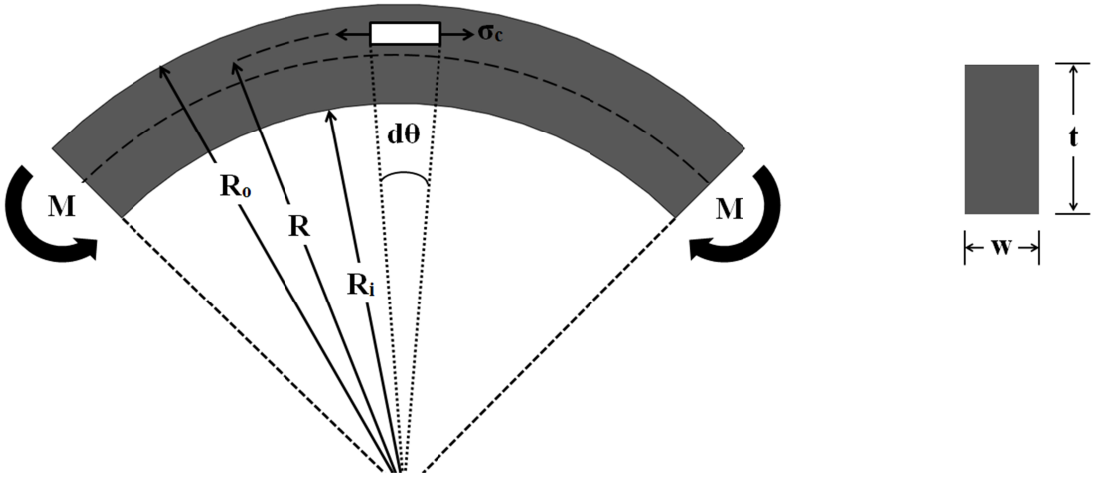

Figure 58- Free-body diagram of a curved beam subject to bending.

The equilibrium equation for polar coordinates is shown below as Eq. (48).

$$\frac{d\sigma_R}{dR} + \frac{1}{R}\frac{d\tau_{R\theta}}{d\theta} + \frac{\sigma_R - \sigma_c}{R} + F_R = 0 \qquad (48)$$

Where "σ_R", "σ_c", "$\tau_{R\theta}$", "F_R", and "R" are the radial stress, circumferential stress, shear stress, radial body force, and radius respectively. Due to symmetry, "$\tau_{R\theta}$" is zero as is

"F_R" due to the absence of body forces. Substitution of the above into Eq. (48) yields the following.

$$\frac{d\sigma_R}{dR} + \frac{\sigma_R - \sigma_c}{R} = 0 \tag{49}$$

In addition, for this case the equation for compatibility is Eq. (50).

$$\frac{d^2(\sigma_R + \sigma_c)}{dR^2} + \frac{1}{R}\frac{d(\sigma_R + \sigma_c)}{dR} = 0 \tag{50}$$

Direct integration of Eq. (50) gives the subsequent equation.

$$\sigma_R + \sigma_c = c_A \ln\frac{R}{R_i} + c_B \tag{51}$$

Solving Eq.'s (49) and (51) together gives the equations from which the circumferential and radial stresses may be calculated.

$$\sigma_c = c_1\left(\ln\frac{R}{R_i} + 1\right) - \frac{c_3}{R^2} + c_2 \tag{52}$$

$$\sigma_R = c_1 \ln\frac{R}{R_i} + \frac{c_3}{R^2} + c_2 \tag{53}$$

The following three boundary conditions were incorporated to solve for the constants in Eq.'s (52) and (53).

1. The circumferential stresses at the ends of the bar produce a moment "M".

$$M = w\int_{R_i}^{R_o} R\sigma_c \, dR \tag{54}$$

2. No circumferential forces act along the upper and lower boundaries of the beam, i.e.

$$\sigma_{R_{R=R_o}} = 0 \tag{55}$$

$$\sigma_{R_{R=R_i}} = 0 \tag{56}$$

3. Because of B.C. #2, the circumferential stress at the bar must be distributed to equal zero.

$$w\int_{R_i}^{R_o} \sigma_c \, dR = 0 \tag{57}$$

Combining Eq.'s (53), (55), and (56) gives the following relationships for "c_1", "c_2", and "c_3".

$$c_3 = -c_2 {R_i}^2 \tag{58}$$

$$c_1 \ln\frac{R_o}{R_i} = c_2\left(\frac{{R_i}^2}{{R_o}^2} - 1\right) \tag{59}$$

The above two equations satisfy the boundary condition shown in Eq. (57). The rearrangement of Eq.'s (58) and (59) yields the following.

$$c_2 = \frac{{R_o}^2 \ln\frac{R_o}{R_i}}{\left({R_i}^2 - {R_o}^2\right)} c_1 \tag{60}$$

$$c_3 = \frac{{R_i}^2{R_o}^2 \ln\frac{R_o}{R_i}}{\left({R_0}^2 - {R_i}^2\right)} c_1 \tag{61}$$

Substitution of Eq.'s (60) and (61) into Eq. (52) and using the boundary condition expressed in Eq. (54) gives the proceeding equation.

$$M = w\int_{R_i}^{R_o} c_1 R\left(\ln\frac{R}{R_i} + 1\right) - c_1\frac{{R_i}^2{R_o}^2 \ln\frac{R_o}{R_i}}{R\left({R_0}^2 - {R_i}^2\right)} + c_1\frac{R\,{R_o}^2 \ln\frac{R_o}{R_i}}{\left({R_i}^2 - {R_o}^2\right)}\, dR \tag{62}$$

When the above equation is integrated, the constant "c_1" is found to be as shown in Eq. (63).

$$c_1 = \frac{4M\left({R_o}^2 - {R_i}^2\right)}{w\,{R_o}^4\left[\left(1 - \frac{{R_i}^2}{{R_o}^2}\right)^2 - 4\frac{{R_i}^2}{{R_o}^2}\ln^2\frac{R_o}{R_i}\right]} \tag{63}$$

Now that all the constants have been determined, they can be substituted into Eq.'s (52) and (53). The final forms of the equations used to calculate circumferential and radial stresses are shown below as Eq.'s (64) and (65) respectively.

$$\sigma_c = \frac{4M\left[\left(1-\frac{{R_i}^2}{{R_o}^2}\right)\left(\ln\frac{R}{R_i}+1\right)-\left(1+\frac{{R_i}^2}{R^2}\right)\ln\frac{R_o}{R_i}\right]}{w\,{R_o}^2\left[\left(1-\frac{{R_i}^2}{{R_o}^2}\right)^2-4\frac{{R_i}^2}{{R_o}^2}\ln^2\frac{R_o}{R_i}\right]} \tag{64}$$

$$\sigma_R = \frac{4M\left[\left(1-\frac{{R_i}^2}{{R_o}^2}\right)\ln\frac{R}{R_i}-\left(1-\frac{{R_i}^2}{R^2}\right)\ln\frac{R_o}{R_i}\right]}{w\,{R_o}^2\left[\left(1-\frac{{R_i}^2}{{R_o}^2}\right)^2-4\frac{{R_i}^2}{{R_o}^2}\ln^2\frac{R_o}{R_i}\right]} \tag{65}$$

The error of using classical beam theory for curved beams was determined by comparing its results to those of Eq. (64), which is considered exact. The results of this comparison are shown in Figure 59. It is shown that the maximum error in any stress calculated in this dissertation was 2.15%, which was incurred at a radius to depth ratio of 16.

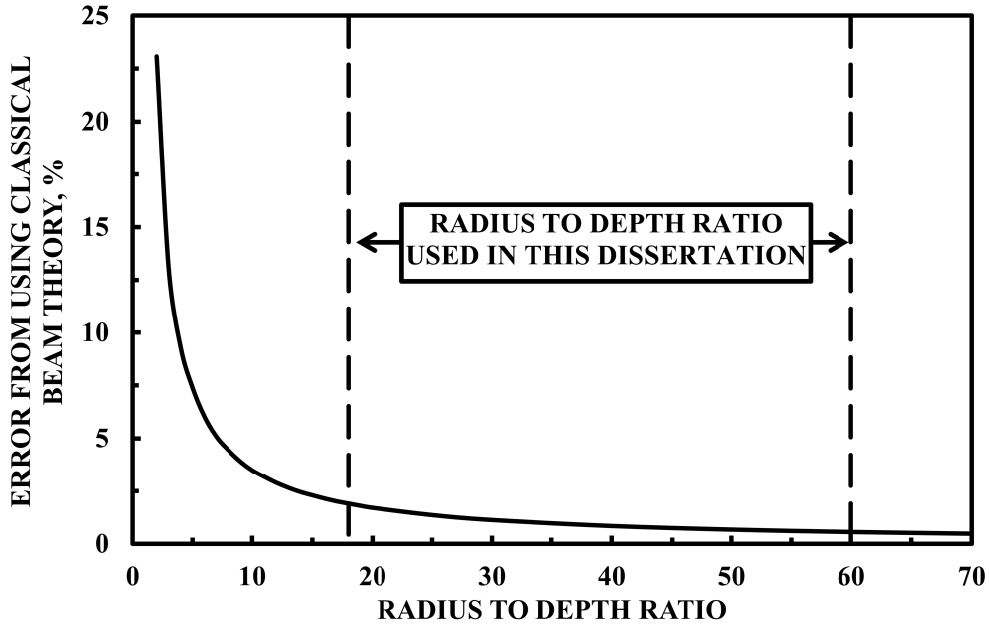

Figure 59- Error of using classical beam theory to calculate flexural strengths of curved beams of varying radius to depth ratios.

APPENDIX D: DISSERTATION PUBLICATIONS

The work presented in this dissertation has been published in the following.

JOURNAL ARTICLE

1. **Anderson, J.P.** and M.C. Altan, *Properties of Composite Cylinders Fabricated by Bladder Assisted Composite Manufacturing (BACM).* Journal of Engineering Materials and Technology, 2012. 134(4): 044501

CONFERENCE PROCEEDINGS

1. **Anderson, J.P.** and M.C. Altan, *Coupled Effect of Humidity Exposure and Cure Pressure on the Formation of Microvoids in Composite Laminates*, in *28th International Conference of the Polymer Processing Society.* 2012, Polymer Processing Society: Pattaya, Thailand.

2. **Anderson, J.P.** and M.C. Altan, *Coupled Effect of Microvoids and High Fiber Content on the Failure Strength of Composite Laminates*, in *Polymer Processing Society Americas Conference*. 2012, Polymer Processing Society: Niagara Falls, Canada.

3. **Anderson, J.P.** and M.C. Altan, *Composite Laminates Fabricated by Bladder Assisted Composite Manufacturing (BACM): Mechanical Properties and Reduction of Microvoids.* in *3rd International Polymeric Composites Symposium and Exhibition*. 2012, International Polymeric Composites: Izmir, Turkey

4. **Anderson, J.P.** and M.C. Altan, *Properties of Composite Cylinders Fabricated by Bladder Assisted Composite Manufacturing (BACM).* in *ASME IMECE*. 2011, ASME: Denver, Colorado

5. **Anderson, J.P.,** J.M. Elizondo, M.C. Saha, and M.C. Altan, *Effect of Heating Methods on the Mechanical Properties and Energy Consumed during Curing of Hollow Composite Parts*, in *Polymer Processing Society 26th Regional Meeting*. 2010, Polymer Processing Society: Istanbul, Turkey.

6. **Anderson, J.P.,** C. Proto, A. Kelly, Z. Siddique, and M.C. Altan, *Fabrication of Hollow Composite Parts Using Inflatable Bladders: Processing and Properties*, in *Polymer Processing Society 26th Annual Meeting*. 2010, Polymer Processing Society: Banff, Canada.